8) Receptor Oriented Apportionment for Big Bend National Park

8.1 Qualitative

8.1.1 Space/Time Pattern Analysis (EOF)

8.1.1.1 Introduction

Spatial and temporal relationships in the BRAVO fine particulate data are examined here using several techniques including Empirical Orthogonal Function (EOF) analysis [*Malm and Gebhart*, 1996, 1997; *Gebhart and Malm*, 1997; *Gebhart et al.*, 2000]. EOF analysis, described in detail in section 2.3.1.1, simplifies the dozens of daily spatial patterns into a few patterns that, when linearly re-combined, explain most of the variance in the data. Examination of spatial and temporal patterns is often useful to qualitatively examine dominant source-receptor relationships and to subjectively form hypotheses about significant source areas and physical factors likely to influence transport and transformation of aerosols in a region [*Malm and Gebhart*, 1996, 1997; *Gebhart and Malm*, 1997; *Gebhart et al.*, 2000; *Malm et al.,* 1990; *Henry et al.,* 1991].

One source of particular interest due in part to the proximity to Big Bend National Park has been the Carbón I (1200 MW) and Carbón II (1400 MW) coal-fired electric generating stations located near Piedras Negras, Coahuila, approximately 20 miles south of the U.S.-Mexico border. These power plants consist of 4 units each that are uncontrolled for SO_2 emissions. The BRAVO site nearest to these plants is Eagle Pass (See section 2.1.1.1 for a detailed description of BRAVO fine particulate monitoring, Figure 1-2 for a map of the study area, and Figure 2-1 for a map of the monitoring locations). Other source areas with high SO_2 emissions, close proximity, and frequent airmass transport to Big Bend include the Lignite Belt in northeast Texas which includes several coal-fired electric generating stations, the Gulf Coast region of southeast Texas and southern Louisiana where there are both large population centers and petrochemical and oil refining activities, the eastern U.S. including the Ohio River Valley with many high-sulfur, coal-burning power plants, industrial areas of Mexico including the Monterrey region, and southern Mexico which includes both Mexico City and an active volcano.

Prior to BRAVO, during September and October 1996, a field study consisting of 19 fine particle monitoring sites located in southern Texas and northern Mexico was conducted by the NPS and Procuraduria Federal de Proteccion al Ambiente (PROFEPA) [*Gebhart et al.*, 2000]. The particulate measurement and analysis techniques employed during this earlier study were essentially the same as during BRAVO. For several reasons it is of interest to compare the temporal, spatial, and interspecies patterns from BRAVO with those from the pilot study. The second half of BRAVO was during the same months of the year as the pilot study so it is possible to examine some inter-annual trends in fine particulate matter. Also, the spatial domains of the two studies overlapped with the 1996 study including sites in Mexico, but not extending as far north into Texas as did BRAVO. If the spatial patterns in the overlapping area are similar for both years, then we might be able to infer that the patterns in the non-overlapping areas were also similar, thus giving us a picture of the typical spatial patterns over a larger geographic area.

8.1.1.2 Imputation of Missing Data

During BRAVO there were 37 sites throughout Texas where speciated fine (< 2.5 μm diameter) particle concentrations were measured. These included four sites with 6-hour duration

samples and the remaining with 24-hour measurements. Summary statistics for most species at all sites are shown in Appendix 8a.

EOF analysis requires, and for other comparisons between sites we would like, a time-by-site matrix of concentrations with no missing values. Several schemes were used to fill missing or below detectable limit elements of the time-by-site matrix for each species. All 6-hour data were averaged to 24-hour concentrations and then missing values were either eliminated or estimated. Time periods and then sites with more than 25% of data missing were eliminated. This reduced the analysis period of June 29–October 31 to July 26–October 30, with August 5 and 6 also removed. Three sites, Padre Island, Guadalupe Mountains, and Wichita Mountains, were also removed, resulting in a matrix of 95 days by 34 sites. Next, all observations immediately preceded and followed by valid data at the same site were approximated by linear interpolation in time. Remaining missing data were filled by inverse distance weighted spatial interpolation. Concentrations below the minimum detectable limit (BDL) were set to 0. For the sulfur matrix, only 0.8% of the data were filled by time interpolation, 2.8% by spatial interpolation, and 0.3% were BDL. Similar fractions of the data matrices for other species were estimated in the same way. Due to the removal of most of July, results of EOF analyses are not expected to be directly comparable to other analyses of BRAVO data that include that time period. EOF analyses were completed for all measured species with adequate data.

8.1.1.3 Results for Sulfur

Because fine sulfate was the largest fraction of both the fine mass and the reconstructed light extinction (see chapter 3), insight into the source regions and transport pathways that lead to high sulfur concentrations at Big Bend are of high interest. Previous analyses of back trajectories arriving at Big Bend National Park over several years [*Gebhart et al.,* 2000, 2001] have also shown that there are dramatic seasonal differences in airmass transport patterns with airmasses more likely to arrive at Big Bend from Mexico during the summer than during other seasons and more likely to arrive from east Texas and other parts of the eastern United States during the fall than during other seasons. Thus it might be expected that sulfur source attributions and spatial patterns in the sulfur concentrations might be different during the early part of BRAVO than later in the study.

Time plots of 24-hour fine particulate elemental sulfur concentrations and some of the other major constituents of fine mass at Big Bend are shown in Figure 8-1. Daily spatial contour maps of sulfur are in Appendix 8b. Time lines and statistics for particulate sulfur for all BRAVO sites are in Appendices 6a and 6b. Maximum sulfur concentrations measured at Big Bend during BRAVO occurred during several 2–3 day episodes, with the highest concentrations occurring on September 1 and 2 (3080 & 2321 ng/m^3), September 15 (2545 ng/m^3), October 12 (2291 ng/m^3), and August 21 (2200 ng/m^3). The September 1–2 episode also had the highest organic carbon and second highest elemental carbon of the BRAVO study. The spatial patterns of measured sulfur on these days are shown chronologically in Figures 8-2 through 8-5. (See Appendix 8a and Figures 1-2 and 2-1 for detailed maps of site names, terrain, and points of interest). The first three of these days coincidentally happened to be days when IMPROVE network samplers were operating, so the spatial domain of sulfur measurements can be extended beyond Texas. The four patterns are all different with August 21 and October 12 being the most similar. These two days had higher sulfur concentrations in northeast Texas and around the Big Bend Area while central Texas had lower values. September 15 had the highest sulfur concentrations around Big Bend and on the southern Gulf Coast while concentrations in northeast Texas were the lowest in

the state. On September 1 the highest sulfur concentrations were in central Texas with the lowest being in three pockets in the east, far west, and southwest.

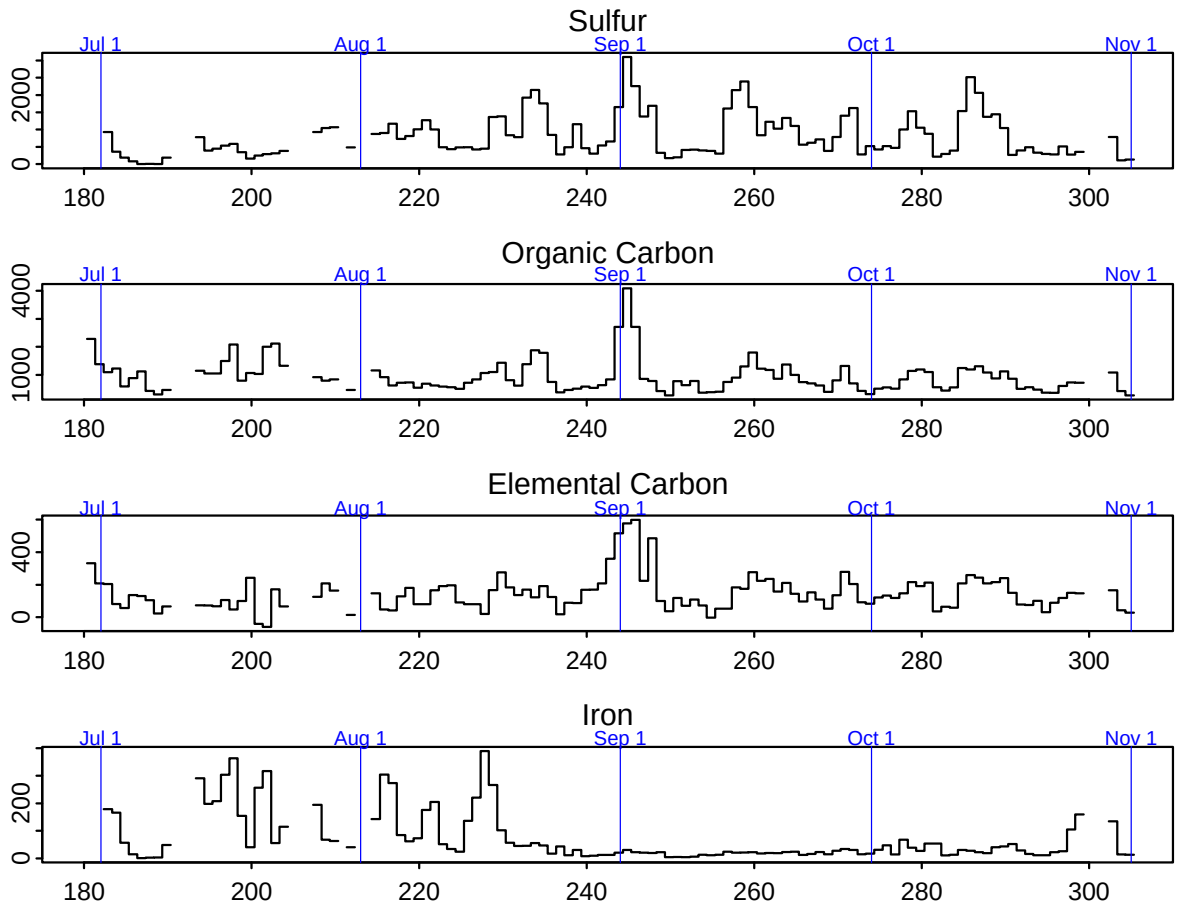

Figure 8-1. Time lines of the major constituents of fine mass (ng/m^3) at Big Bend. Labels on the x-axis are the day of the year. The vertical blue lines show the beginning of each month.

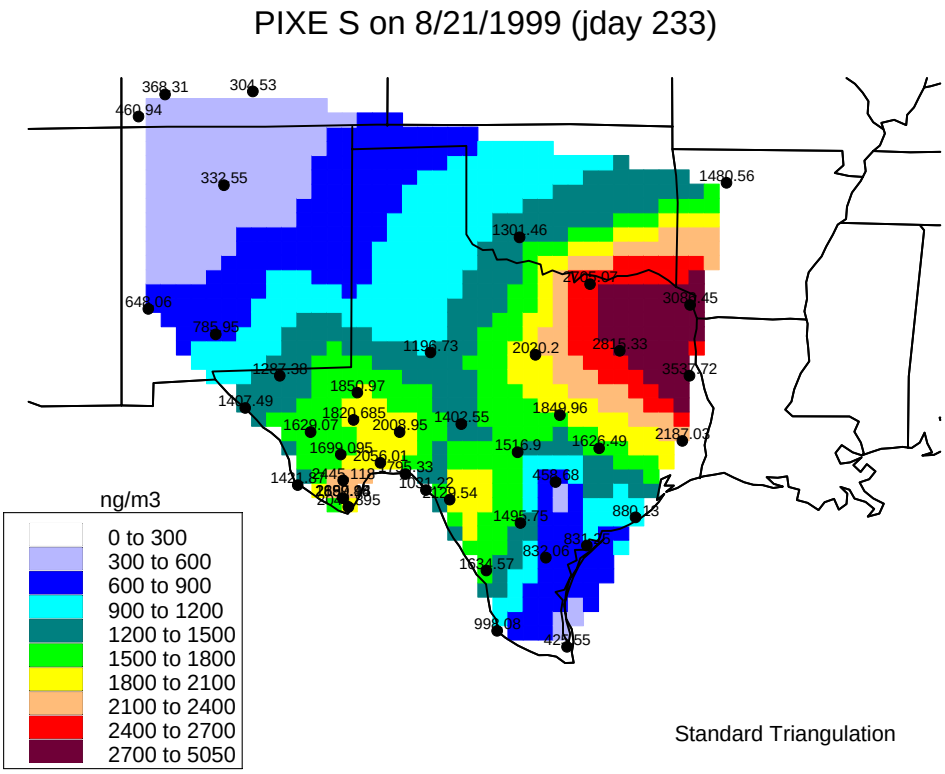

Figure 8-2. Spatial pattern of sulfur on August 21 when S at Big Bend was 2200 ng/m^3.

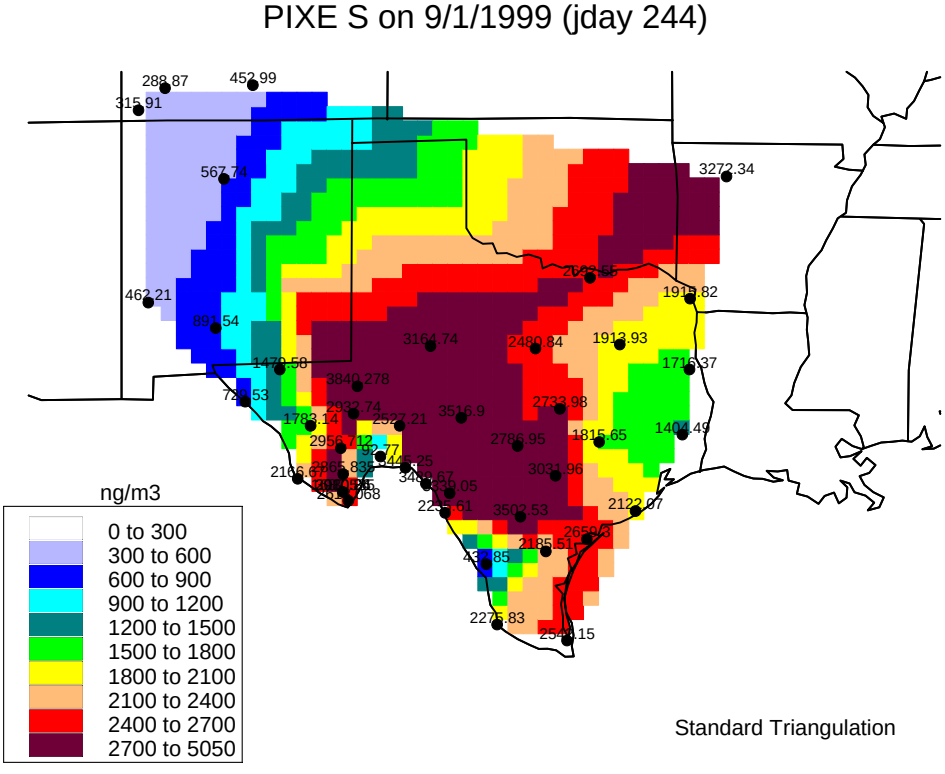

Figure 8-3. Spatial pattern of sulfur on September 1 when S at Big Bend was 3080 ng/m^3.

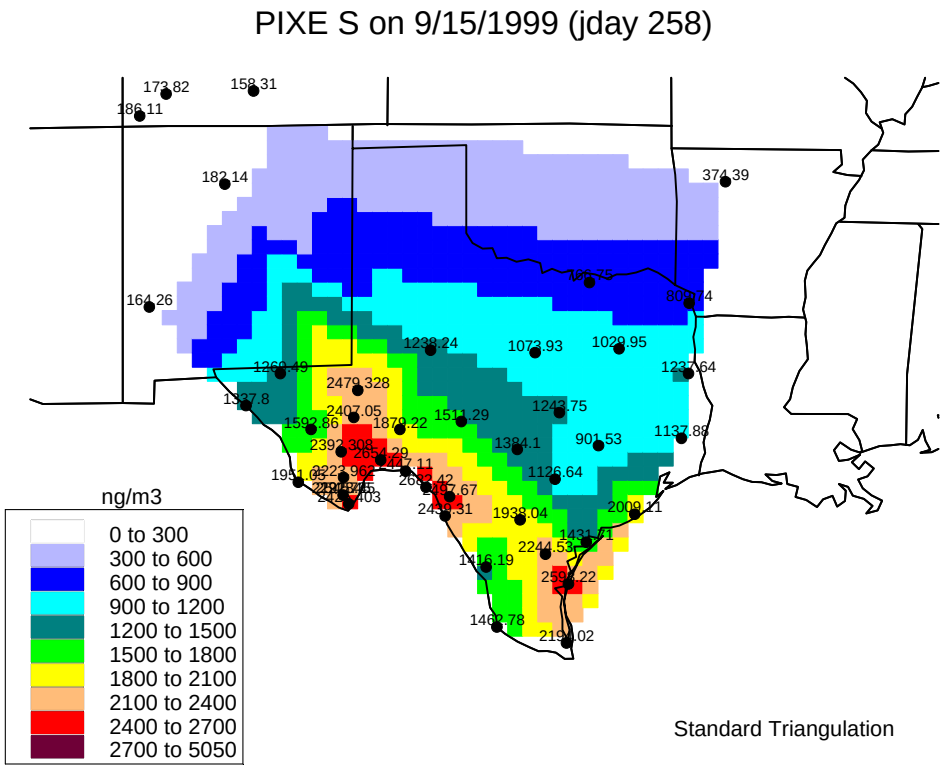

Figure 8-4. Spatial pattern of sulfur on September 15 when S at Big Bend was 2545 ng/m^3.

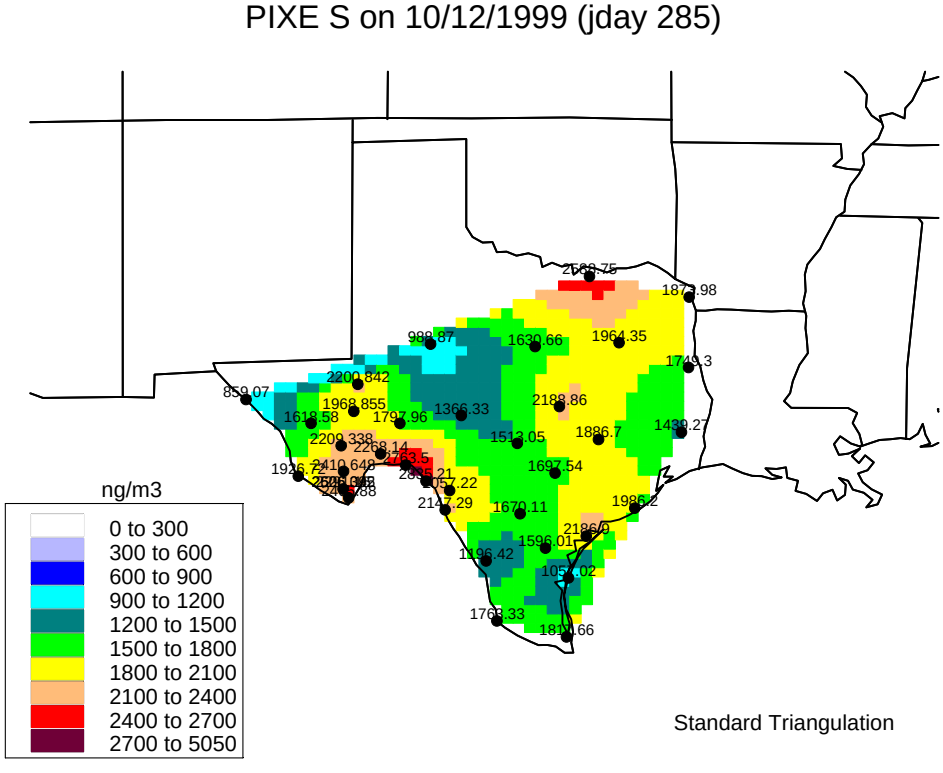

Figure 8-5. Spatial pattern of sulfur on October 12 when S at Big Bend was 2291 ng/m^3.

Mean sulfur concentrations during BRAVO are shown in Figure 8-6. Concentrations are highest on average in the northeast corner of the monitoring domain and lower towards the southwest, except an area east of Big Bend near the international border where there is a local maximum. That perturbation in the spatial pattern is indicative of at least some local influence from the nearby Carbón I/II plants.

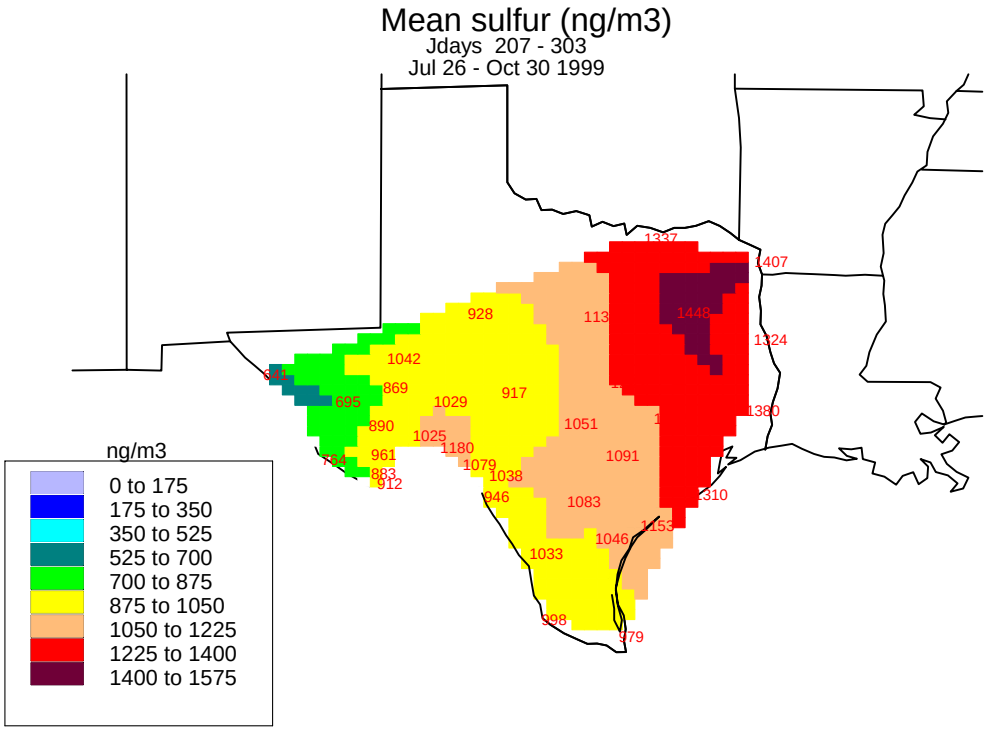

Figure 8-6. Mean sulfur concentrations for July 26–October 30, the portion of the study period when all sites had sufficient data.

Correlations of the sulfur concentrations at Big Bend to sulfur measured at other BRAVO sites are 0.6 or greater out to approximately 400 km from Big Bend and fall to below 0.3 at sites in eastern and northeastern Texas that are 700 km or more from the park as shown in Figure 8-7.

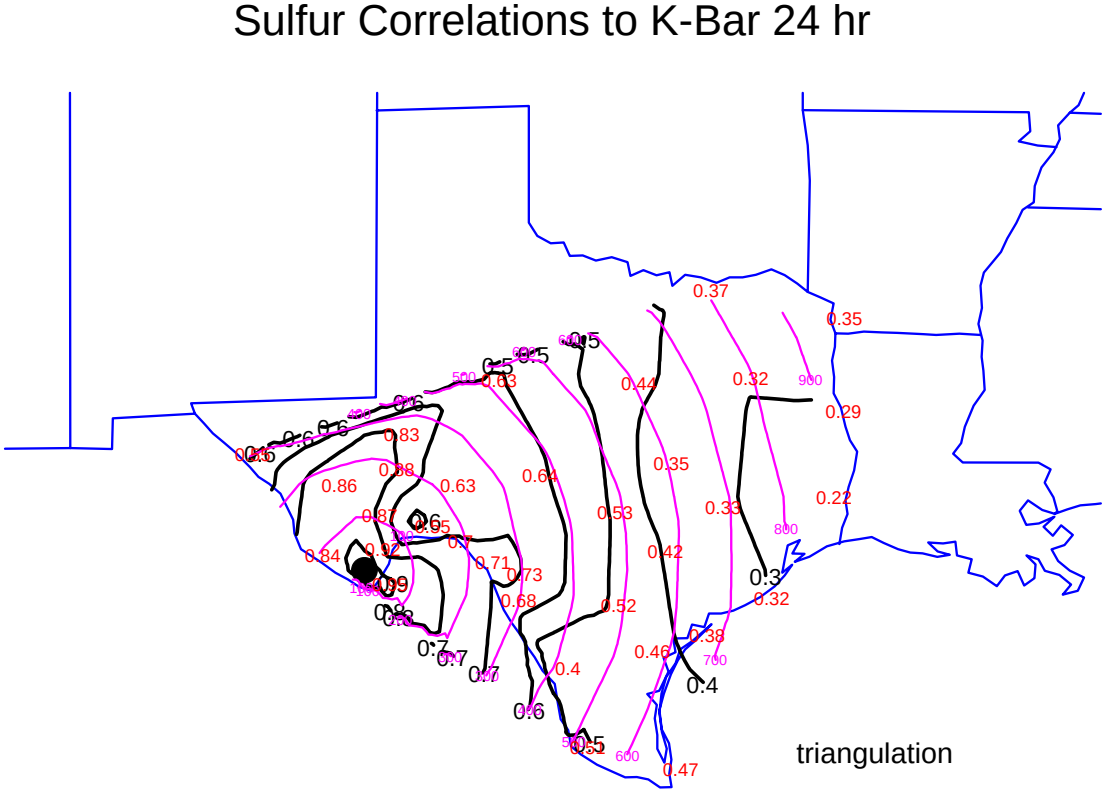

Figure 8-7. Correlations of sulfur measured at Big Bend to sulfur measured at other sites. Light magenta lines are distance in km from Big Bend.

Timeplots of the sulfur concentrations at sites other than Big Bend show that sulfur measured at locations within 200–300 km of each other are temporally very similar, though dissimilar to groups of more distant sites. A more compact illustration of this is shown in the monthly boxplots in Figure 8-8. The centerline of each box is the median concentration, tops and bottoms of the boxes are the 25th and 75th percentiles and the whiskers extend to 1.5 times the interquartile range. Values more extreme are shown as individual lines. The top left graph is for four sites located nearest to the Carbón I/II electric generating stations in northern Mexico, the top right graph is for five sites in the northeast corner of Texas in the lignite belt, the bottom left graph is for four sites in and near Big Bend National Park in southwest Texas, and the bottom right for four sites in southeast Texas near Houston. Sites in different areas of the state experienced their highest sulfur concentrations during different months of the study, with northeast Texas having maximum values during August, while sites closer to Big Bend had maximums during September. Sites nearest Carbón I/II experienced less monthly variation in sulfur concentrations than did sites in other corners of the monitoring domain. The relative lack of temporal variability at these sites, meaning the sulfur concentration is more or less constant no matter the predominant wind direction, is an indication of some relatively constant impact by nearby sources, possibly the Carbón I/II plants.

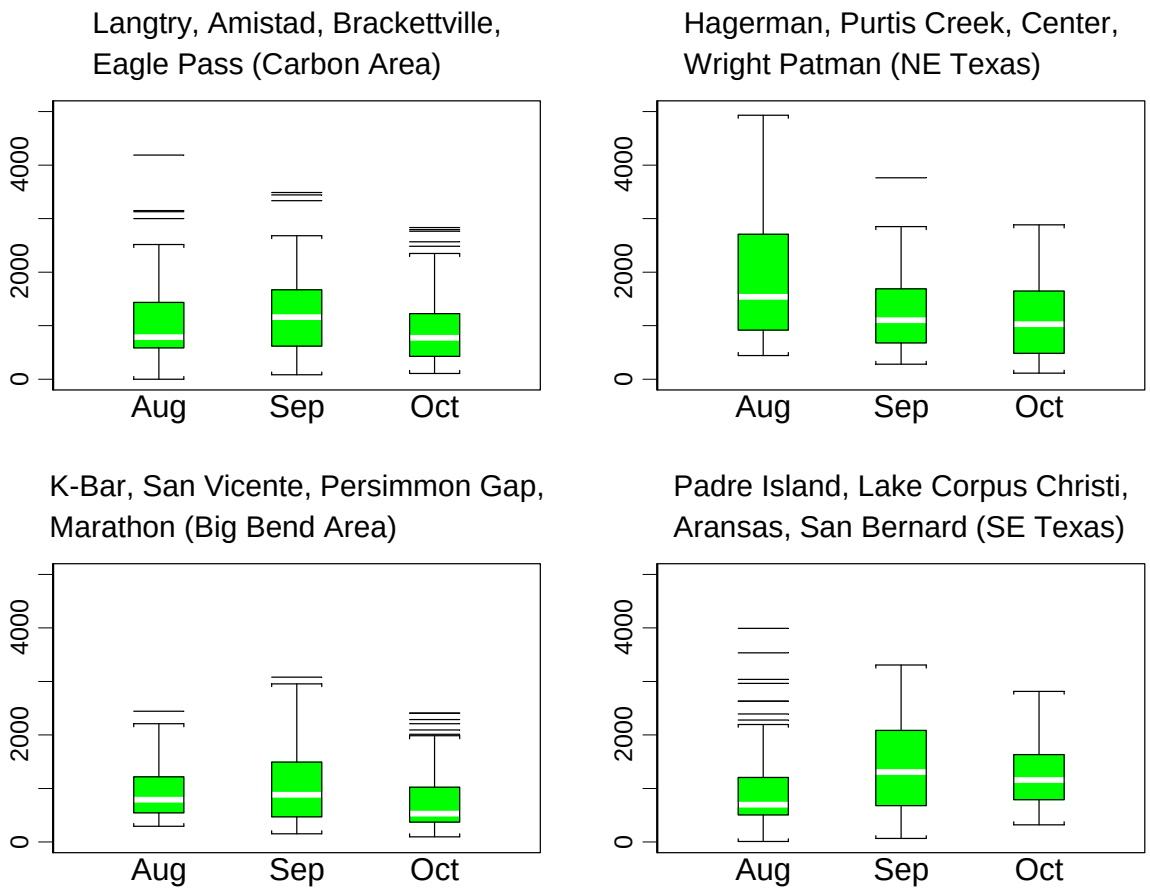

Figure 8-8. Boxplots of sulfur concentrations (ng/m^3) by month in four sections of the monitoring domain.

Seven fine particulate monitoring sites were common to both the 1996 and 1999 field studies. At five of these sites the differences between the mean September and October 1996 and mean September and October 1999 sulfur concentrations were 10% or less. The largest differences were 22% at Amistad and 12% at Fort Lancaster with 1996 being higher than 1999 for both. At Big Bend the difference between 1996 and 1999 was only 9 ng/m^3 or about 1% with 1999 being slightly higher. Since the sulfur concentrations appear to be quite similar between the two studies, the 1996 and 1999 means for these two months were plotted on a single map to visualize the "typical" mean sulfur concentrations for September and October over a larger area that includes both northeast Mexico sites of 1996 and the northeast Texas sites of 1999. This is shown in Figure 8-9.

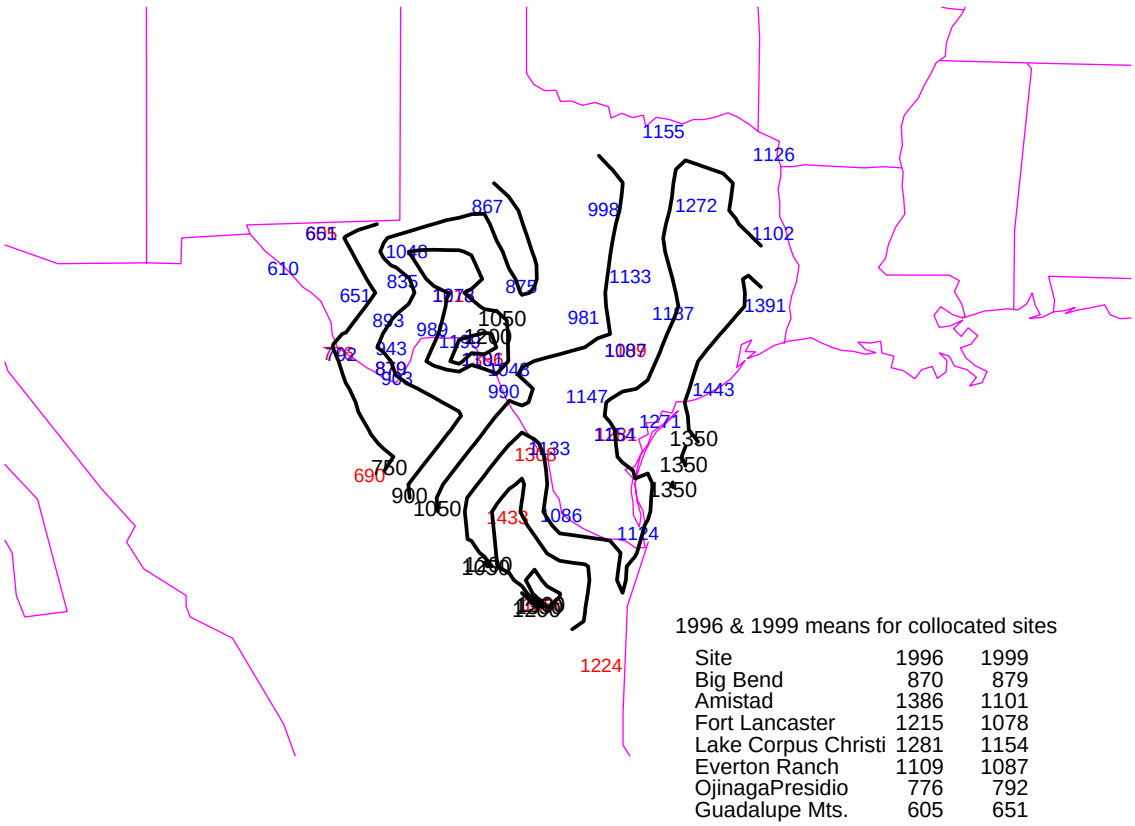

Figure 8-9. Overlaid mean sulfur concentrations during September and October 1996 and 1999. Sites listed in the bottom right corner are sites common to both years and the mean concentrations during each study period.

In general, mean fine sulfur across Texas decreases from east to west during September and October, but with a noticeable perturbation near and to the northwest of the Carbón I/II plants. Sulfur concentrations in northeast Mexico follow a similar east-west gradient, but with higher concentrations around the Monterrey area. The lower concentrations on the coast than inland in Mexico indicate that, although U.S. emissions may be transported across this area enroute to Big Bend, Mexican sources are certainly adding to the sulfur load in the airmass. Also, it is again evident by comparing the study-long (summer and fall) means in Figure 8-6 with the fall-only means in Figure 8-9 that the spatial patterns of sulfur within Texas vary seasonally. Northeast Texas has higher concentrations during July and August than during the fall, while sites closer to the Gulf Coast have similar concentrations during both seasons.

EOF analysis of the raw data cross product matrix for sulfur results in four factors (Figures 8-10 through 8-12 show EOFs 1–3) that cumulatively explain 82% of the variance. The factors were rotated using the Varimax criteria. The first rotated factor, explaining 33% of the variance, has highest values in the southwest and northeast corners of the state with lower values between. This indicates two likely source areas and transport pathways for sulfur for the days weighted highly for this pattern. First, sulfur is likely being transported into Texas from the

northeast or there are sulfur sources in the northeast corner of the state that influence the concentrations there. Also, sulfur is either being transported into Texas from the south or being generated in southwest Texas. The highest time weights for this pattern include the days of some of the highest concentrations at Big Bend including especially September 15, and to a lesser extent September 1, October 12, and the mid-August episode. This factor could represent local stagnation with light southerly flows yielding high concentrations in southwest Texas from nearby Mexican sources, while high concentrations in northeast Texas are due to local northeast Texas emissions or sources in nearby states. However, this pattern could also result from moderate wind speeds if wind directions in northeast Texas are arriving from the northeast while those in southwest Texas are from southerly directions. It's also possible that the lower concentrations in the center of Texas are due to conditions that caused enhanced deposition or reduced oxidation in this area.

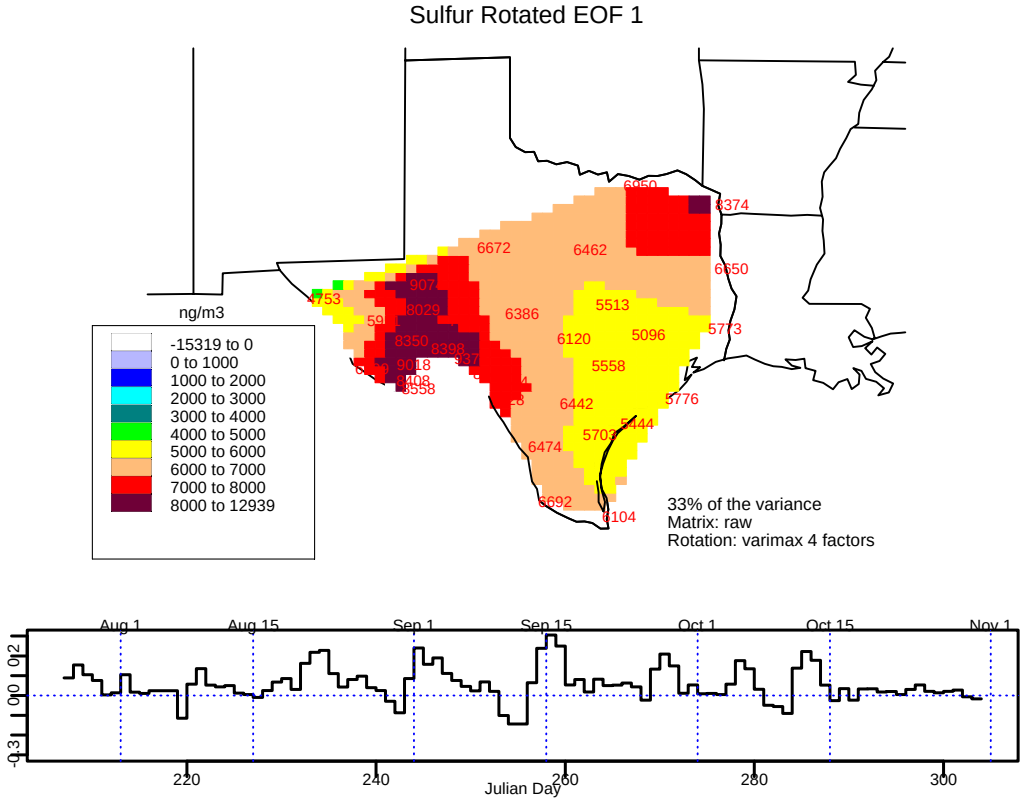

Figure 8-10. EOF 1 for sulfur.

The spatial pattern for rotated EOF 2, explaining 31% of the variance, is indicative of transport from northeast to southwest. This pattern has the strongest positive time weights on August 29–30, just before the high sulfur concentration at Big Bend on September 1. The highest value is in northeast Texas, with lower values all around. It is not possible to determine from EOF analysis alone whether this is because the source of the sulfate is in this location or whether the sources are primarily upwind, but the combined oxidation, transport, and deposition result in peak concentrations in this location. It seems most likely that the known sulfur sources

in northeast Texas are contributing to the sulfate load in the air being transported from east and northeast of the state.

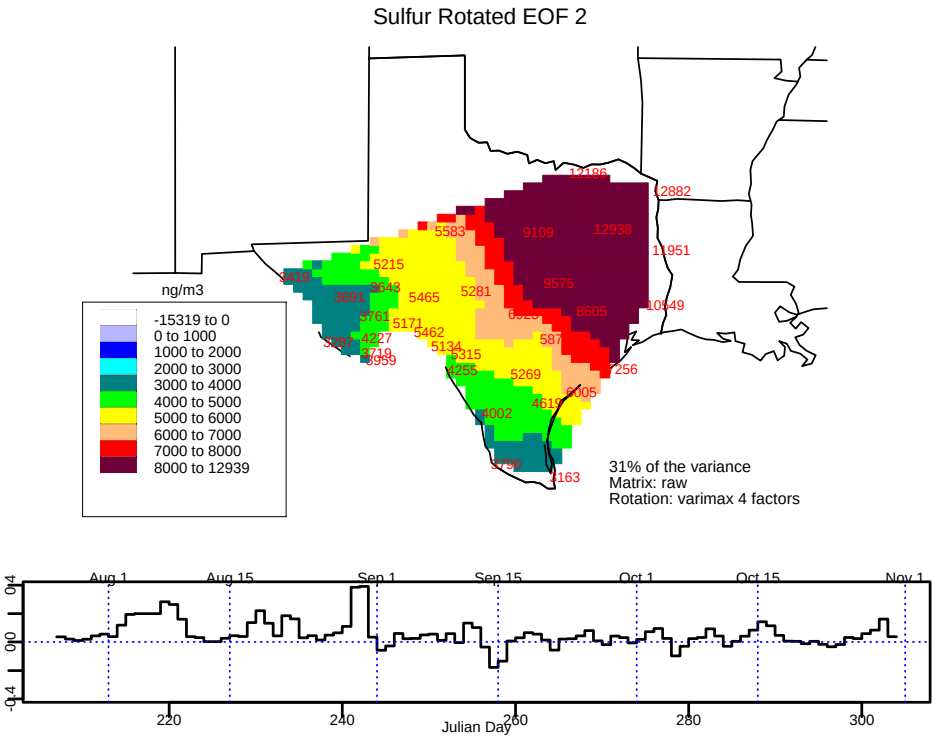

Figure 8-11. EOF 2 for sulfur.

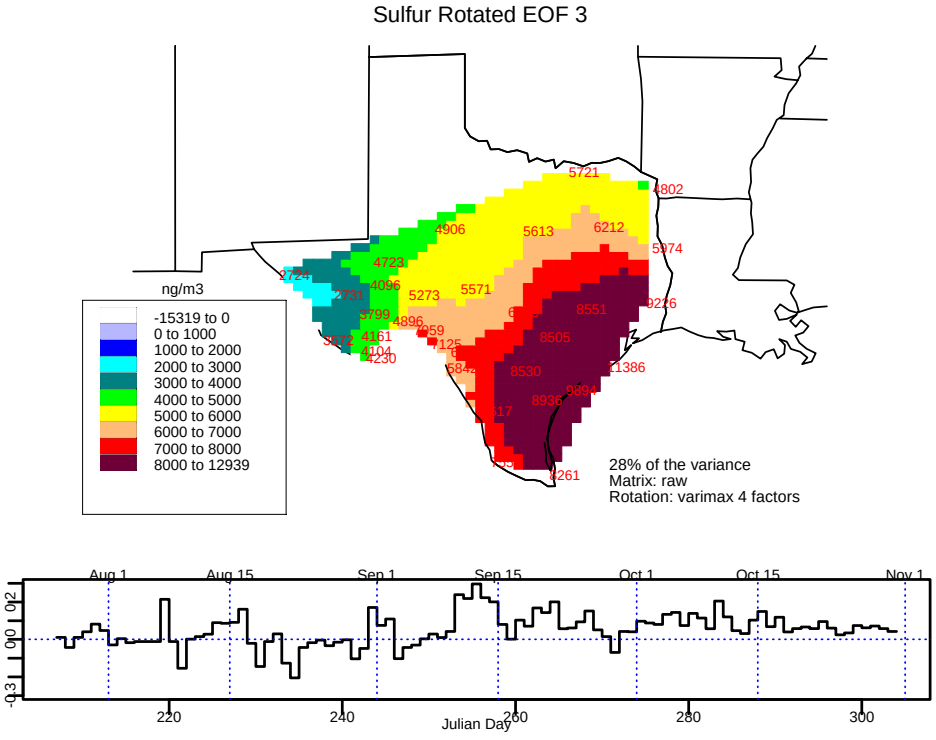

Figure 8-12. EOF 3 for sulfur.

EOF 3, explaining 28% of the variance, has highest values along the Texas Gulf Coast, suggestive of transport from the Gulf of Mexico or from the Houston area inland to central Texas. Highest time weights for this pattern are just prior to the September 15 episode at Big Bend.

The fourth factor explains only 3% of the variance and is not shown, but has highest concentrations in central Texas with lower values around the edges.

8.1.1.4 Iron

Spatial and temporal patterns of iron, representative of fine soil, are quite different from sulfur as illustrated in the time line of fine iron at Big Bend shown in Figure 8-1. By far the highest iron concentrations are during the summer and, in contrast to sulfur, mean iron concentrations are highest at the southernmost monitoring sites rather than at those in northeast Texas. While fine soil is, on average, less than 15% of the measured fine mass at Big Bend, it was greater than 50% during a few days early in the study. Figure 8-13 shows unrotated EOF 1 for iron, which explains 76% of the variance in the iron concentrations. Note that the only time factors significantly different from zero occur during July and early August. Rotating the iron factors resulted in four spatial patterns that all had high concentrations at southern sites. Previous analysis of historical particulate data at Big Bend [*Perry et al*., 1997; *Gebhart et al.*, 2001] has indicated frequent episodes of Saharan dust impacting the park during the summer. The spatial and temporal patterns in the BRAVO iron data suggest a similar phenomenon early in the BRAVO study, with the decreasing concentrations from south to north indicating the predominant transport pathway.

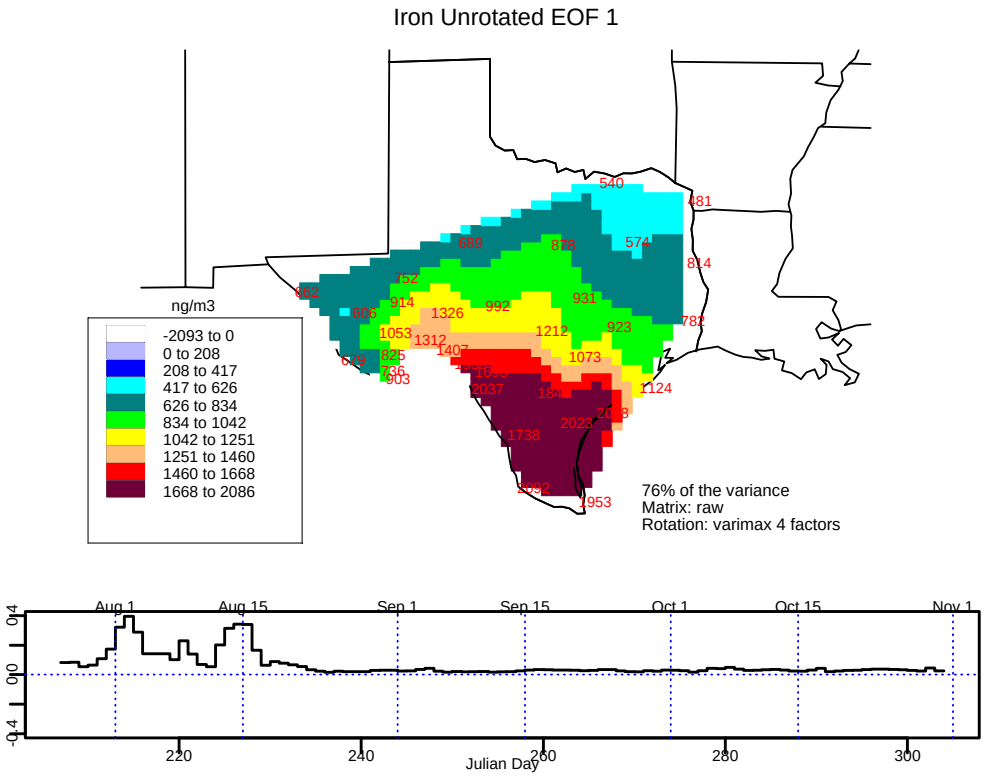

Figure 8-13. EOF 1 for iron.

Correlations of iron measured at Big Bend with iron measured at other BRAVO sites are 0.7 or higher out to approximately 200 km with some sites more than 300 km away having correlations this high. At several sites near and to the north of Big Bend, including San Vicente (0.961), Monahans Sandhills (0.930), McDonald Observatory (0.921), Fort Stockton (0.917), and Marathon (0.890), the correlations were 0.9 or greater. Even the most distant sites in northeast Texas have correlations of at least 0.25.

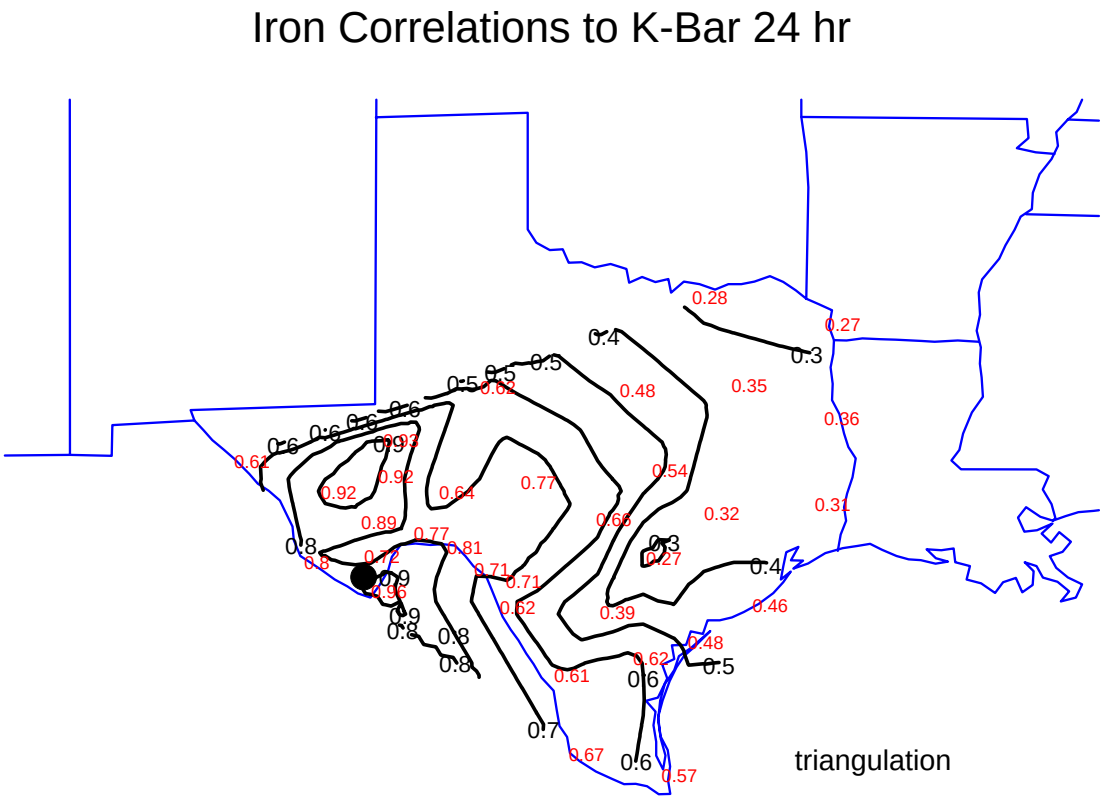

Figure 8-14. Correlations of iron measured at Big Bend to iron measured at other BRAVO sites.

High Al/Ca ratios have been associated with Saharan dust, which is known to be lower in Ca than North American soils [*Perry et al.*, 1997; *Gebhart et al.*, 2001]. During BRAVO, Al/Ca ratios were never greater than 1 at Big Bend after August 22, but were often between 2 and 3 during the early half of the study, with values greater than 3 on July 8, and August 3, 4, and 18. Figure 8-15, shows aluminum vs. calcium for all sites. Summer values are shown in red and fall values in black. This graph shows a clear separation between the seasons with calcium-poor fine soil concentrations being common throughout Texas during the summer, but not during the fall. Calcium concentrations at Big Bend are relatively constant throughout the study, indicating the local soil concentration of this element is relatively constant. During the Saharan dust episodes of the summer, Ca does not increase, but the other soil elements do. The correlations between iron and other elements associated with soil, Si, K, Al, Ti, and Sr, are all 0.9 or higher for Big Bend alone. For all BRAVO sites combined, the same is true except the correlation between Fe and Ti is slightly lower at 0.83. The Fe to Ca correlation is 0.68 at Big Bend and 0.57 for all BRAVO sites combined. Therefore scatter plots of almost any soil element against calcium would be similar in pattern to that shown in Figure 8-15. Aluminum is shown for consistency

with earlier literature, but Fe or Si would have fewer values below detectable limits.

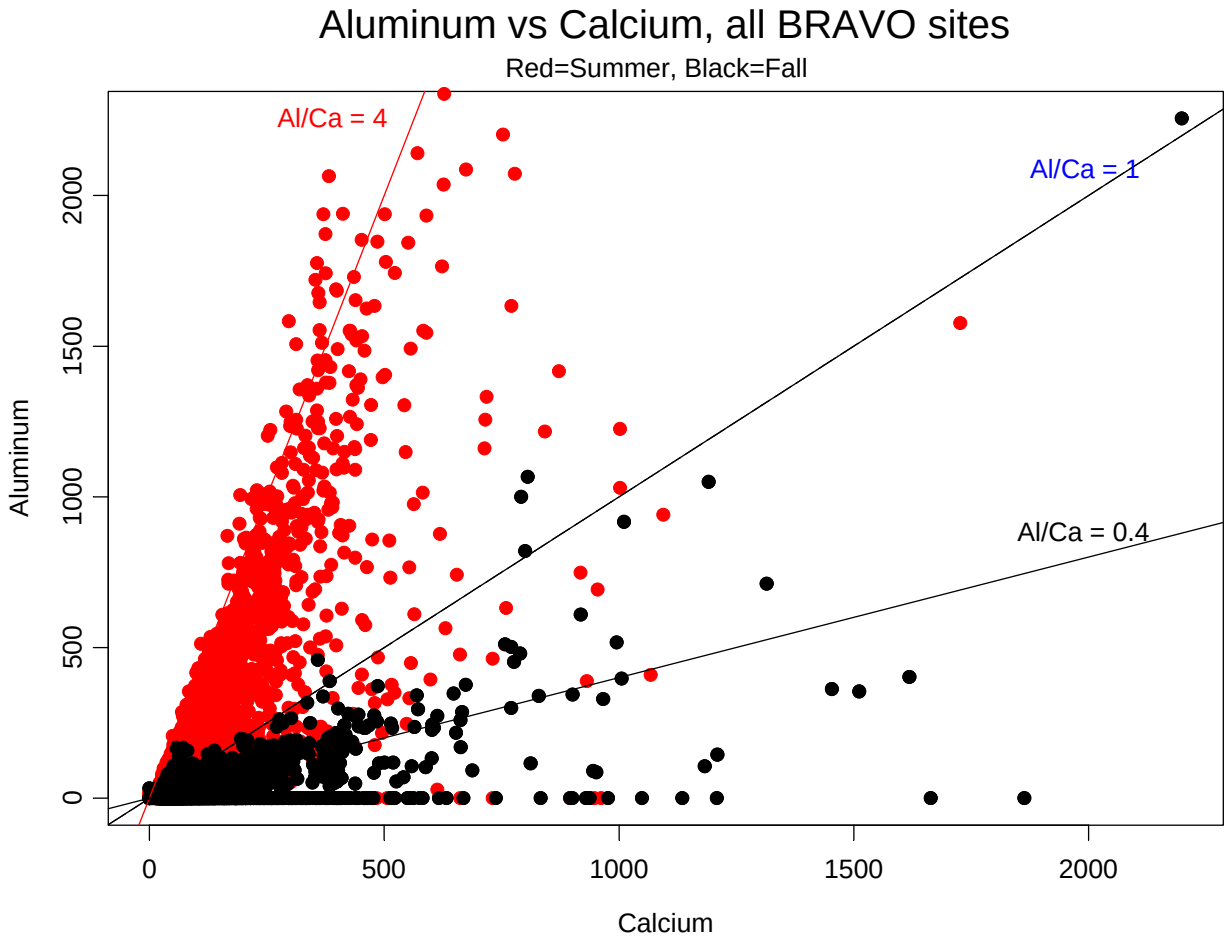

Figure 8-15. Aluminum vs. calcium (ng/m^3). Several lines have been added for reference.

Mean concentrations of iron during September and October 1996 were different enough from means during 1999 that it was not reasonable to plot them on the same map as was done for sulfur. All sites except Presidio/Ojinaga had 15–40% higher mean iron concentrations during fall 1999 than fall 1996.

8.1.1.5 Selenium

Selenium is of interest due to its association with coal-burning sources such as electric generating stations [*Olmez et al.*, 1988; *Malm and Gebhart*, 1997; *Gebhart and Malm*, 1997] and because it is more highly correlated with sulfur at Big Bend than are any other trace elements (0.79 during BRAVO, 0.73 during the 1996 Scoping Study—see section 1.2). During the 1996 Scoping Study, selenium was found to be indicative of airmasses originating in the United States as opposed to Mexico [*Gebhart et al.*, 2000]. Figure 8-16 shows the time lines of selenium and several other trace elements at Big Bend during BRAVO. The highest selenium concentration (0.83 ng/m^3) at Big Bend was measured on October 12 during one of the four highest sulfur episodes. Selenium was also moderately high (0.63 and 0.61 ng/m^3) on September 15 and August 21 during two other high sulfur concentrations, but much lower (0.38 ng/m^3) on

September 1 when the maximum sulfur was measured. This may indicate that the sulfur episodes of October 12, September 15, and August 21 were more heavily influenced by coal-burning sources than was September 1. Back trajectories support this hypothesis. Airmasses arriving at Big Bend on September 1 generally bypassed the lignite belt coal-fired plants in northeast Texas, while airmasses arriving during the remaining three episodes are more likely to have passed over that region. (See Appendices 4b, c, and d for daily trajectory plots.)

Figure 8-17 shows the mean selenium concentrations during BRAVO. The highest mean (1.03 ng/m^3) was at Purtis Creek in northeast Texas with lower concentrations at sites in all directions. This indicates sources of selenium within Texas. In general the mean selenium concentrations are higher in the eastern part of the state than in the western. There are also local maxima at Eagle Pass and Everton Ranch with the Eagle Pass value indicating that the Carbón I/II plants are also noticeable sources of selenium.

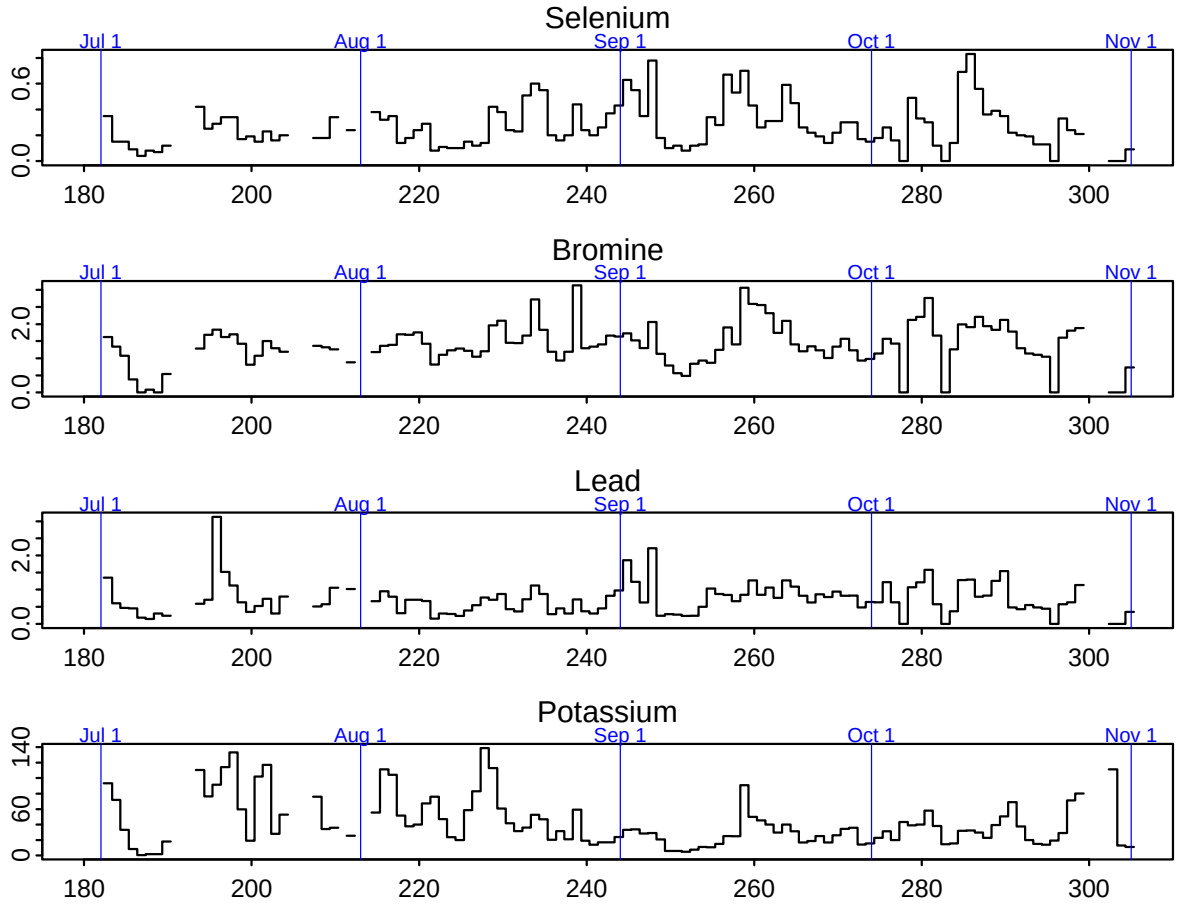

Figure 8-16. Time lines of several trace elements (ng/m^3) measured at Big Bend National Park during BRAVO. Labels on the x-axis are the day of the year. The vertical blue lines show the beginning of each month.

The spatial patterns for the four highest sulfur episodes at Big Bend are shown in Figures 8-18 through 8-21. On August 21 and September 1 there are selenium concentrations greater than 1.9 ng/m^3 in northeast Texas with generally lower concentrations all around. On October

12 the highest measured value is 1.54 ng/m^3 at Hagerman, west of and lower than the peak concentrations on August 21 and September 1. On September 15, Se concentrations are generally lower across the state, but still with the highest concentration, 1.22 ng/m^3, in northeast Texas.

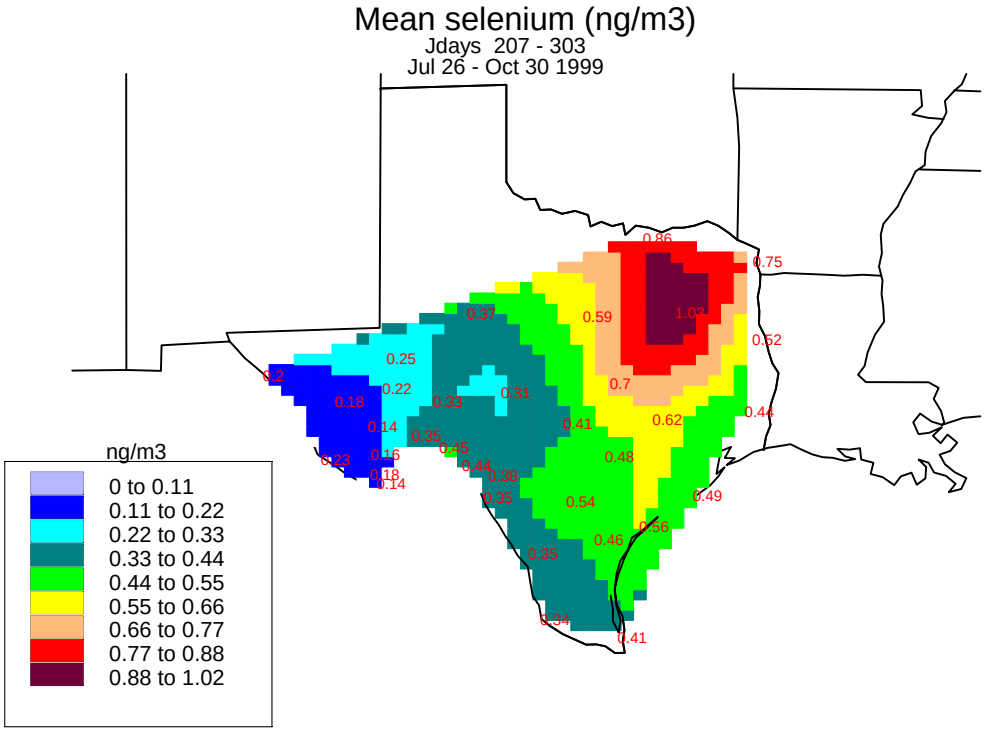

Figure 8-17. Mean selenium concentrations.

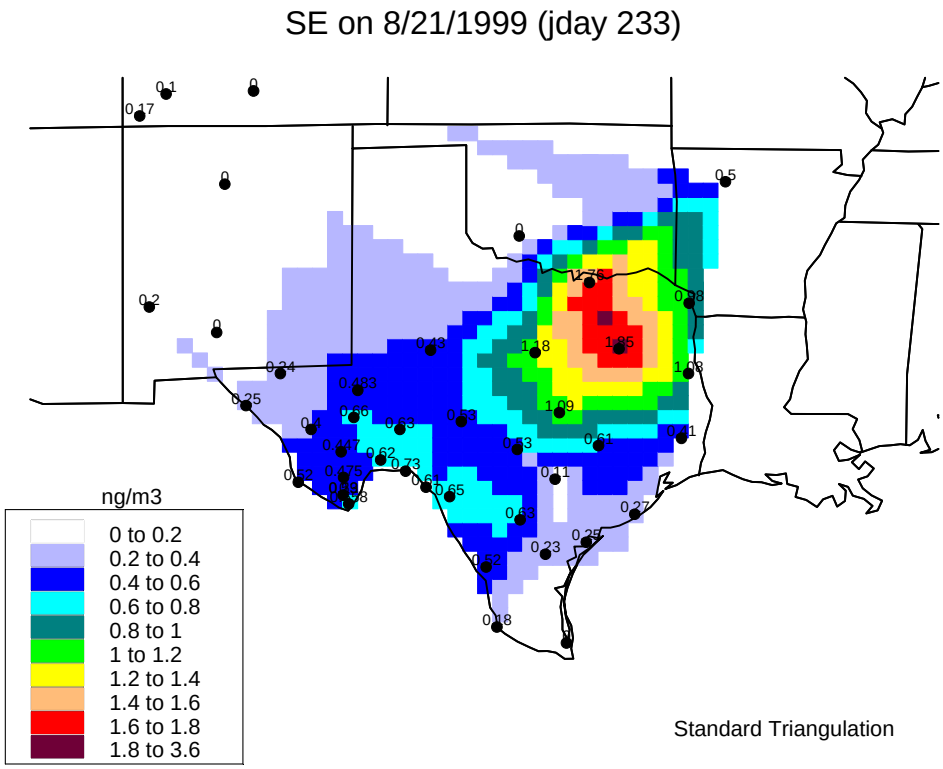

Figure 8-18. Selenium concentrations on August 21.

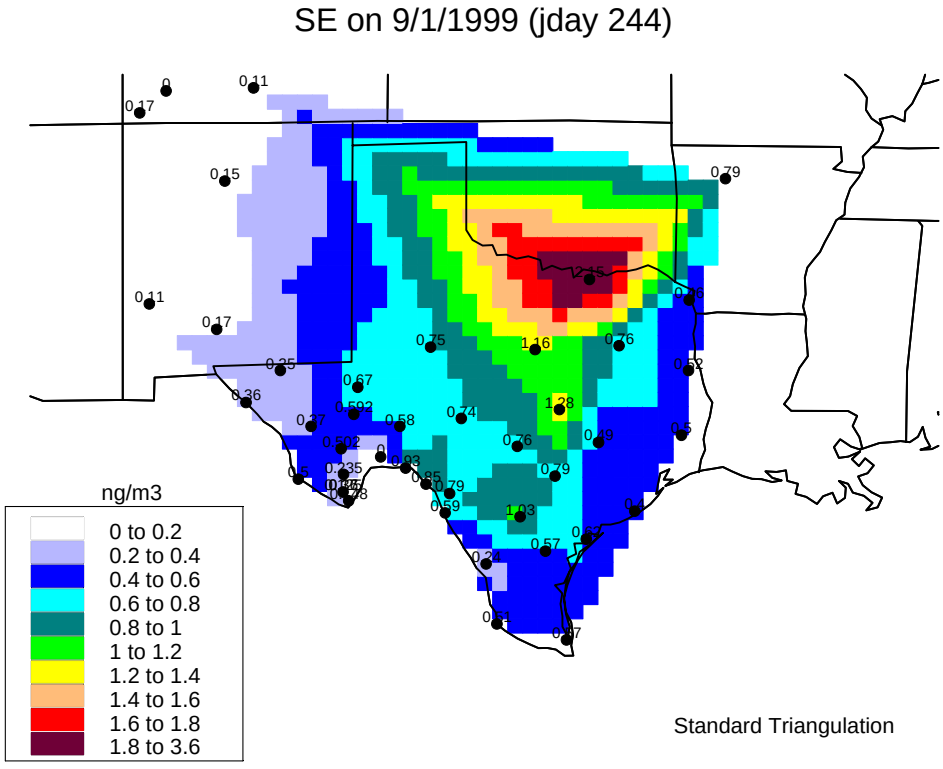

Figure 8-19. Selenium concentrations on September 1.

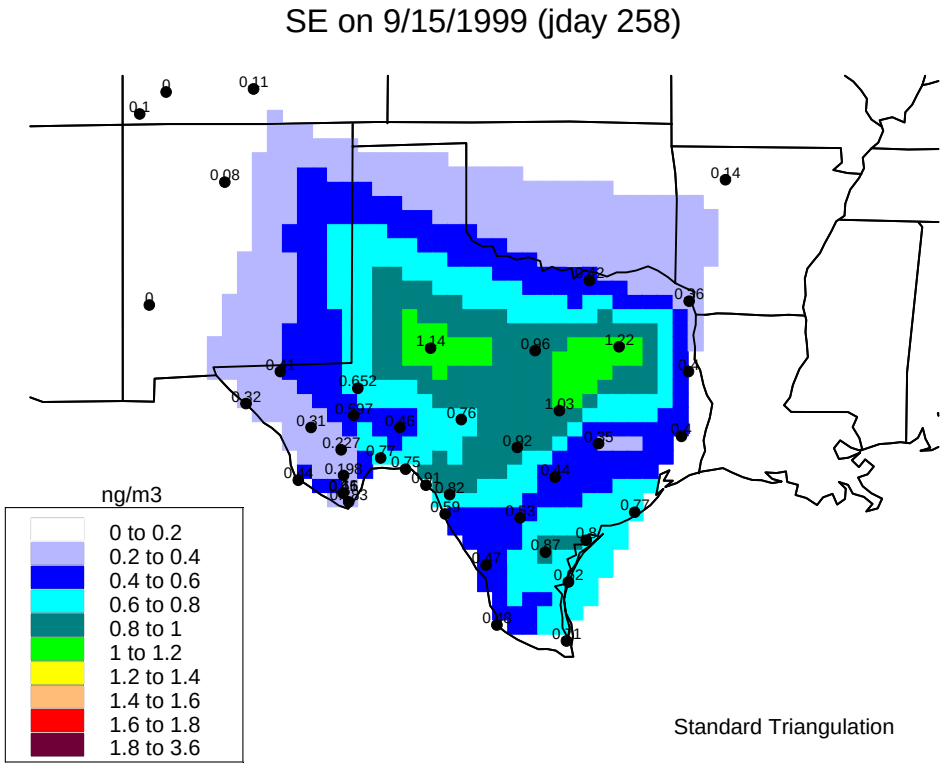

Figure 8-20. Selenium concentrations on September 15.

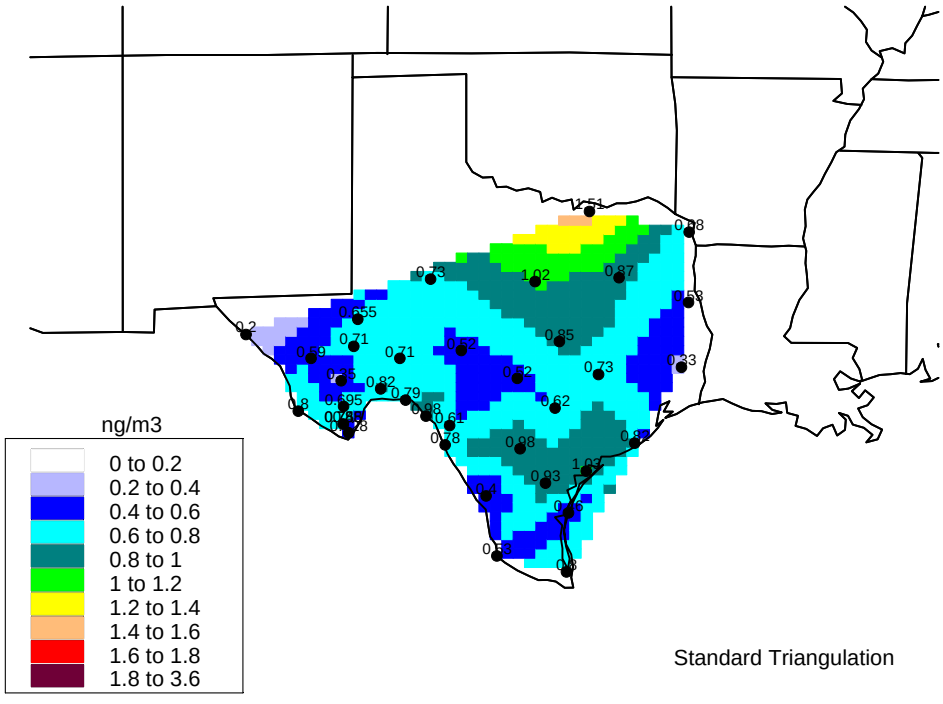

Figure 8-21. Selenium concentrations on October 12.

Correlations of selenium measured at Big Bend to selenium measured at other BRAVO sites, shown in Figure 8-22, are much lower than the corresponding correlations for sulfur, showing that selenium is less spatially homogeneous than sulfur. Correlations greater than 0.5 are generally seen only at sites within about 200 km and selenium measured at sites in northeast Texas are negatively correlated with selenium measured at Big Bend. Because selenium is a primary species, while sulfate is secondary, the spatial patterns in selenium are more indicative of sources of selenium than the spatial patterns in sulfate are of locations of SO_2 sources. Spatial patterns in sulfates are complicated by the locations of clouds, oxidants, and other factors that influence the locations of chemical processes.

EOFs (not shown) and correlation maps similar to Figure 8-22 for other sites also indicate the selenium measured across Texas is generally not highly correlated across the state. Monthly box plots of selenium for four different sections of Texas, shown in Figure 8-23, also illustrate the spatial differences in selenium. Northeast Texas (upper right), as seen in the spatial maps, has the highest concentrations and generally there are high values during all three months, with the greatest median in August and a maximum in October. In southeast Texas (lower right) selenium concentrations are much larger during October than during other months, indicating concentrations influenced by the differing transport patterns across the months. Selenium concentrations measured around Eagle Pass (upper left) and Big Bend (lower left) are much lower than in eastern Texas and without much monthly variation, though values in the Eagle Pass area, like values in southeast Texas, are highest during October.

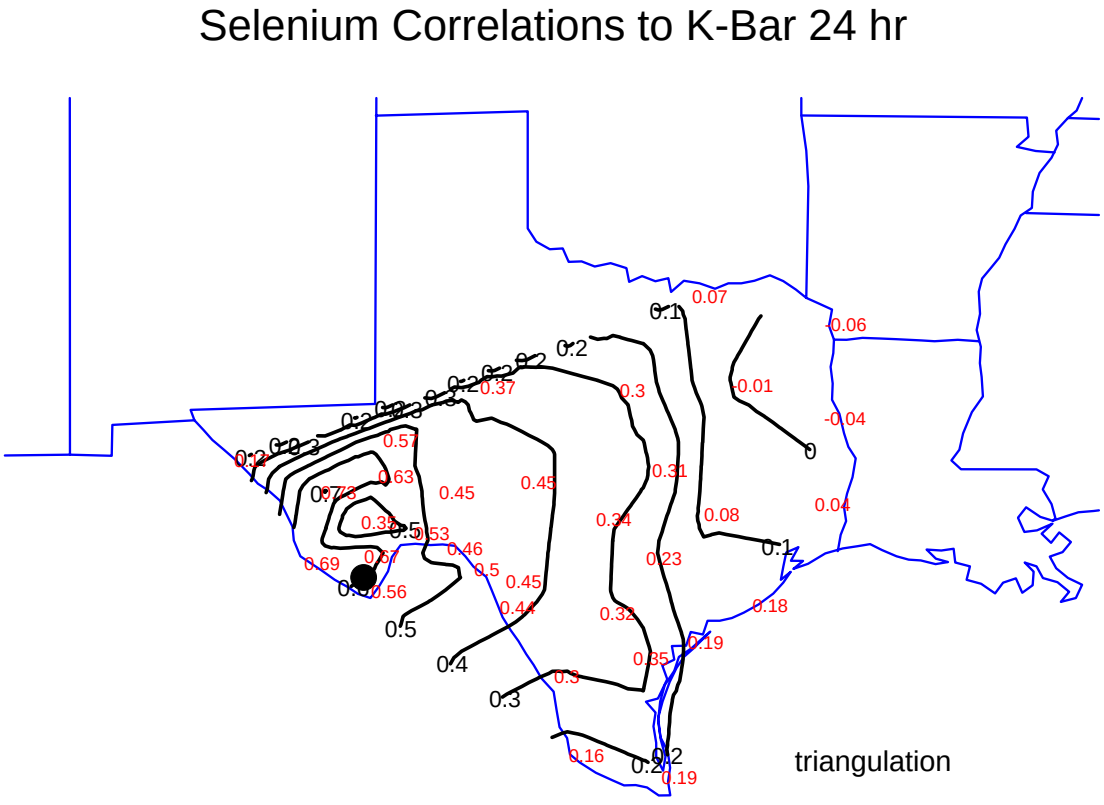

Figure 8-22. Correlations of selenium at Big Bend to selenium at other sites.

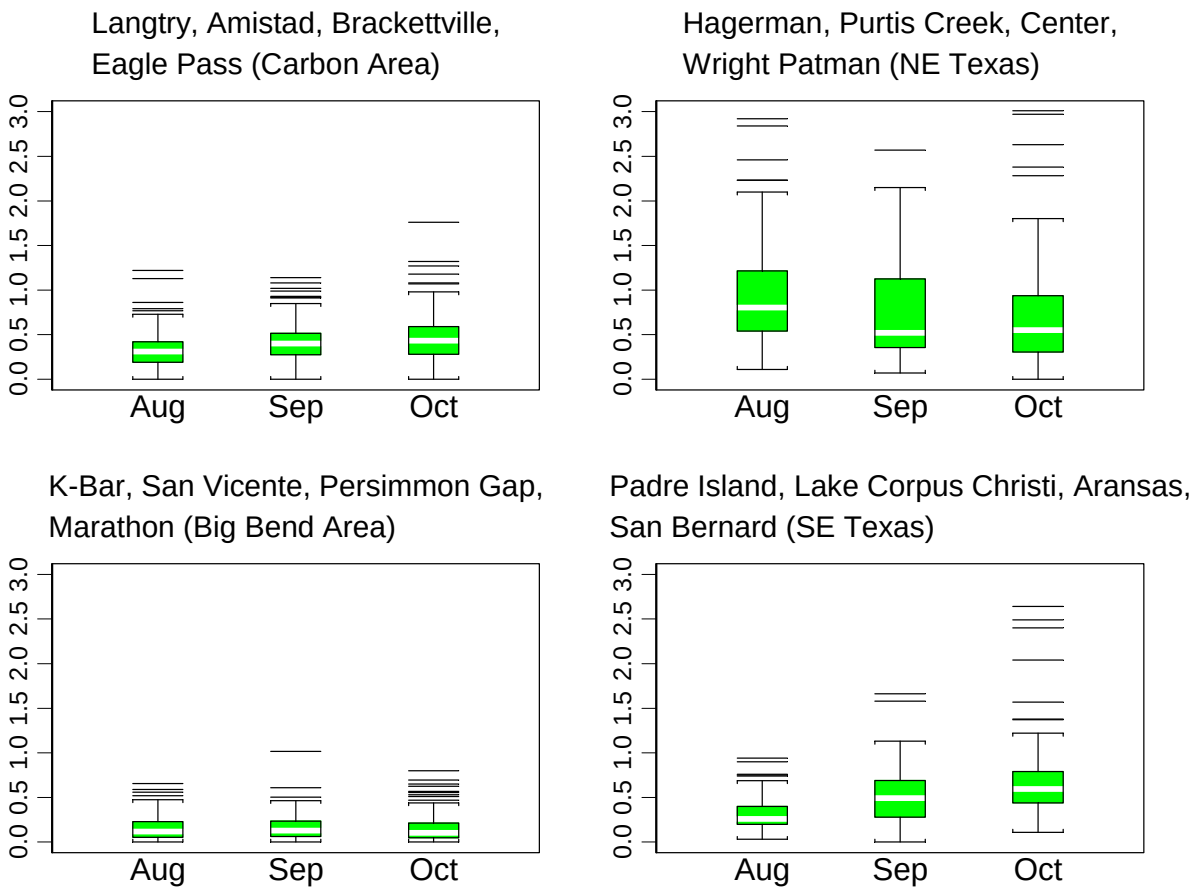

Figure 8-23. Monthly box plots of selenium (ng/m^3) for four different sections of the monitoring domain.

8.1.1.6 Vanadium & Other Tracers of Mexico

Vanadium concentrations, as well as lead, zinc, nickel, and manganese, were much higher at sites in Mexico than in Texas during the 1996 pilot study [*Gebhart et al.*, 2000]. Figure 8-24 shows the time lines of all of these species except lead at Big Bend during BRAVO. Lead was shown previously in Figure 8-16.

There is an unusual trace element day, October 29, near the end of the study when back trajectories indicate transport from northeast Mexico early in the day, with a wind shift due to a frontal passage and trajectories from the west, including both northern Mexico and southern Arizona and New Mexico, later in the day. October 29 had the highest coarse mass concentration measured at Big Bend during BRAVO, probably due to local blowing dust associated with high wind speeds. There were also high concentrations of fine K, V, Mn, and Br; only moderate concentrations of fine S, OC, EC, and Fe; and very low Se and Ni. The high V and Mn are consistent with transport from Mexico, though the high correlations of Mn with other soil elements indicate that Mn is usually mostly due to dust. Organic carbon, Br, and K can be indicators of smoke. But while non-soil K measured on October 29 at Big Bend was 30 ng/m^3, the 6th highest value at this site during BRAVO, the OC/EC ratio, another indicator of smoke, was only at about the 60th percentile for this site at 6.5. The carbon fractions O3 and O4 were higher than usual, but all other carbon fractions had moderate or lower concentrations on

this day. The mixed smoke indicators may be because there was smoke present, but perhaps only during either the early or the later half of the day and the mid-day wind shift makes the 24-hour concentrations difficult to interpret.

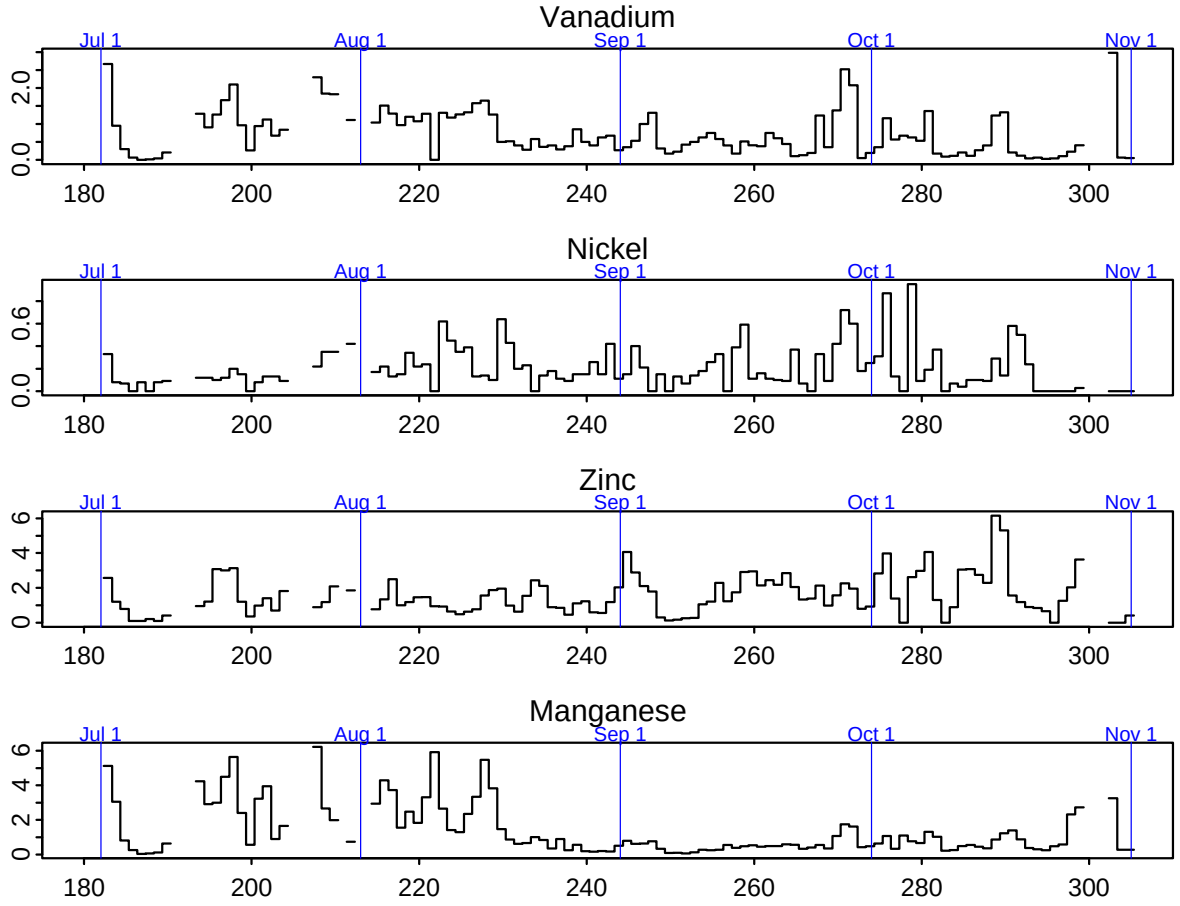

Figure 8-24. Time lines of several trace elements (ng/m^3) at Big Bend. Labels on the x-axis are the day of the year. The vertical blue lines show the beginning of each month.

Though there were no monitoring sites in Mexico during BRAVO, the concentrations of vanadium during BRAVO were mostly below minimum detectable limits except at sites near the Mexican border. Like iron, the highest concentrations of vanadium also occurred mostly during the summer rather than fall. Figure 8-25 illustrates mean vanadium during BRAVO showing the general south to north gradient and also generally higher values along the Texas Gulf Coast than inland in Texas. The combination of the spatial pattern of highest concentrations along the Mexican border, along with the temporal pattern of higher values during summer than fall, both indicate that vanadium is more likely to arrive at Big Bend from Mexico than from the United States. Because vanadium was so often below detectable limits, little further analysis is possible.

Nickel and vanadium, though both previously associated with transport from Mexico and both associated with residual oil combustion, are not highly correlated at Big Bend. Nickel was highest at Big Bend during August to early October in contrast to vanadium which was highest during July. The back trajectory patterns for high vanadium and high nickel concentrations are somewhat similar in that both are associated with transport from Mexico, but high nickel days

have more northerly transport across the Gulf and along the U.S. Gulf Coast, while high vanadium days do not. Airmasses associated with high vanadium arrive from farther south in Mexico. Non-correlation between nickel and vanadium has also been observed in the northeastern U.S. and may be explained by high variability of the ratios of these elements in different crude oil stocks. [*Poirot*, 2004]

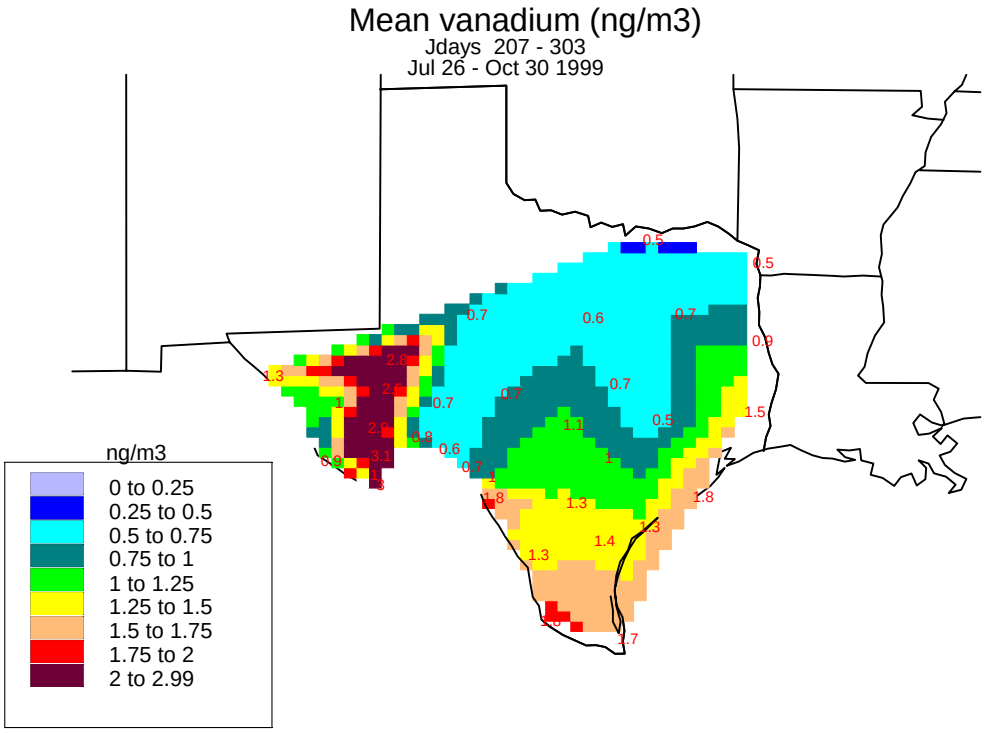

Figure 8-25. Mean vanadium.

8.1.1.7 Sodium

During the 1996 Scoping Study, sodium was of interest as a trace element due to its high correlation with sulfur at Big Bend (0.661). However, during BRAVO sodium (shown in Figure 8-26) had almost no correlation with sulfur (0.039), though relatively high sodium (244 ng/m^3) was measured at Big Bend on September 1 which was the day of the maximum sulfur concentration there. The highest sodium concentrations at Big Bend during BRAVO were very early in the study, June 29–July 2 and July 16, when the concentrations were 318–392 ng/m^3. Examination of the sodium concentrations at Big Bend measured in the IMPROVE network for 1988–2002 also shows that the highest concentrations generally occur during the summer, especially May through July, while the lowest concentrations are during the winter.

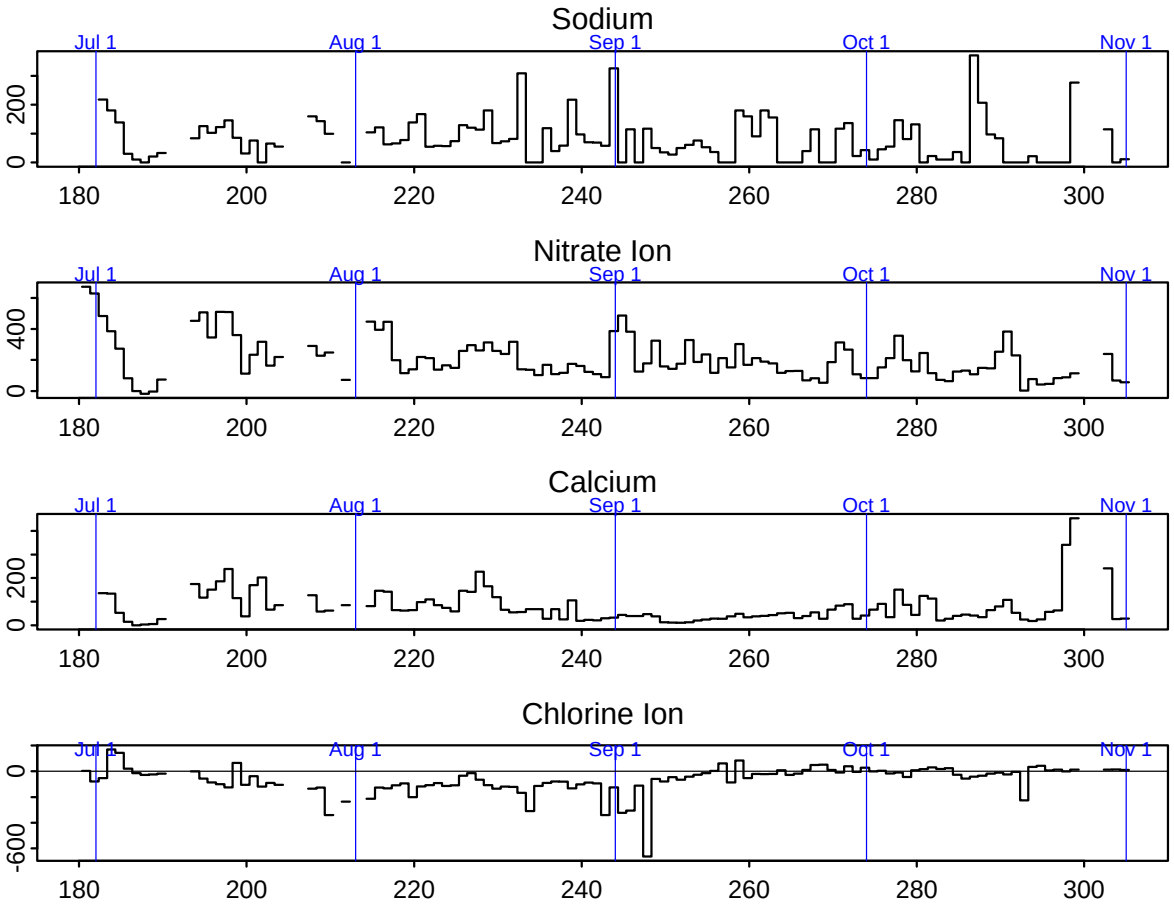

Figure 8-26. Time lines of Na, NO^-_3, Ca, and Cl^- (ng/m^3) at Big Bend. Labels on the x-axis are the day of the year. The vertical blue lines show the beginning of each month.

Spatially, the highest mean sodium concentrations during BRAVO were at sites long the Gulf Coast (Figure 8-27), suggesting transport across the Gulf of Mexico and indicating sea-salt as a source, though an additional sodium source south of the BRAVO area, as hypothesized during the pilot study, cannot be ruled out by the spatial patterns alone. *Collett et al.* [2001] found that during BRAVO the sum of sodium and calcium was highly correlated with coarse particle nitrate measured at Big Bend, suggesting that soil and sea salt particles provide a surface for condensation of nitric acid.

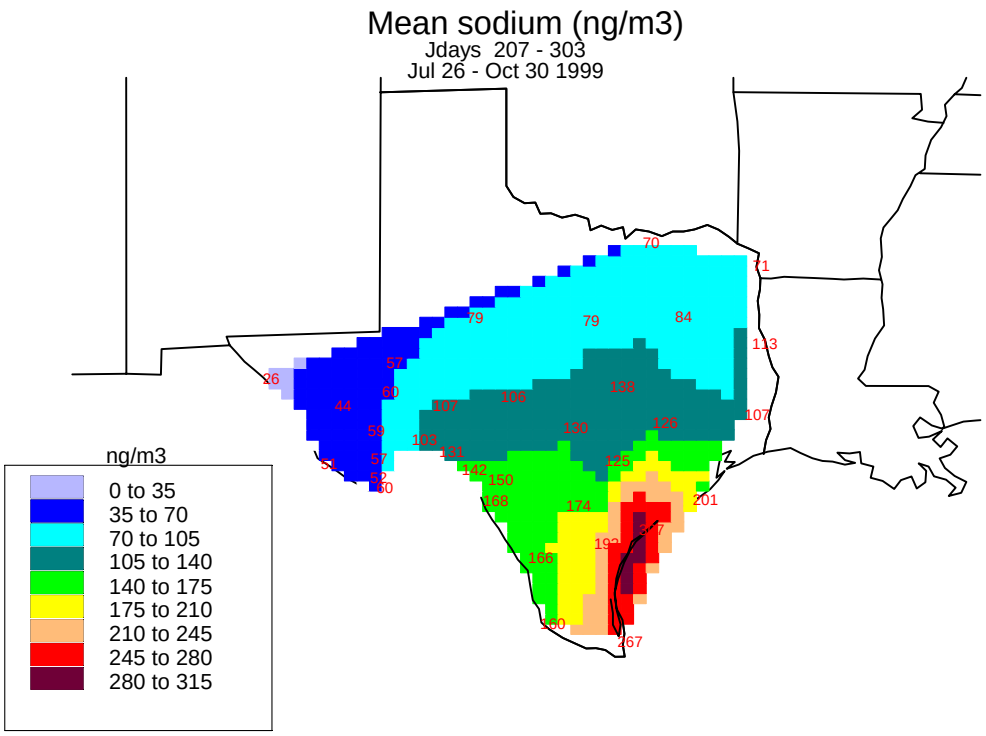

Figure 8-27. Mean sodium concentrations.

For the seven sites which had measurements during both the 1996 and 1999 studies, the 1999 concentrations during September and October were all 50–80% lower than in 1996 as shown in Table 8-1. Also, the number of concentrations below the minimum detection limit (MDL) was much higher during BRAVO than during the scoping study. In 1996 only 2% of the non-missing sodium was below MDL, while in BRAVO it was 46%.

The IMPROVE sodium data, collected at Big Bend since 1988 (Figure 8-28), does not show a long term decline, but does indicate that sodium concentrations measured during 1996 were unusually high.

The reasons for the highly different concentrations in 1996 and 1999 aren't known but there are at least three possibilities. 1) Transport patterns influencing sodium concentrations at Big Bend during the two studies may have been different, and in particular, transport of airmasses across the Gulf of Mexico to Texas may have been less frequent during 1999 than during 1996. Since sodium tends to be highest during the summer, it's possible that summer-like meteorology persisted longer than usual into the fall during 1996; 2) Sodium emissions or the sodium to sulfur ratios in emissions in one or more important source regions are variable and for some reason were higher than usual during 1996; or 3) Some important aspect of the measurement and/or analysis techniques for sodium may have been different during the two study periods. PIXE was used to analyze the filters for sodium in 1996. PIXE was also used at all sites while both PIXE and XRF were used at Big Bend during BRAVO. Either the first or third scenarios seem more likely than the second.

Table 8-1. Mean sodium concentrations (ng/m3) during the 1996 Scoping Study and during September and October of 1999 during BRAVO. Values in parentheses are the means with the zeros (below MDL) removed.

Site	Mean Na September & October 1996	Mean Na September & October 1999	Change (1999–1996)	% Change (Change/1996)
Big Bend	118	42 (77)	-76	-64%
Amistad	207	100 (153)	-107	-52%
Ft. Lancaster	163	95 (142)	-68	-58%
Lake Corpus Christi	318	164 (182)	-154	-48%
Everton Ranch	184	79 (119)	-105	-57%
Ojinaga/Presidio	212	44 (89)	-168	-79%
Guadalupe Mts.	100	25 (65)	-75	-75%

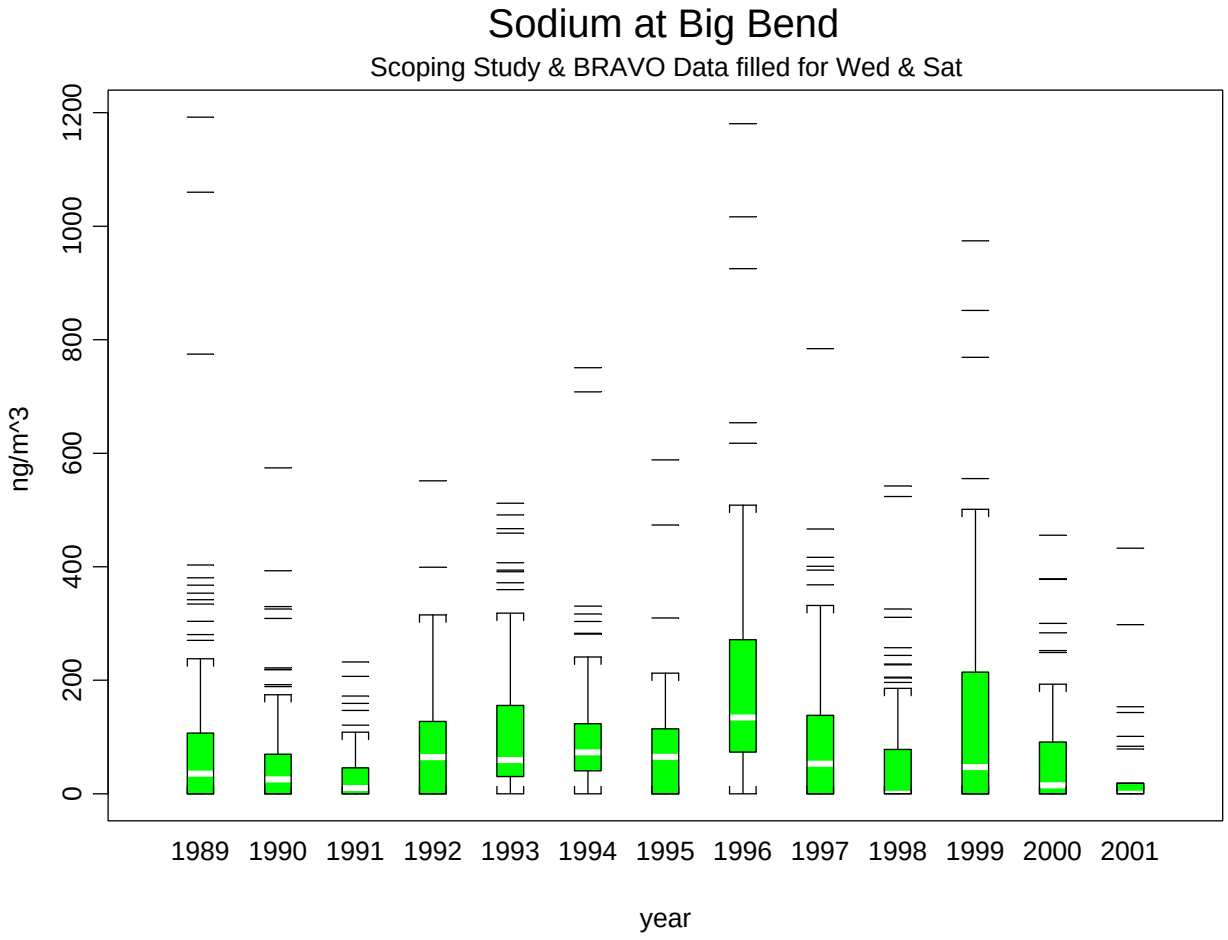

Figure 8-28. Box plots of sodium concentrations at Big Bend by year from the IMPROVE network.

8.1.1.8 Bromine

After selenium, the trace element next most highly correlated with sulfur at Big Bend during BRAVO was bromine. Correlations between sulfur and bromine were 0.57 during

BRAVO and 0.34 during the 1996 Scoping Study. The sulfur episodes on September 15 and August 21 were associated with high bromine, though the sulfur episodes of September 1 and October 12 were not. Spatial patterns of mean bromine (Figure 8-29) show highest bromine concentrations at sites along the Gulf Coast. The site with the highest mean concentration of bromine (3.13 ng/m^3) was at San Bernard, just south of Houston, the lowest (1.375 ng/m^3) at McDonald Observatory, and second lowest (1.41 ng/m^3) at Big Bend. Sites north and west, though farther from the Gulf, had higher bromine concentrations than Big Bend. A similar spatial pattern was seen in 1996. For most of the sites common to both studies, the mean fall bromine concentrations were similar. A combined 1996 and 1999 spatial pattern for September and October is shown in Figure 8-30.

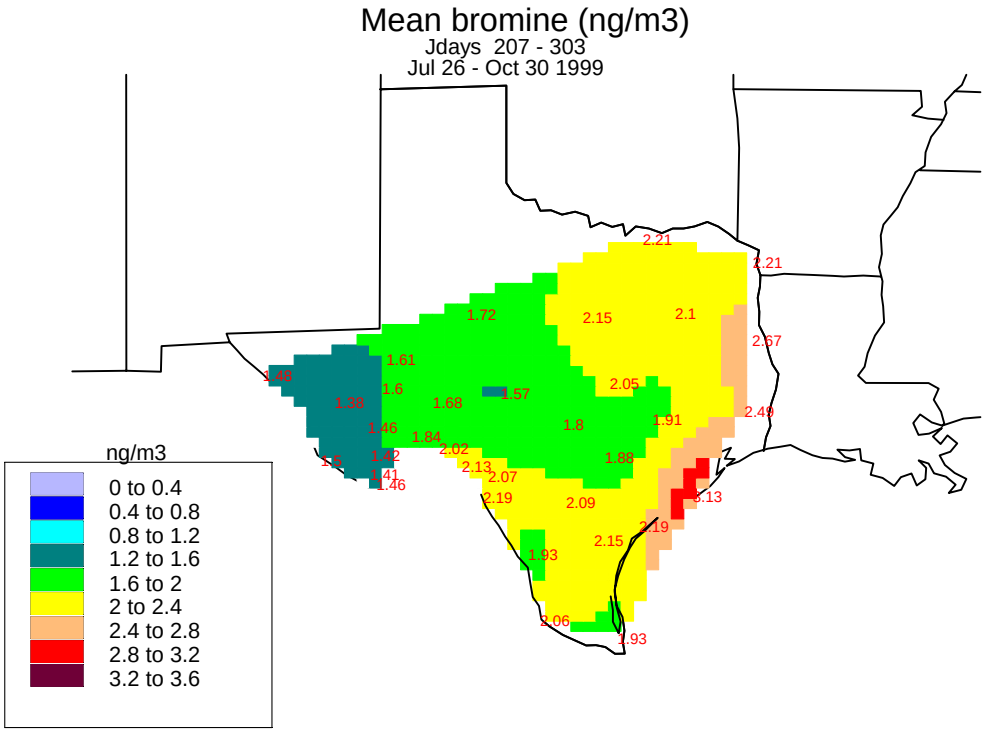

Figure 8-29. Mean bromine concentrations.

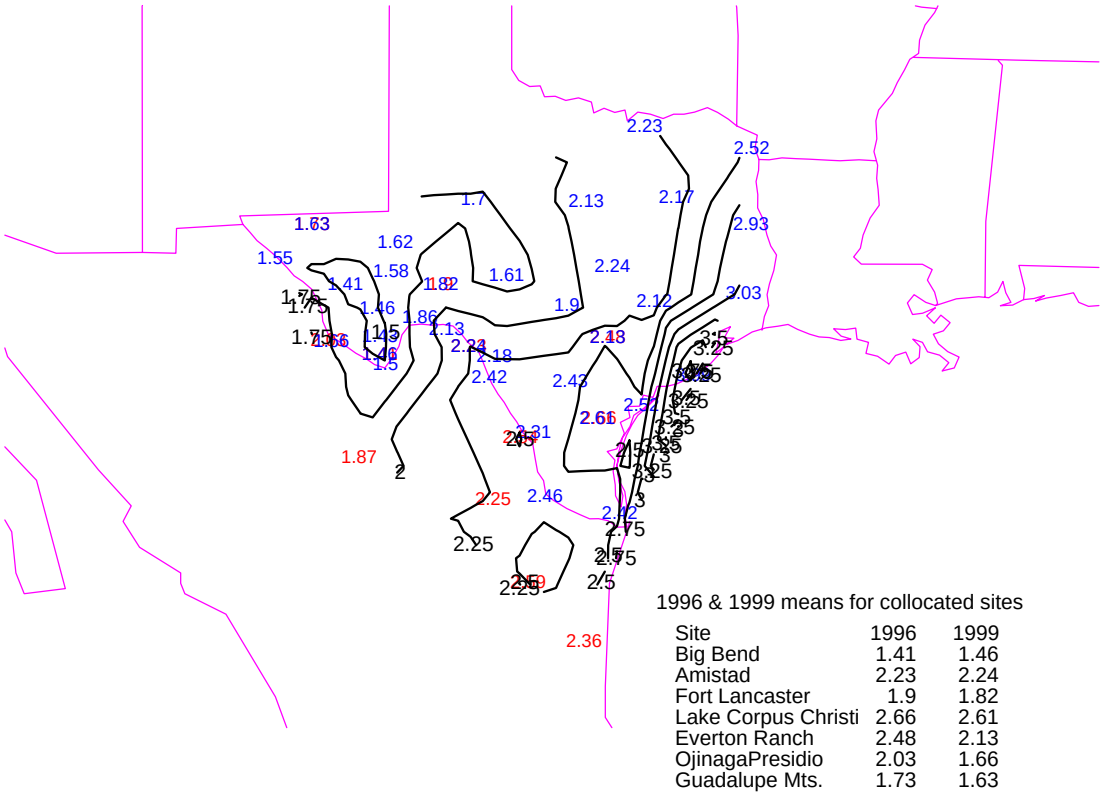

Figure 8-30. Combined 1996 and 1999 spatial pattern for Bromine.

8.1.1.9 Lead

Lead concentrations were much higher in Mexico than in Texas during the 1996 study [*Gebhart et al.*, 2000]. Previous analysis of lead concentrations collected at Big Bend since 1988 [*Gebhart et al.*, 2001] show that lead at Big Bend is highest during October–December and lowest during the summer. Also, back trajectory analysis of both the historical data and the 1996 Scoping Study data showed that lead concentrations were higher when airmasses were transported to the park from Mexico than when they were from the U.S. except during July and August when the reverse was true.

Mean lead concentrations during BRAVO, shown in Figure 8-31, show two local maximums, one in northeast Texas and another on the Texas-Mexico border at Eagle Pass.

Lead concentrations measured at Big Bend are negatively correlated with lead measured in the northeast half of the study area and no sites had correlations greater than 0.5 with the measurements at Big Bend indicating little spatial homogeneity across Texas and also indicating different sources of lead at Big Bend than in northeast Texas.

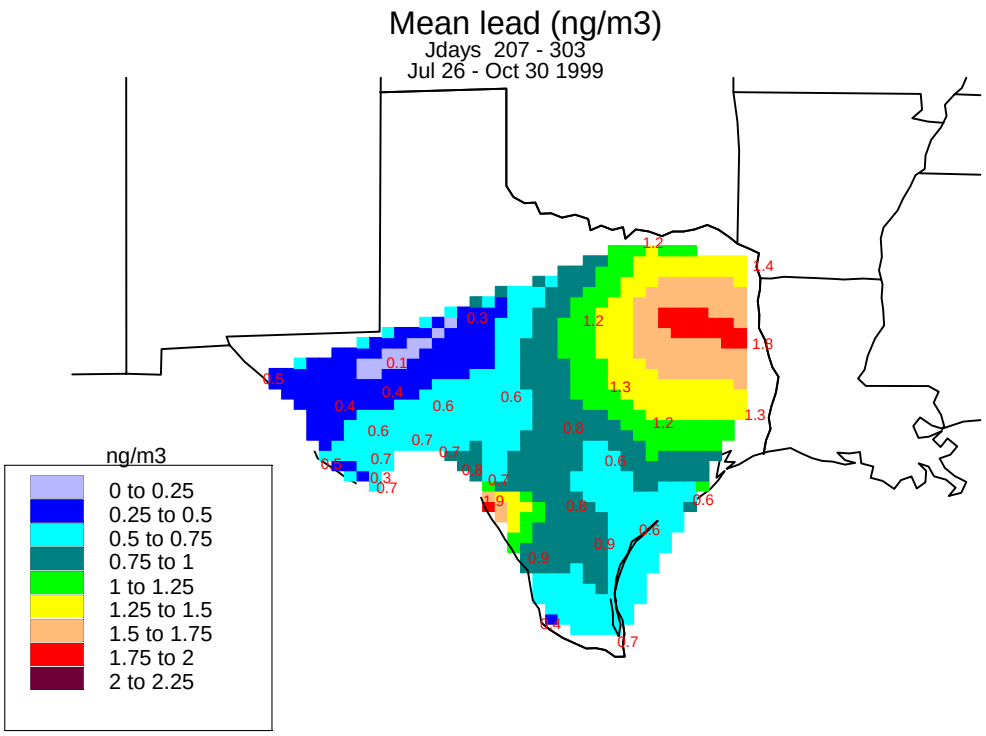

Figure 8-31. Mean lead concentrations.

Lead concentrations at Big Bend as measured in the IMPROVE network have dropped dramatically since measurements were begun in 1988 (see Figure 8-32). During 1988–1991 annual mean concentrations ranged from 2–3 ng/m^3, with maximums of 9–11 ng/m^3, while since 1997 mean concentrations have been 0.6–1.1 ng/m^3, with maximums of 3–7 ng/m^3. Comparing data from the BRAVO study to data from sites collocated in the 1996 study shows that the decline in lead occurred throughout the southern half of Texas. In 1999 the mean lead concentrations at the 7 collocated sites were 60–75% lower than at the same sites in 1996.

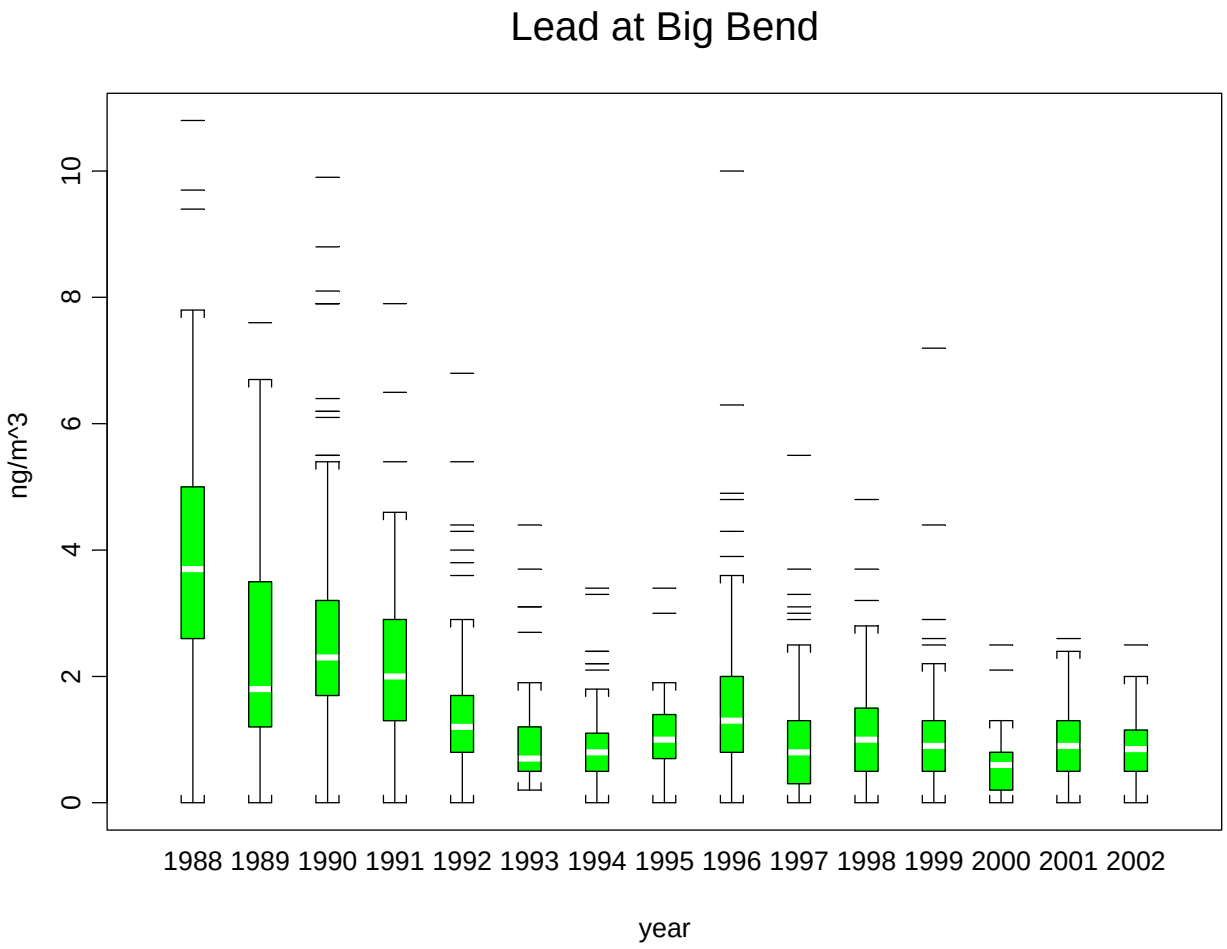

Figure 8-32. Box plots of lead at Big Bend by year.

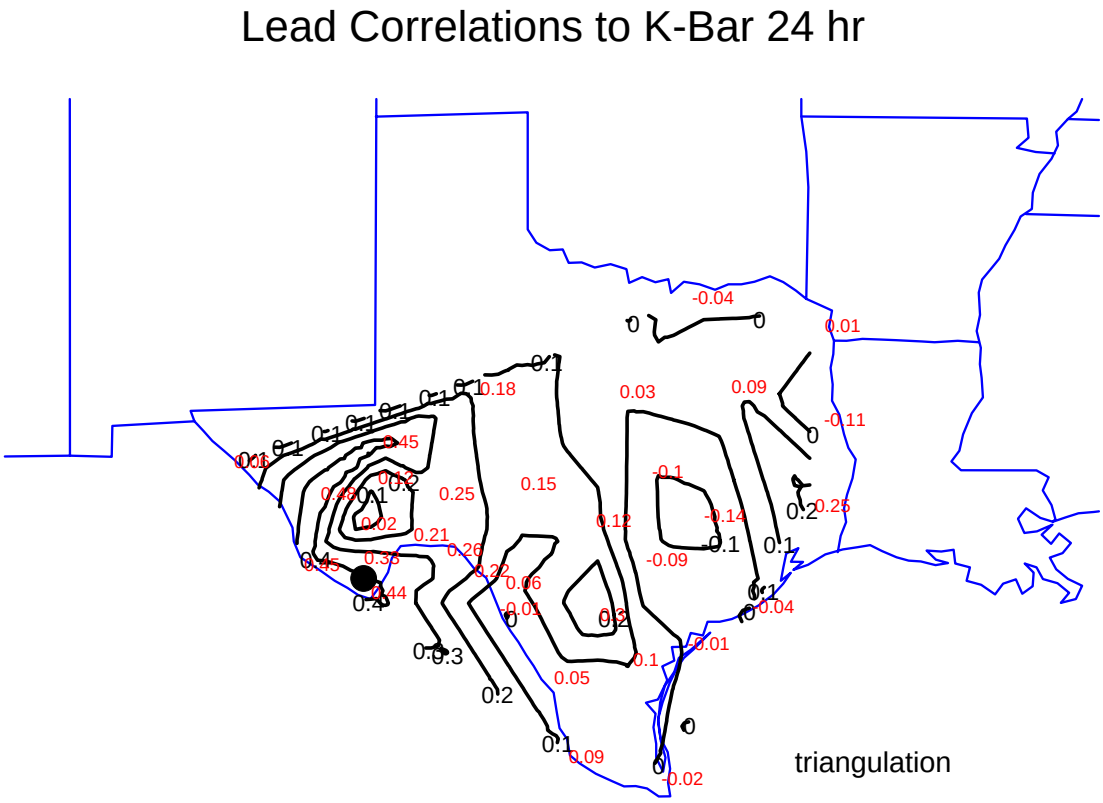

Figure 8-33. Correlations of lead at Big Bend to lead at other BRAVO sites.

8.1.1.10 Discussion of Spatial and Temporal Patterns

Examination of the spatial and temporal patterns in several fine particulate species measured during BRAVO suggests that there are unique sources for different aerosol types and that transport patterns are seasonal with more transport from Mexico to southern Texas during the summer than during the fall. Sulfur is of interest due to its large contribution to fine mass and light scattering at Big Bend National Park. Sulfur concentrations at Big Bend were highest during four episodes. September 1 and 2 had the highest sulfur and highest organic and elemental carbon concentrations, respectively, measured at Big Bend as well as moderately high zinc. The second highest sulfur on September 15 also had high sodium, the highest non-soil potassium, and moderately high selenium, bromine, arsenic, and zinc. October 12 was characterized by high sulfur, selenium, and arsenic. August 22 had moderately high sulfur and selenium. Sulfur concentrations measured within a few hundred km are generally highly correlated, but measurements in southwestern Texas were not highly correlated with measurements in northeast Texas and different regions of the state showing different seasonal patterns in sulfur concentrations. Highest sulfur concentrations measured during BRAVO were in northeast Texas during the summer while highest concentrations at Big Bend were during the fall. Spatial patterns in sulfur concentrations show influence from the Carbón I & II power plants on sulfur concentrations especially north and west of the plants, though the contribution is not quantifiable by these analyses.

Spatial and temporal patterns in the iron concentrations and the abrupt drop in Al/Ca ratios from summer to fall are evidence of Saharan dust episodes during the summer.

The trace element most associated with sulfur at Big Bend is selenium which is usually associated with coal combustion. Selenium concentrations were highest in northeast Texas with evidence of selenium sources within the state, at the Carbón I & II plants, and possibly entering Texas from the east. Sodium was highly correlated with sulfur in the 1996 Scoping Study, but was much less related to sulfur during BRAVO and seems to be primarily related to transport of airmasses across the Gulf of Mexico, though the difference may be attributable to measurement differences between the two studies. Vanadium was often below detectable limits, but is most frequently measurable at the southernmost sites. This seems to confirm earlier analyses that found vanadium to be associated with transport from Mexico into Texas. Bromine was second only to selenium in correlation to sulfur at Big Bend and was highest at Gulf Coast sites. Lead concentrations in southern Texas have dropped dramatically since the 1996 study.

8.1.2 Factor Analysis

Fine particulate concentrations measured with the IMPROVE sampler at K-Bar were examined to determine which species varied together during BRAVO. These analyses are of interest as a qualitative way of understanding which fine particulate species may be associated with common source areas or source types. It can also give an idea of which species are likely to fall together as source types in more quantitative multivariate receptor modeling which determines source types by common variations between species. Such models include Chemical Mass Balance (CMB), UNMIX, and Positive Matrix Factorization (PMF).

Input data for this analysis is from the May 19, 2003, "high sensitivity" data set that was generated for K-Bar only by re-analyzing the filters from the 24-hour IMPROVE sampler using higher sensitivity XRF analysis. This significantly improved the minimum detection limits of many of the trace elements. Several species, including SO_2, Cd, Ag, Ba, Co, Mg, Au, Y, Zr, Rb, Hg, and P were not included in the factor analysis because there were too many values below detectable limits. All remaining species had very few values below or near the detection limit. Figure 8-34 is a compact representation of the correlation matrix for data measured at K-Bar. The species are labeled on the diagonal of the matrix with the names given by scientists at University of California-Davis who measured and analyzed these data. In most cases the labels are the standard elemental abbreviations from the periodic table of elements. In some cases a "P" has been appended in front of the standard abbreviation to indicate that the element was originally measured using PIXE. When these data were later re-analyzed by XRF, the label remained the same. Labels in the top right corner of the figure (O1, O2, O3, OP, E1, E2, E3) refer to the organic and elemental carbon fractions. Details of the measurement techniques are given in section 2.1.1.

The row and column containing the label give the correlations of that species with all others. The colors are based on a topographic color scheme with the highest values being the brown through white-like mountains and the lowest values being blue like sea level. The highest correlations (near 1) are between sulfur, sulfate, and ammonium and also between the various soil elements, Fe, Si, Ti, Al, etc. The lowest correlations are between Cl ion and E3, one of the elemental carbon fractions. This same correlation matrix is also shown in tabular form in Table 8-2.

Although the correlation matrix is informative, factor analysis is as a more systematic method of identifying groups of species which are correlated or anti-correlated with each other.

Input to this factor analysis was the correlation matrix of the centered and scaled high sensitivity data collected at K-Bar. Varimax rotation was used.

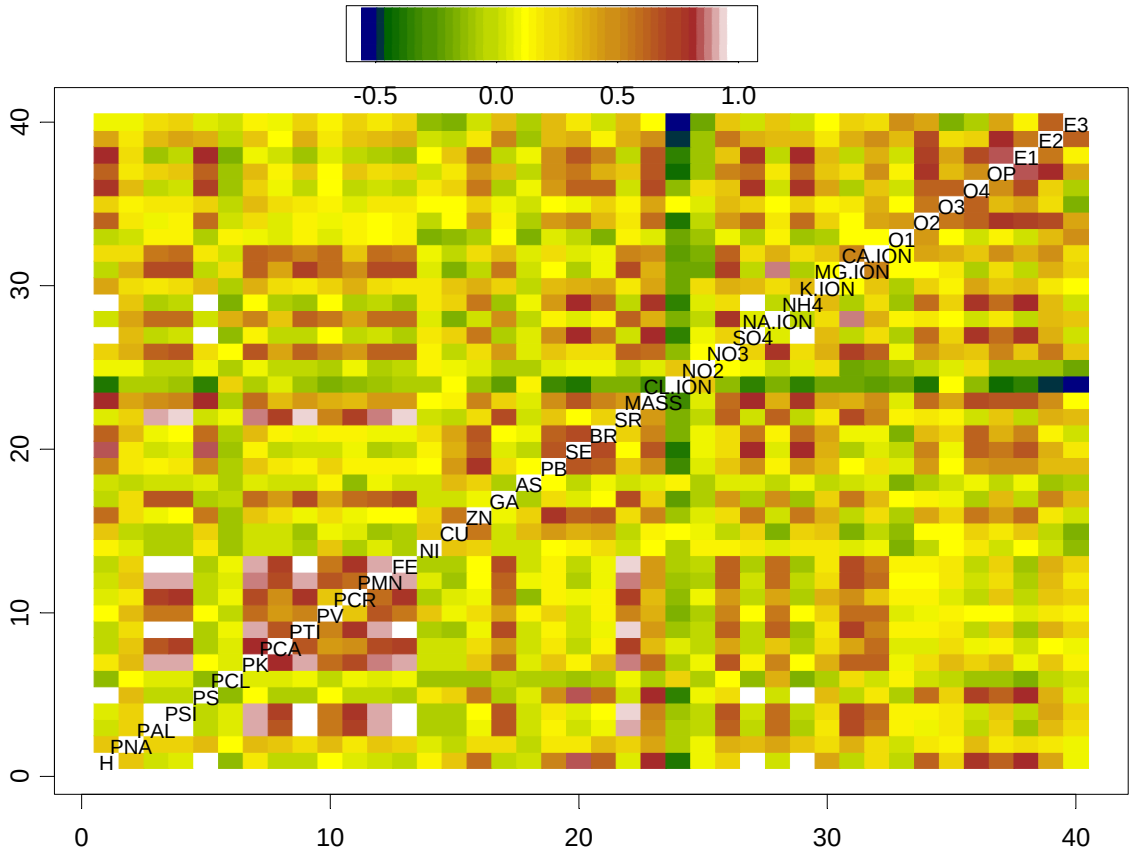

Figure 8-34. Correlations between fine particle species measured at K-Bar during BRAVO.

Figures 8-35 and 8-36 below show the variance and cumulative variance explained as increasing numbers of factors are added to the analysis. The number of factors to retain for rotation is somewhat subjective. There are several methods commonly used including the scree test [*Cattell,* 1966] which is to plot the variance explained by each factor, as in Figure 8-35 and then choose a number of factors where there is a large drop in the variance explained. Solutions with from 3 to 8 factors were all tried. The largest drop is with three factors; however, at least four factors seem to be required to get most of the physically meaningful divisions between the factors. There are four patterns that always emerge with four or more factors. These have arbitrarily been labeled "soil", "sulfur", "carbons with high EC", and "carbons with high O3 and O4." Another moderate drop in the scree plot is at eight factors. Also, as can be seen in Figure 8-36, eight factors explain between 80 and 90% of the total variance in the fine particle measurements. This was chosen as a reasonable number of factors to use.

Table 8-2. Correlations between fine particle species measured at K-Bar during BRAVO.

	H	Na	Al	Si	S	Cl	K	Ca	Ti	V	Cr	Mn	Fe	Ni	Cu	Zn	Ga	As	Pb	Se
H	1.00	0.30	0.00	0.04	0.98	-0.13	0.19	-0.01	-0.01	0.11	0.04	0.02	-0.02	0.17	0.29	0.58	-0.01	0.02	0.52	0.85
Na	0.30	1.00	0.26	0.28	0.32	0.13	0.33	0.29	0.25	0.35	0.21	0.29	0.25	0.04	-0.01	0.22	0.22	-0.03	0.17	0.20
Al	0.00	0.26	1.00	0.99	-0.04	0.06	0.89	0.67	0.98	0.54	0.75	0.89	0.98	-0.06	-0.07	0.10	0.66	0.02	0.15	0.00
Si	0.04	0.28	0.99	1.00	0.00	0.06	0.92	0.73	0.98	0.56	0.75	0.91	0.99	-0.05	-0.06	0.14	0.67	0.02	0.19	0.03
S	0.98	0.32	-0.04	0.00	1.00	-0.14	0.14	-0.06	-0.05	0.12	-0.01	-0.01	-0.07	0.20	0.27	0.56	-0.05	0.05	0.48	0.83
Cl	-0.13	0.13	0.06	0.06	-0.14	1.00	0.05	0.03	0.08	-0.04	0.08	0.04	0.07	-0.10	-0.08	-0.08	-0.01	-0.05	-0.06	-0.10
K	0.19	0.33	0.89	0.92	0.14	0.05	1.00	0.79	0.89	0.59	0.70	0.86	0.91	0.03	0.01	0.29	0.58	0.05	0.29	0.16
CA	-0.01	0.29	0.67	0.73	-0.06	0.03	0.79	1.00	0.66	0.46	0.48	0.71	0.73	0.00	0.02	0.24	0.44	0.02	0.19	-0.03
Ti	-0.01	0.25	0.98	0.98	-0.05	0.08	0.89	0.66	1.00	0.53	0.78	0.90	0.99	-0.07	-0.08	0.08	0.69	0.01	0.16	0.00
V	0.11	0.35	0.54	0.56	0.12	-0.04	0.59	0.46	0.53	1.00	0.30	0.67	0.54	0.31	0.08	0.23	0.42	0.16	0.27	0.03
Cr	0.04	0.21	0.75	0.75	-0.01	0.08	0.70	0.48	0.78	0.30	1.00	0.58	0.76	-0.06	0.06	0.08	0.60	-0.13	0.17	0.10
Mn	0.02	0.29	0.89	0.91	-0.01	0.04	0.86	0.71	0.90	0.67	0.58	1.00	0.91	0.03	-0.09	0.12	0.61	0.10	0.15	-0.05
Fe	-0.02	0.25	0.98	0.99	-0.07	0.07	0.91	0.73	0.99	0.54	0.76	0.91	1.00	-0.07	-0.07	0.11	0.68	0.02	0.17	-0.01
Ni	0.17	0.04	-0.06	-0.05	0.20	-0.10	0.03	0.00	-0.07	0.31	-0.06	0.03	-0.07	1.00	0.31	0.26	0.01	0.03	0.13	0.15
Cu	0.29	-0.01	-0.07	-0.06	0.27	-0.08	0.01	0.02	-0.08	0.08	0.06	-0.09	-0.07	0.31	1.00	0.57	0.03	0.34	0.44	0.36
Zn	0.58	0.22	0.10	0.14	0.56	-0.08	0.29	0.24	0.08	0.23	0.08	0.12	0.11	0.26	0.57	1.00	0.07	0.26	0.77	0.61
Ga	-0.01	0.22	0.66	0.67	-0.05	-0.01	0.58	0.44	0.69	0.42	0.60	0.61	0.68	0.01	0.03	0.07	1.00	-0.06	0.24	0.06
As	0.02	-0.03	0.02	0.02	0.05	-0.05	0.05	0.02	0.01	0.16	-0.13	0.10	0.02	0.03	0.34	0.26	-0.06	1.00	0.11	-0.04
Pb	0.52	0.17	0.15	0.19	0.48	-0.06	0.29	0.19	0.16	0.27	0.17	0.15	0.17	0.13	0.44	0.77	0.24	0.11	1.00	0.65
Se	0.85	0.20	0.00	0.03	0.83	-0.10	0.16	-0.03	0.00	0.03	0.10	-0.05	-0.01	0.15	0.36	0.61	0.06	-0.04	0.65	1.00
Br	0.61	0.34	0.08	0.10	0.59	-0.06	0.32	0.17	0.07	0.14	0.15	0.08	0.08	0.24	0.42	0.67	0.13	0.10	0.61	0.71
Sr	0.05	0.28	0.91	0.93	0.00	0.09	0.88	0.72	0.94	0.52	0.73	0.86	0.94	0.00	-0.01	0.22	0.69	0.03	0.31	0.13
PM2.5	0.82	0.40	0.47	0.50	0.79	-0.06	0.59	0.33	0.46	0.37	0.35	0.45	0.45	0.11	0.16	0.51	0.26	0.04	0.47	0.65
Cl-	-0.38	-0.07	-0.06	-0.08	-0.36	0.27	-0.05	0.04	-0.09	-0.18	-0.14	-0.10	-0.07	-0.06	0.13	-0.08	-0.25	0.16	-0.31	-0.38
NO2	0.09	0.07	-0.03	-0.04	0.07	-0.05	0.08	-0.03	-0.03	-0.06	0.09	-0.07	-0.02	0.14	0.09	0.03	-0.07	-0.04	0.04	0.10
NO3-	0.26	0.37	0.62	0.65	0.25	0.13	0.65	0.40	0.64	0.53	0.45	0.61	0.62	0.15	-0.03	0.23	0.46	0.03	0.30	0.22
SO4--	0.98	0.32	-0.01	0.02	0.99	-0.13	0.15	-0.03	-0.03	0.12	-0.02	0.02	-0.04	0.20	0.26	0.55	-0.05	0.06	0.46	0.82
NA+	0.03	0.41	0.59	0.59	0.03	0.38	0.53	0.31	0.62	0.54	0.40	0.58	0.59	0.06	-0.17	0.00	0.49	-0.02	0.15	0.05
NH4+	0.97	0.28	-0.07	-0.04	0.98	-0.17	0.11	-0.05	-0.09	0.12	-0.07	-0.01	-0.09	0.21	0.28	0.56	-0.09	0.10	0.46	0.79
K+	0.42	0.21	0.19	0.22	0.34	-0.07	0.36	0.25	0.19	0.27	0.37	0.23	0.19	0.19	0.32	0.36	0.27	-0.01	0.33	0.36
MG+	-0.04	0.36	0.70	0.70	-0.02	0.23	0.62	0.42	0.71	0.59	0.47	0.70	0.70	0.03	-0.18	-0.01	0.56	0.02	0.11	-0.05
CA++	0.24	0.24	0.54	0.59	0.21	0.01	0.61	0.57	0.52	0.58	0.31	0.59	0.55	0.08	-0.03	0.23	0.32	0.06	0.23	0.05
O1	-0.03	0.02	0.14	0.16	-0.06	0.16	0.07	0.05	0.17	0.05	0.14	0.10	0.16	-0.17	-0.14	-0.05	0.12	-0.15	0.06	-0.02
O2	0.62	0.20	0.09	0.15	0.59	0.00	0.21	0.05	0.15	0.08	0.14	0.11	0.15	-0.01	0.11	0.40	0.16	-0.07	0.43	0.53
O3	0.26	0.17	0.18	0.20	0.25	-0.02	0.32	0.21	0.19	0.14	0.06	0.20	0.21	0.10	0.11	0.28	0.09	0.02	0.14	0.08
O4	0.78	0.33	-0.02	0.01	0.75	-0.08	0.25	0.09	-0.04	0.12	-0.02	0.01	-0.02	0.18	0.26	0.54	-0.05	0.09	0.44	0.61
OP	0.64	0.19	0.26	0.31	0.61	-0.09	0.33	0.17	0.29	0.13	0.30	0.23	0.28	0.00	0.19	0.45	0.33	-0.01	0.48	0.56
E1	0.80	0.24	-0.08	-0.03	0.79	-0.15	0.09	0.02	-0.08	0.03	-0.03	-0.04	-0.08	0.13	0.30	0.58	-0.01	0.08	0.48	0.64
E2	0.40	0.18	0.35	0.39	0.38	-0.01	0.32	0.14	0.38	0.20	0.31	0.32	0.36	0.00	-0.01	0.20	0.50	-0.09	0.34	0.37
E3	0.09	0.08	0.22	0.26	0.04	0.03	0.17	0.09	0.28	0.16	0.28	0.20	0.26	-0.13	-0.15	0.02	0.35	-0.07	0.34	0.20

	Br	Sr	PM2.5	Cl-	NO2	NO3-	SO4--	NA+	NH4+	K+	MG+	Ca++	O1	O2	O3	O4	OP	E1	E2	E3
H	0.61	0.05	0.82	-0.38	0.09	0.26	0.98	0.03	0.97	0.42	-0.04	0.24	-0.03	0.62	0.26	0.78	0.64	0.80	0.40	0.09
Na	0.34	0.28	0.40	-0.07	0.07	0.37	0.32	0.41	0.28	0.21	0.36	0.24	0.02	0.20	0.17	0.33	0.19	0.24	0.18	0.08
Al	0.08	0.91	0.47	-0.06	-0.03	0.62	-0.01	0.59	-0.07	0.19	0.70	0.54	0.14	0.09	0.18	-0.02	0.26	-0.08	0.35	0.22
Si	0.10	0.93	0.50	-0.08	-0.04	0.65	0.02	0.59	-0.04	0.22	0.70	0.59	0.16	0.15	0.20	0.01	0.31	-0.03	0.39	0.26
S	0.59	0.00	0.79	-0.36	0.07	0.25	0.99	0.03	0.98	0.34	-0.02	0.21	-0.06	0.59	0.25	0.75	0.61	0.79	0.38	0.04
Cl	-0.06	0.09	-0.06	0.27	-0.05	0.13	-0.13	0.38	-0.17	-0.07	0.23	0.01	0.16	0.00	-0.02	-0.08	-0.09	-0.15	-0.01	0.03
K	0.32	0.88	0.59	-0.05	0.08	0.65	0.15	0.53	0.11	0.36	0.62	0.61	0.07	0.21	0.32	0.25	0.33	0.09	0.32	0.17
CA	0.17	0.72	0.33	0.04	-0.03	0.40	-0.03	0.31	-0.05	0.25	0.42	0.57	0.05	0.05	0.21	0.09	0.17	0.02	0.14	0.09
Ti	0.07	0.94	0.46	-0.09	-0.03	0.64	-0.03	0.62	-0.09	0.19	0.71	0.52	0.17	0.15	0.19	-0.04	0.29	-0.08	0.38	0.28
V	0.14	0.52	0.37	-0.18	-0.06	0.53	0.12	0.54	0.12	0.27	0.59	0.58	0.05	0.08	0.14	0.12	0.13	0.03	0.20	0.16
Cr	0.15	0.73	0.35	-0.14	0.09	0.45	-0.02	0.40	-0.07	0.37	0.47	0.31	0.14	0.14	0.06	-0.02	0.30	-0.03	0.31	0.28
Mn	0.08	0.86	0.45	-0.10	-0.07	0.61	0.02	0.58	-0.01	0.23	0.70	0.59	0.10	0.11	0.20	0.01	0.23	-0.04	0.32	0.20
Fe	0.08	0.94	0.45	-0.07	-0.02	0.62	-0.04	0.59	-0.09	0.19	0.70	0.55	0.16	0.15	0.21	-0.02	0.28	-0.08	0.36	0.26
Ni	0.24	0.00	0.11	-0.06	0.14	0.15	0.20	0.06	0.21	0.19	0.03	0.08	-0.17	-0.01	0.10	0.18	0.00	0.13	0.00	-0.13
Cu	0.42	-0.01	0.16	0.13	0.09	-0.03	0.26	-0.17	0.28	0.32	-0.18	-0.03	-0.14	0.11	0.11	0.26	0.19	0.30	-0.01	-0.15
Zn	0.67	0.22	0.51	-0.08	0.03	0.23	0.55	0.00	0.56	0.36	-0.01	0.23	-0.05	0.40	0.28	0.54	0.45	0.58	0.20	0.02
Ga	0.13	0.69	0.26	-0.25	-0.07	0.46	-0.05	0.49	-0.09	0.27	0.56	0.32	0.12	0.16	0.09	-0.05	0.33	-0.01	0.50	0.35
As	0.10	0.03	0.04	0.16	-0.04	0.03	0.06	-0.02	0.10	-0.01	0.02	0.06	-0.15	-0.07	0.02	0.09	-0.01	0.08	-0.09	-0.07
Pb	0.61	0.31	0.47	-0.31	0.04	0.30	0.46	0.15	0.46	0.33	0.11	0.23	0.06	0.43	0.14	0.44	0.48	0.48	0.34	0.34
Se	0.71	0.13	0.65	-0.38	0.10	0.22	0.82	0.05	0.79	0.36	-0.05	0.05	-0.02	0.53	0.08	0.61	0.56	0.64	0.37	0.20
Br	1.00	0.25	0.50	-0.18	0.10	0.25	0.57	0.14	0.57	0.42	0.10	0.08	-0.17	0.33	0.28	0.61	0.37	0.51	0.15	0.00
Sr	0.25	1.00	0.45	-0.16	-0.01	0.63	0.02	0.63	-0.04	0.21	0.71	0.50	0.17	0.20	0.16	0.02	0.32	-0.03	0.39	0.32
PM2.5	0.50	0.45	1.00	-0.31	0.05	0.57	0.81	0.38	0.77	0.40	0.37	0.47	0.05	0.58	0.42	0.68	0.68	0.66	0.49	0.14
Cl-	-0.18	-0.16	-0.31	1.00	0.29	-0.14	-0.34	-0.15	-0.36	-0.22	-0.19	-0.23	-0.19	-0.40	0.12	-0.12	-0.42	-0.35	-0.48	-0.54
NO2	0.10	-0.01	0.05	0.29	1.00	0.12	0.09	-0.03	0.05	0.22	-0.19	-0.17	-0.11	-0.03	0.05	0.22	-0.09	-0.11	-0.10	-0.19
NO3-	0.25	0.63	0.57	-0.14	0.12	1.00	0.26	0.78	0.21	0.37	0.73	0.61	0.10	0.45	0.34	0.30	0.50	0.28	0.55	0.30
SO4--	0.57	0.02	0.81	-0.34	0.09	0.26	1.00	0.04	0.98	0.35	-0.01	0.23	-0.06	0.58	0.26	0.76	0.60	0.78	0.37	0.03
NA+	0.14	0.63	0.38	-0.15	-0.03	0.78	0.04	1.00	-0.02	0.22	0.86	0.38	0.16	0.19	0.13	0.02	0.20	-0.04	0.35	0.30
NH4+	0.57	-0.04	0.77	-0.36	0.05	0.21	0.98	-0.02	1.00	0.35	-0.06	0.23	-0.10	0.57	0.27	0.78	0.58	0.80	0.34	0.00
K+	0.42	0.21	0.40	-0.22	0.22	0.37	0.35	0.22	0.35	1.00	0.13	0.31	-0.07	0.25	0.17	0.42	0.30	0.33	0.20	0.12
MG+	0.10	0.71	0.37	-0.19	-0.19	0.73	-0.01	0.86	-0.06	0.13	1.00	0.51	0.13	0.12	0.18	-0.06	0.23	-0.04	0.37	0.28
CA++	0.08	0.50	0.47	-0.23	-0.17	0.61	0.23	0.38	0.23	0.31	0.51	1.00	0.11	0.40	0.36	0.30	0.48	0.37	0.49	0.23
O1	-0.17	0.17	0.05	-0.19	-0.11	0.10	-0.06	0.16	-0.10	-0.07	0.13	0.11	1.00	0.45	0.12	0.01	0.16	0.00	0.35	0.48
O2	0.33	0.20	0.58	-0.40	-0.03	0.45	0.58	0.19	0.57	0.25	0.12	0.40	0.45	1.00	0.54	0.63	0.75	0.72	0.69	0.40
O3	0.28	0.16	0.42	0.12	0.05	0.34	0.26	0.13	0.27	0.17	0.18	0.36	0.12	0.54	1.00	0.63	0.32	0.40	0.23	-0.18
O4	0.61	0.02	0.68	-0.12	0.22	0.30	0.76	0.02	0.78	0.42	-0.06	0.30	0.01	0.63	0.63	1.00	0.49	0.70	0.28	-0.05
OP	0.37	0.32	0.68	-0.42	-0.09	0.50	0.60	0.20	0.58	0.30	0.23	0.48	0.16	0.75	0.32	0.49	1.00	0.85	0.82	0.40
E1	0.51	-0.03	0.66	-0.35	-0.11	0.28	0.78	-0.04	0.80	0.33	-0.04	0.37	0.00	0.72	0.40	0.70	0.85	1.00	0.54	0.15
E2	0.15	0.39	0.49	-0.48	-0.10	0.55	0.37	0.35	0.34	0.20	0.37	0.49	0.35	0.69	0.23	0.28	0.82	0.54	1.00	0.63
E3	0.00	0.32	0.14	-0.54	-0.19	0.30	0.03	0.30	0.00	0.12	0.28	0.23	0.48	0.40	-0.18	-0.05	0.40	0.15	0.63	1.00

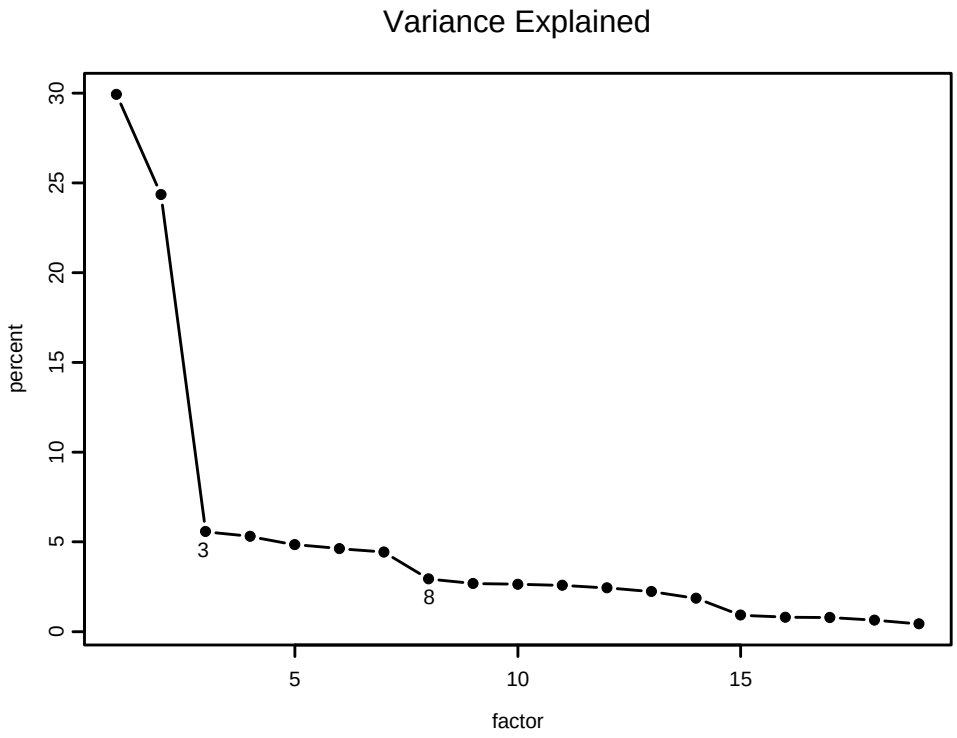

Figure 8-35. Variance explained by each factor in a factor analysis of measured fine particle concentrations at K-Bar.

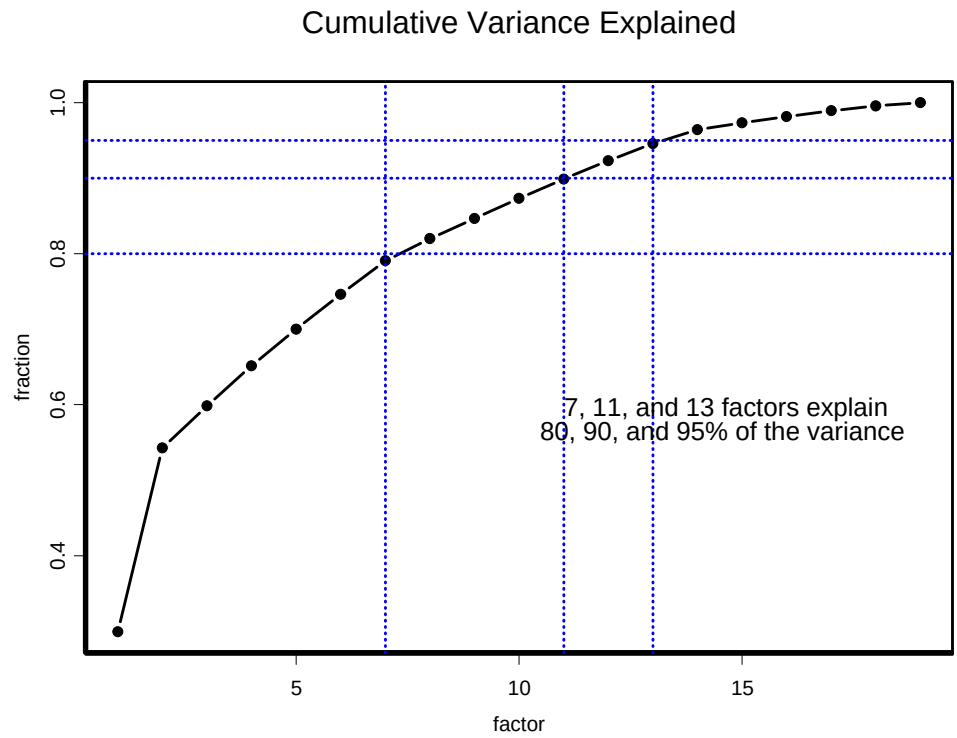

Figure 8-36. Cumulative variance explained by each factor in a factor analysis of measured fine particle concentrations at K-Bar.

Factor one (Figure 8-37) is clearly a soil factor. The typical soil elements of Al, K, Ca, Ti, Cr, Mn, Fe, Ga, Mg, and Sr all load strongly together on this factor which explains 35% of the variance. The daily factor scores also are high only early during the study, prior to about August 15, when other analyses (see section 8.1.1) have shown that there is likely impact from Saharan dust. The relatively high loading for V may either be indicative of V in soil or V may have been added to the airmass as it traversed across Mexico. Vanadium is usually thought to be indicative of the Mexican oil industry along the Gulf Coast. Also loading strongly on this factor are Na^+, NO^-_3, but not NH^+_4. This is further confirmation of the findings of *Collett et al.*, [2001] that the nitrate at Big Bend is mostly not in the form of ammonium nitrate, but more likely as sodium nitrate

The second factor (Figure 8-38), explaining 28% of the variance, is the sulfur factor on which the highest factor loadings are for S, SO_4, NH_4, H, all components of ammonium sulfate, as well as fine mass, of which ammonium sulfate is the largest fraction. Several trace elements also load strongly on this factor including especially Se, and to a lesser extent, Zn, Pb, and Br. The mid-temperature carbons, especially O4, OP, and E1, are also strong loaders on factor two. This factor has the highest factor score on September 1, which was the day of both highest sulfate and highest organic carbon concentrations during BRAVO. The factor scores tend to be near zero or negative during July and after mid-October. The temporal pattern of the factor scores combined with knowledge of the transport patterns indicate that this factor is more likely associated with sources in the U.S. than in Mexico. Transport from the eastern U.S. to Big Bend is most common during September. Additionally, Se emissions are thought to be higher from U.S. coal-fired generating stations than from Mexican sources, which also suggests that this factor indicates sources of U.S. origin. Back trajectories arriving at Big Bend on September 1 cross all three of the large major source regions, Mexico, Texas, and the eastern U.S. The relatively high mid-temperature carbon content on a sulfur factor has consistently been observed elsewhere. In a previous study in Toronto, Canada, where good quality NH_4 and organic acid data were collected, the high mid-temperature OC/S fraction was uniquely associated with acidic sulfates, and suggestive of an acid-catalyzed secondary organic aerosol (SOA) formation mechanism [*Poirot*, 2004].

Factor 3 (Figure 8-39) which explains 11% of the variance, also has the peak factor score on September 1, though the species with the largest loadings, all carbon fractions except O3 and O4, are different from factor 2. Also different from factor 2 are the higher factor scores during July and near-zero scores during mid-September through the end of October. Other analyses of the organic aerosol measured during BRAVO [*Brown et al.*, 2002] have shown that only about 6% of the organic matter measured during BRAVO was due to smoke while more than half was secondary organic aerosol.

Factor 4 (Figure 8-40) is noteworthy for the high factor loadings of several trace elements including especially Zn, Cu, Pb, and Br. This collection of trace elements may be indicative of smelting sources. Factor scores are generally low, but tend to be near zero or negative up until about September 11, after which there are higher magnitudes of both positive and negative scores, with the highest positive scores on October 14–15, October 7, and October 1–2. Back trajectories on these dates are somewhat unique in all having more transport from the western U.S. than did most days during BRAVO. As there are known smelters in that region of the country, the designation of this factor as a smelter factor may be accurate.

Factor 5 (Figure 8-41), explaining 6% of the variance, is weighted highest for the carbon fractions, O2, O3, and O4. O3 and O4 are the fractions that had near-zero loadings for factor 3, while the other carbon fractions loaded highly.

Factor 6 (Figure 8-42) is indicative of marine influence. The species that load highest are those associated with sea salt, Cl, Na, Mg, and also NO_3 which other BRAVO analyses have shown is likely reacting with sea salt to form ammonium nitrate. The factor scores are all generally low with the highest score on July 2. Back trajectories on this day show high speed trajectories arriving from across the Gulf of Mexico.

Factor 7 (Figure 8-43), with high loadings of Ni and V, is indicative of Mexican oil industry influence (see discussion in section 8.1.1.6.). Consistent with the source attribution modeling results discussed later in section 8.2, this factor has some influence on many days, but rarely a large influence. Highest factor scores occur on July 1, about July 28, and September 28–29. All of these days have trajectories arriving from Mexico and on some days also from the western U.S.

Factor 8 (Figure 8-44), explains about 3% of the variance. Species loading the strongest are Cr, NO_2, and K, with highest factor scores on September 14 and September 11, and with most other days having relatively low or negative scores. Back trajectories arriving on these days are not very similar, though both have trajectories that crossed the Gulf of Mexico and Gulf Coast areas.

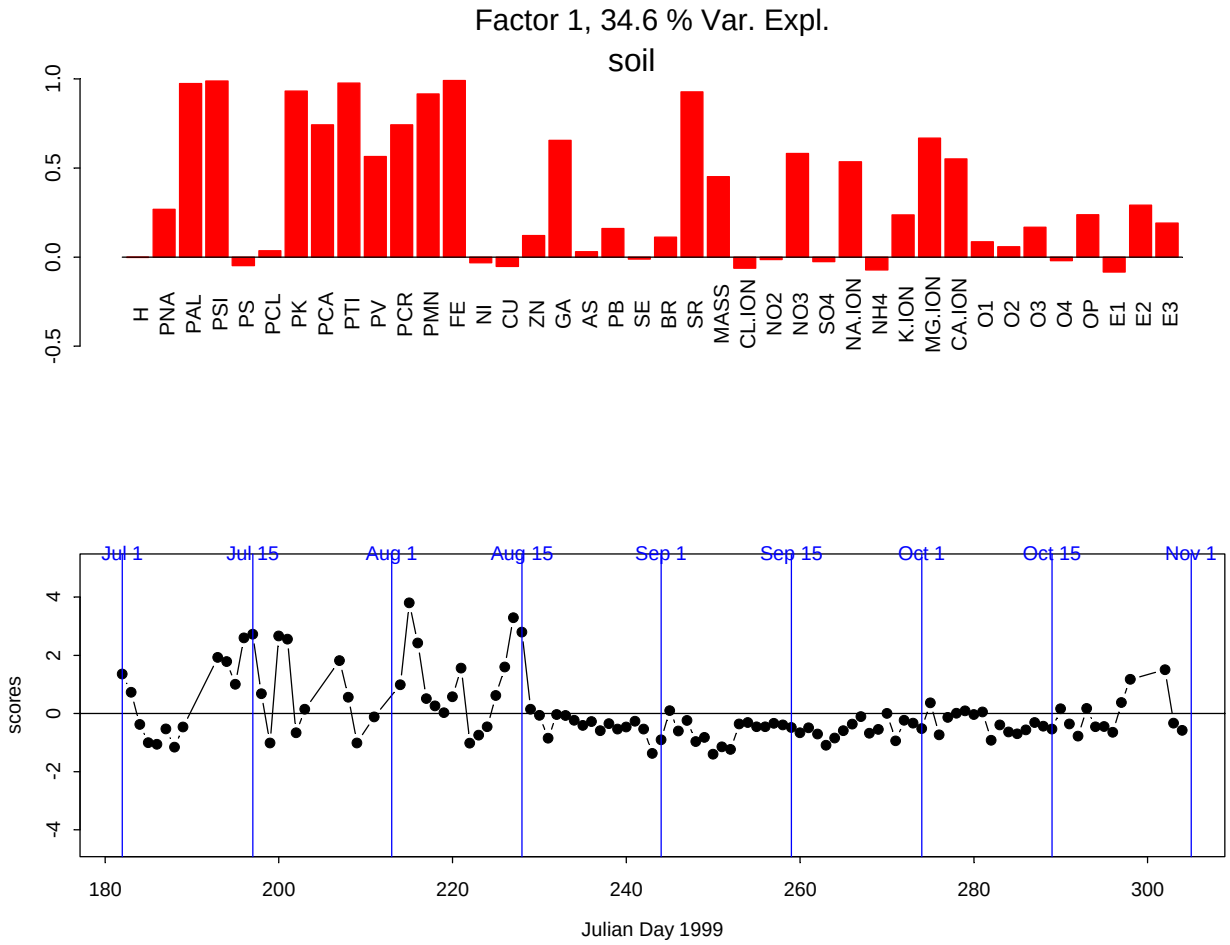

Figure 8-37. Factor loadings in the bar graph and daily factor scores in the line graph for factor one of eight factors.

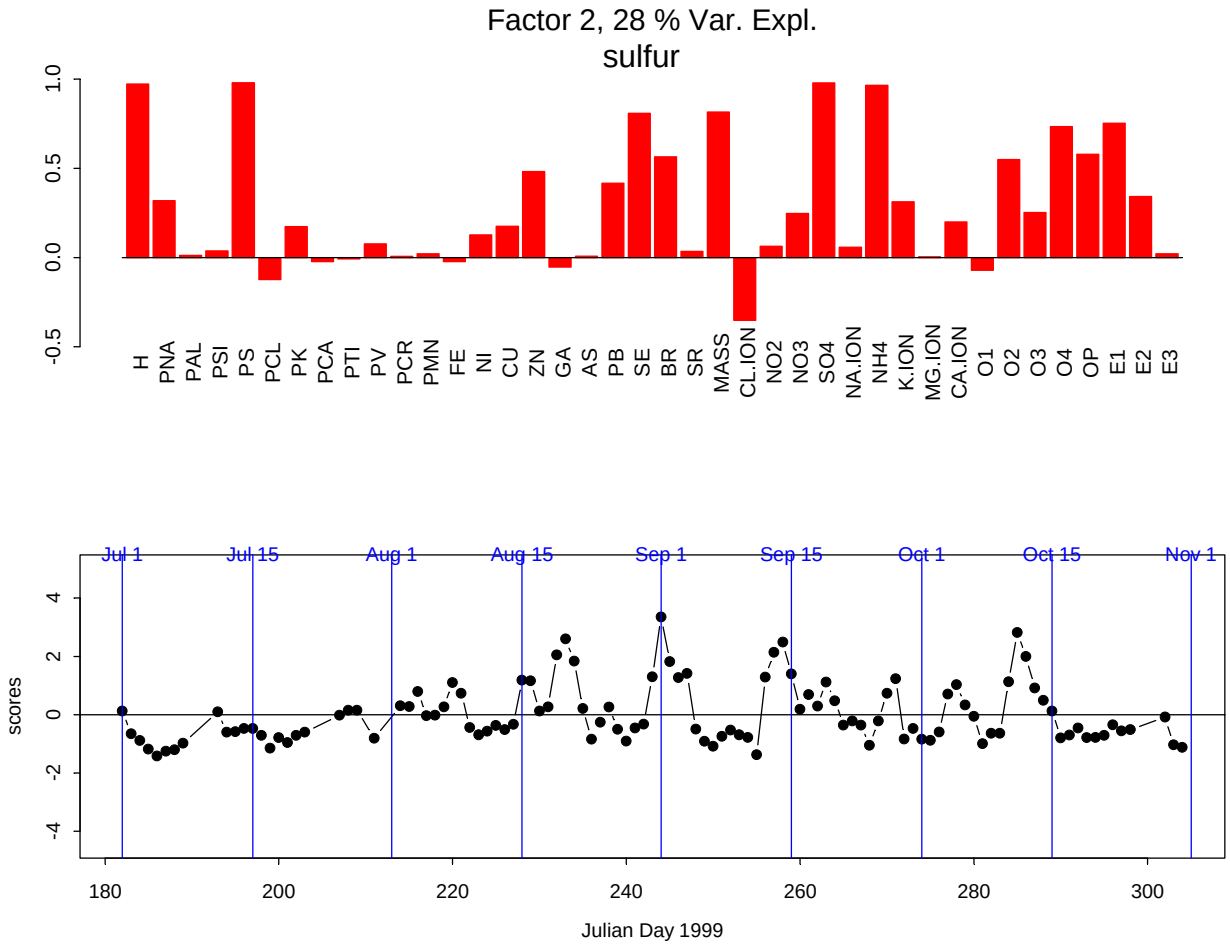

Figure 8-38. Factor loadings in the bar graph and daily factor scores in the line graph for factor two of eight factors.

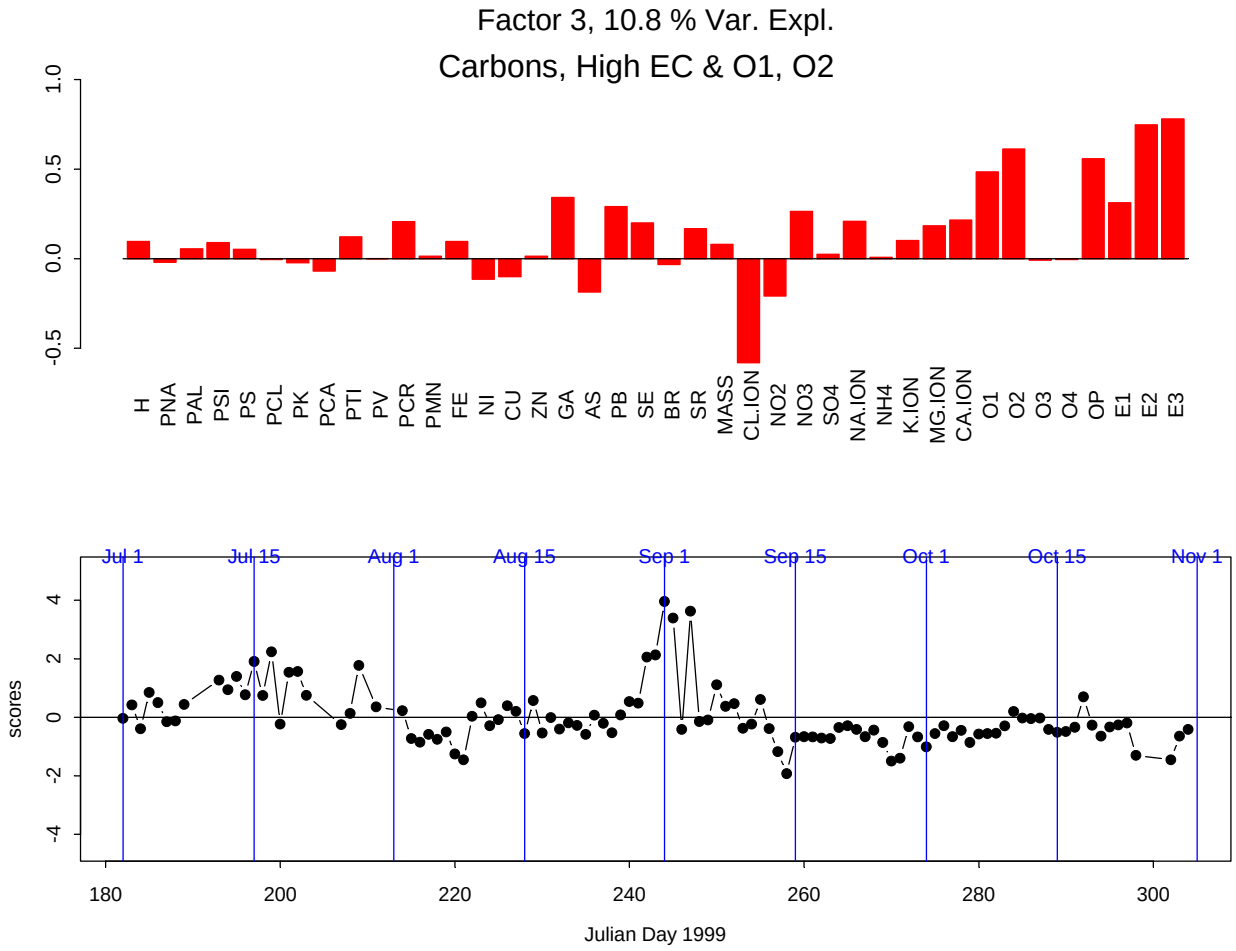

Figure 8-39. Factor loadings in the bar graph and daily factor scores in the line graph for factor three of eight factors.

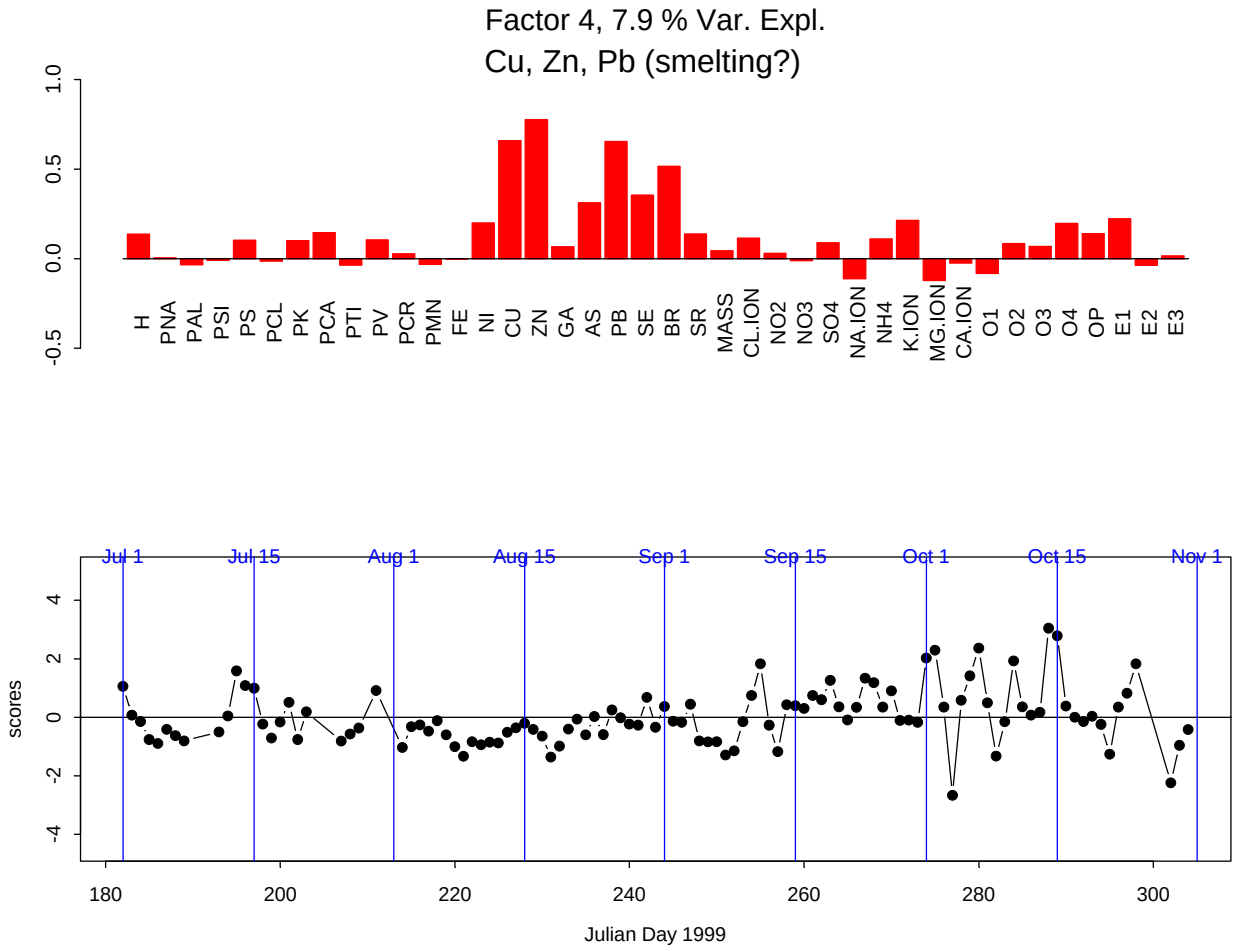

Figure 8-40. Factor loadings in the bar graph and daily factor scores in the line graph for factor four of eight factors.

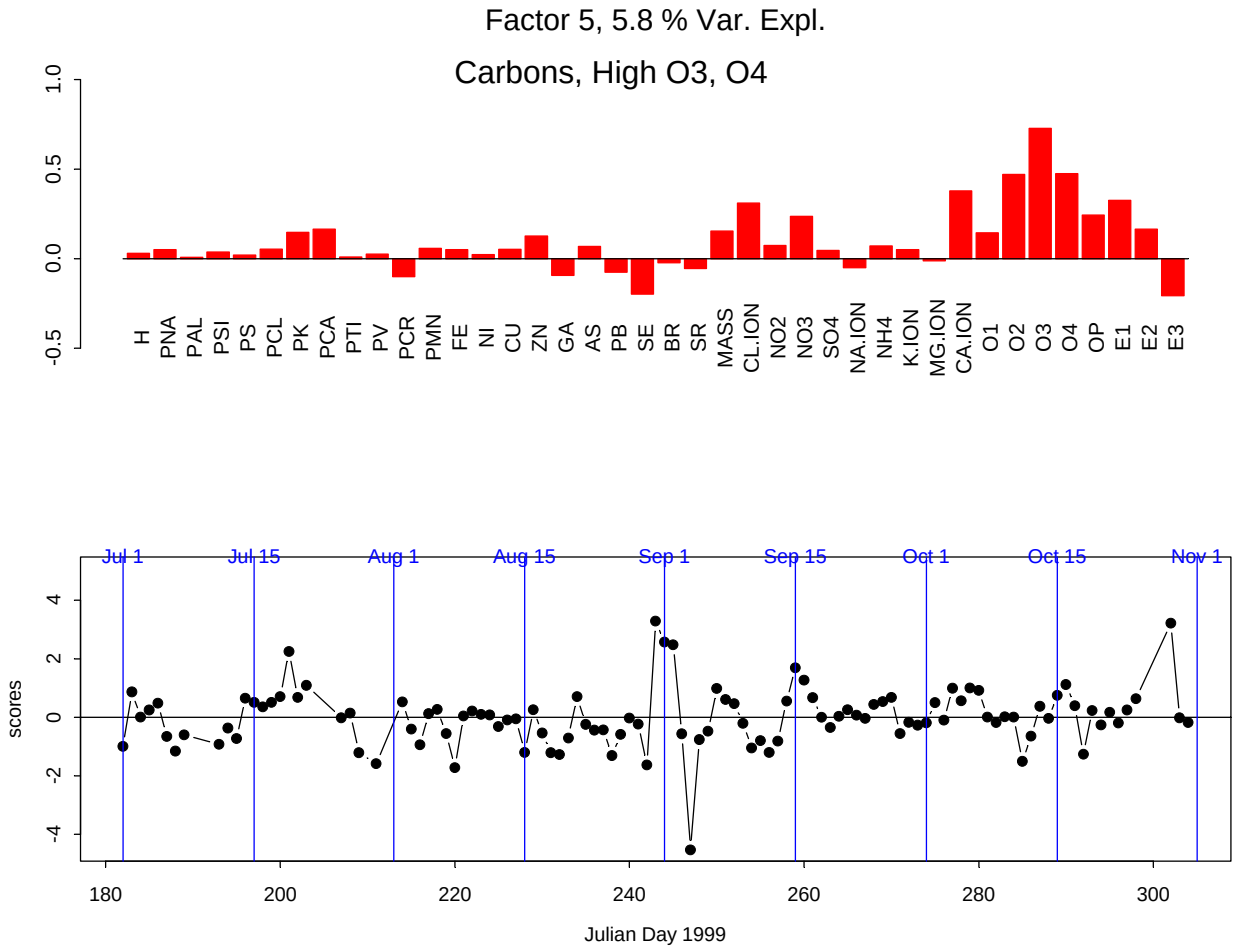

Figure 8-41. Factor loadings in the bar graph and daily factor scores in the line graph for factor five of eight factors.

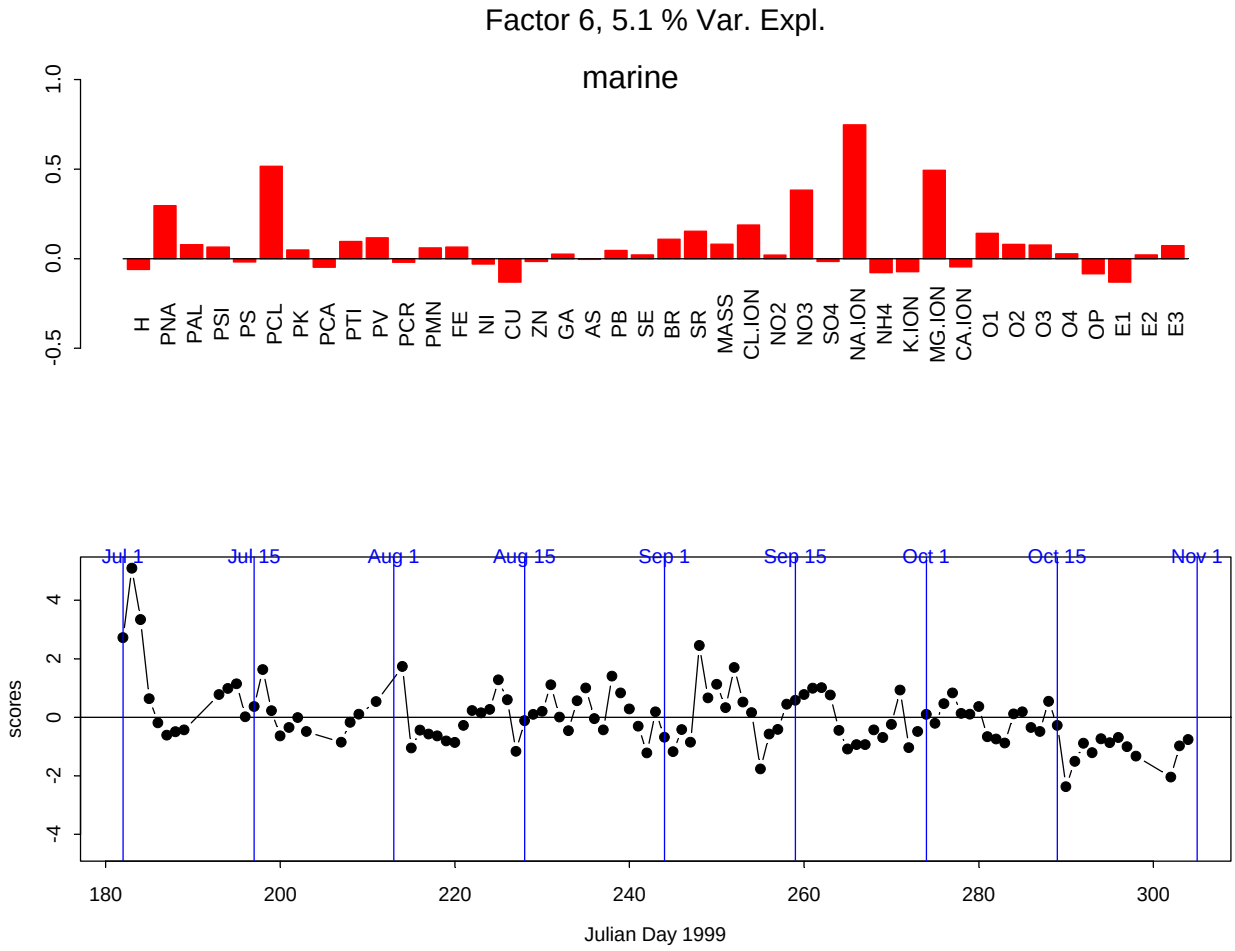

Figure 8-42. Factor loadings in the bar graph and daily factor scores in the line graph for factor six of eight factors.

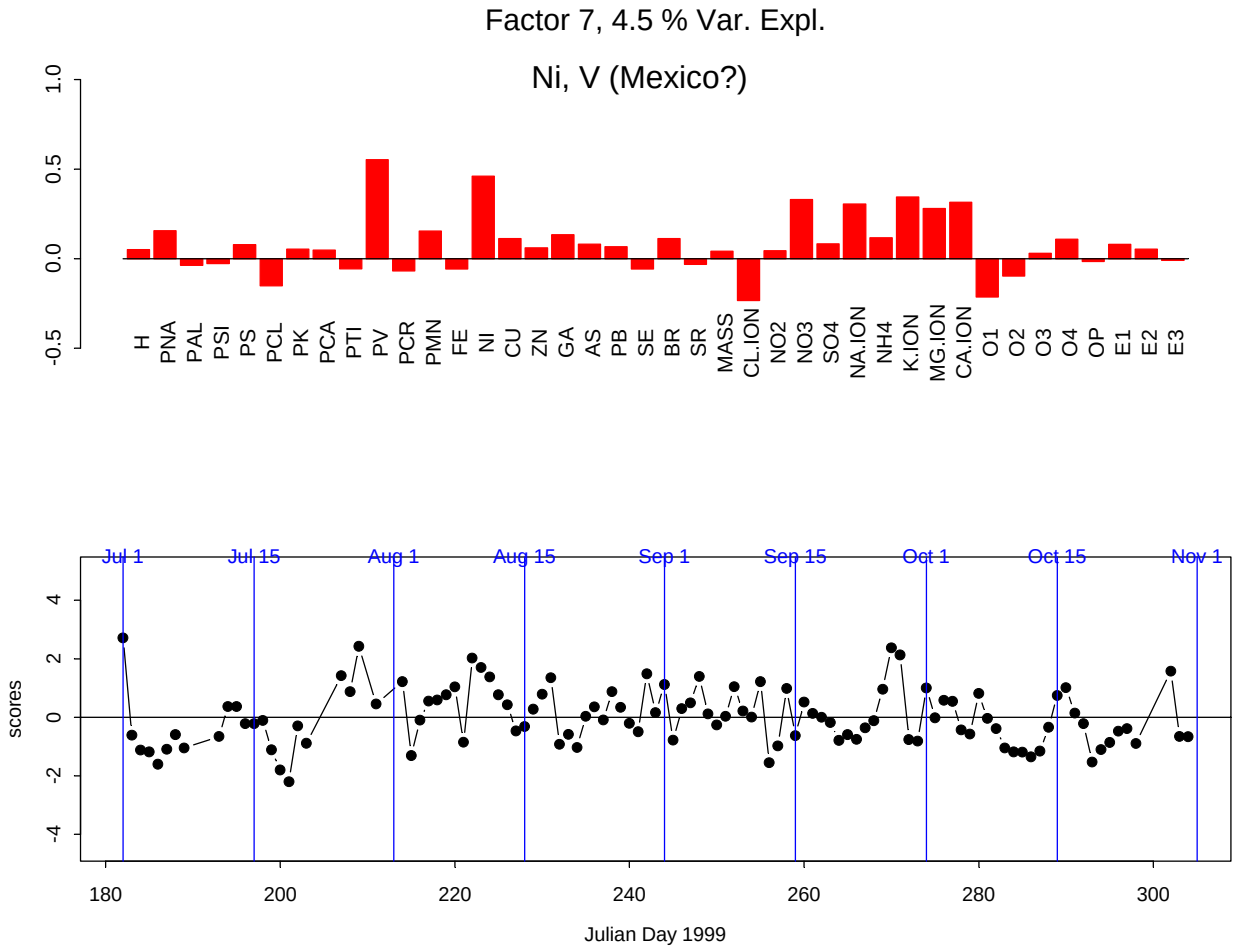

Figure 8-43. Factor loadings in the bar graph and daily factor scores in the line graph for factor seven of eight factors.

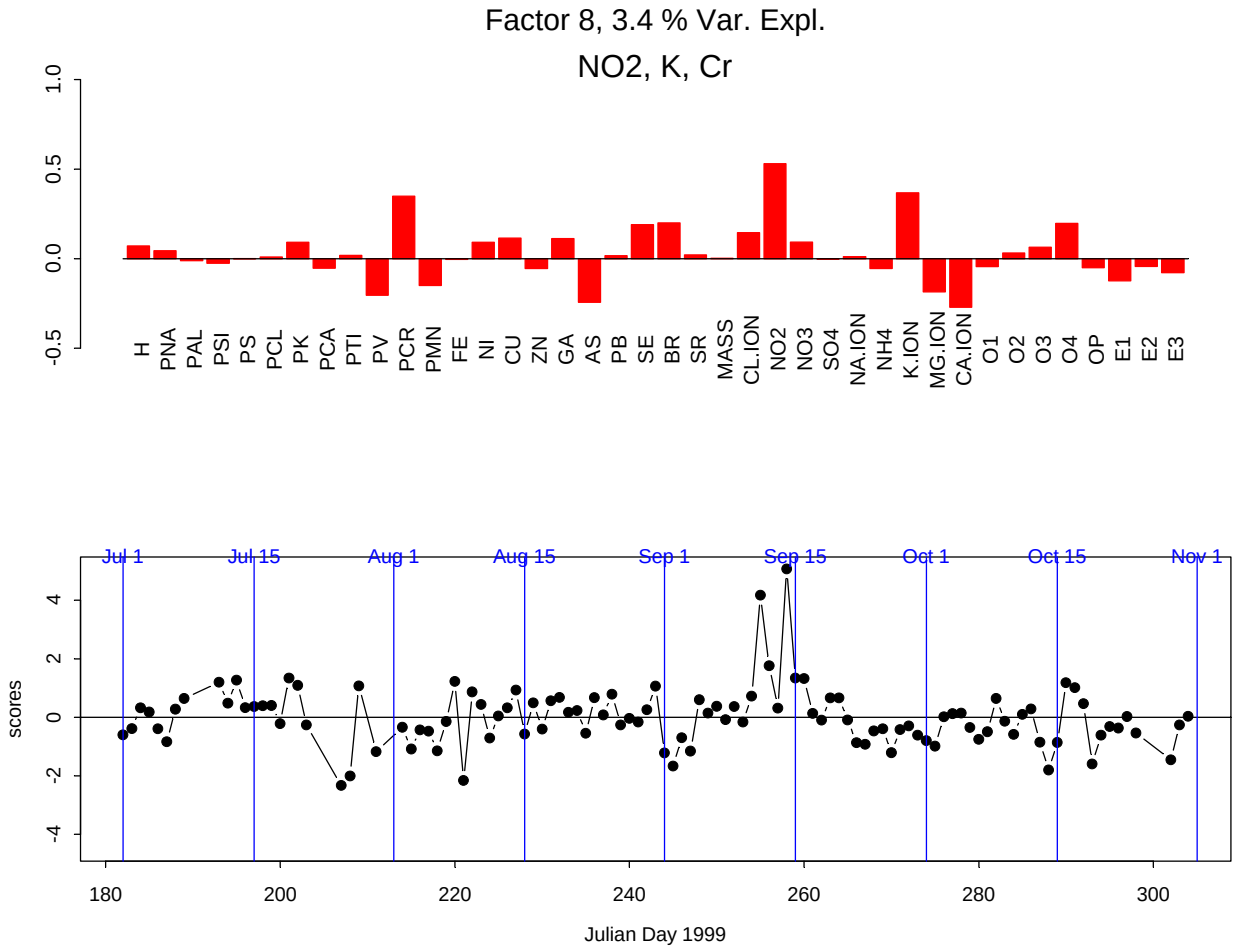

Figure 8-44. Factor loadings in the bar graph and daily factor scores in the line graph for factor eight of eight factors.

8.1.3 Evaluation of Airmass Transport to Big Bend National Park

The primary goal of BRAVO was to identify and quantify the contributions of specific U.S. and Mexican source regions and source types to the haze at Big Bend National Park. To address this goal, airmass histories were aggregated together using residence time analysis techniques (section 2.3.1.3) to develop relationships between long-range and trans-boundary transport and Big Bend's fine particle sulfur concentrations during BRAVO. The study focused on the sulfur concentrations because ammoniated sulfates comprised the majority of the fine mass and light scattering during the Big Bend study [*Malm et al.*, 2003] (see chapter 3).

In this section, the residence time analyses are first evaluated against the BRAVO tracer data. Then the airmass transport directions, speeds, and heights associated with average, high (above the 80th percentile), and low (below the 20th percentile) particulate sulfur concentrations at Big Bend are assessed. In addition, the transport pathways associated with individual Big Bend sulfur episodes are examined, and potential source regions for particle sulfur, sulfur dioxide, and selenium, a power plant tracer, are identified.

This work complements the other BRAVO source attribution analyses presented in this chapter in that the results help to delineate the boundaries of the source regions contributing to Big Bend on the highest sulfur days and identify regions that are not likely to contribute to the highest sulfur levels. These results also help to better understand, interpret, and support or call into question the attribution results.

8.1.3.1 Residence Time Analysis and Airmass History Calculation

The CAPITA Monte Carlo model (section 3.2.3) was used to generate five-day backward airmass histories from Big Bend every two hours from July through October. Each airmass history was composed of 75 particles or individual trajectories. In addition to the particles, three-dimensional location, temperature, humidity, and precipitation were saved along the airmass histories pathway. Two sets of airmass histories were generated with one using the combined EDAS/FNL meteorological data and the other using the 36 km MM5 meteorological data (sections 2.1.3.1–2.1.3.3). It was found in section 5.3 that both meteorological data sets simulated the measured tracer data with about equal skill, properly transporting tracer to Big Bend during the measured multi-day tracer events, and not transporting tracer to Big Bend when the tracer was near the background levels for multi-day periods. Therefore neither wind field could be considered superior, so both wind fields were used in the analysis. These airmass histories are able to characterize regional scale transport. However, they are poorly suited for and not intended for the identification of local flows or nearby source influences (<150 km).

The airmass history technique applied in this work is based upon the residence time analysis (section 3.3). The residence time analysis results in a probability density field identifying the most likely regions in which an airmass will reside en route to the receptor. The most likely transport directions to a receptor are then along the ridges of the probability fields. In this analysis, the airmass histories were sorted according to whether the sulfur was low (below the 20^{th} percentile) or high (above the 80^{th} percentile) and were aggregated together creating transport pathways during the high and low sulfur days. The implication from these sulfur sorted residence time PDFs is that sources, or lack of sources, along the most likely airmass transport pathways are responsible for Big Bend's air quality.

The residence time PDF is the result of the frequency that an airmass is transported over a region en route to the receptor and the length of time it spent over that region. In this analysis, the residence time PDF was decomposed into these two components by calculating a transport direction frequency and an accumulation potential where their product is equal to the residence time PDF (see Appendix 8c). The transport direction frequency is the fraction of time an airmass traverses a given region normalized by a characteristic length of the region to account for different sized regions. Therefore this addresses the question as to what fraction of the receptor concentrations are potentially influenced by emissions from a given region. The accumulation potential can be thought of as an inverse of a characteristic transport speed and is related to the inverse of the speed an airmass was transported over a grid cell and the number of times it traverses the grid cell due to recirculation or flow reversals. This is a better index for determining the exposure of an airmass to a source region's emission than the measured wind speed. For example, fast recirculating winds would spend more time over a source region than slower but directionally persistent winds. Therefore the recirculating airmass would be exposed to a region's emissions for a longer period of time, increasing the potential for pollutants to accumulate.

An important characteristic of airmass transport is the height of the airmasses when traversing a region. An elevated airmass is unlikely to accumulate emissions from surface sources. In this analysis, the airmass height is characterized by averaging the height of all particles that crossed the grid cell.

Relationships between the everyday and air quality sorted residence time analyses can be generated to further enhance the identification of potentially contributing source regions [*Ashbaugh et al*., 1985; *Vasconcelos et al*., 1996; *Stohl,* 1998]. These techniques rely on the triangulation of the source regions by the airmass histories crossing over a true contributing source region following different routes and arriving at the receptor carrying elevated levels of pollutants. Two metrics used in this analysis are the residence time conditional probability (CP) and incremental probability (IP) analyses (sections 3.3.1.3 and 3.3.1.4). The conditional probability is the likelihood that if an airmass passes through a given area it will arrive at the receptor with a high or low concentration. The incremental probability identifies regions that are more or less likely to be traversed during periods of high or low sulfur compared to an average day. These are complementary analyses in that the conditional probabilities tend to identify potential source regions further from the receptor than the incremental probabilities.

This analysis was originally conducted using the combined EDAS and FNL meteorological data. Most of the analysis was duplicated using the MM5 meteorological data when they became available. The following discussion is based upon the EDAS/FNL results, and differences in the transport patterns using the MM5 data are presented or discussed.

8.1.3.2 Evaluation of the Airmass History Techniques.

To evaluate the airmass history analyses' ability to properly identify the airmass transport pathways and known source locations, a residence time analysis was conducted for the upper 20th percentile of the Big Bend 24-hour averaged tracer concentrations. The analysis was conducted for the Eagle Pass tracer (ocPDCH) using data from July through October. Data for the San Antonio tracer, PDCB and the Parish power plant tracer, PTCH, were only released from these sites from September 17 through the end of October. Therefore, only data from September 19 through October 30 were used. iPPCH was continuously released from the Big Brown power plant throughout the study. However, only the tracer data from September 19 through October were used, since prior to this date the data had poor quality with a large fraction below zero. The tracer from Big Brown was intended to represent dispersion of all elevated sources from northeastern Texas and will be referred to as the northeastern tracer. Similarly, the Parish power plant tracer was intended to represent dispersion from Houston source and will be referred to as the Houston tracer.

The results are presented in Figure 8-45 as the residence time PDF weighted by the distance from the Big Bend receptor and the conditional and incremental probabilities. For all four tracers, the airmass transport pathways in the distance weighted residence time PDF correctly include the tracer release sites. However, the Houston release site is at the southern edge of the average airmass transport pathway. Examination of individual trajectories showed a northerly bias in the airmass histories during several of the Houston tracer hits at Big Bend. The conditional and incremental probabilities for the Eagle Pass and San Antonio tracers also properly identified the tracer release sites with the highest probabilities, CP > 0.5 and IP ≥ $1.6*10^{6}$ km^{-2}. The incremental probability had a strong decreasing gradient from these tracer release locations. However, for the conditional probabilities, other regions also had CP > 0.5

hundreds of kilometers from the tracer release sites, such as in southern Oklahoma for the Eagle Pass tracer. The conditional probability for the Houston tracer showed the region of the largest probability northeast of the release site, which was expected from the examination of the distance weighted residence time plots. The incremental probabilities for both the northeast Texas and San Antonio tracers did not clearly identify a potential source region, but did identify a transport pathway encompassing a region from most of eastern Texas to Eagle Pass.

The airmass transport pathways from the three eastern Texas tracer release sites, San Antonio, Houston, and northeast Texas, included the region around the Carbón power plants in Mexico. However, transport from the Eagle Pass tracer release site was not necessarily associated with transport from eastern Texas. Therefore these collinearities in airmass transport pathways over major sulfur dioxide source regions present difficulties in truly separating these source areas in these analyses.

The residence time analysis results using the MM5 trajectories are presented in Figure 8-46. The same general conclusions drawn from the EDAS trajectories can be made about the MM5 results. However, the MM5 results tend to show more distant transport results. This is most evident in the distance weighted residence time. For example, the MM5 results show the highest distance weighted probabilities in Arkansas, and for the EDAS/FNL results it is along the Texas-Louisiana border.

In chapter 4 it was shown that Big Bend airmass histories did not always traverse the tracer release site when there was measured tracer at the receptor. For example, the day with the largest northeast tracer concentration at Big Bend had airmass histories to the west of the tracer release site. However, the residence time results indicate that on average the airmass traversed the northeast Texas tracer release site, indicating that the errors in transport are random.

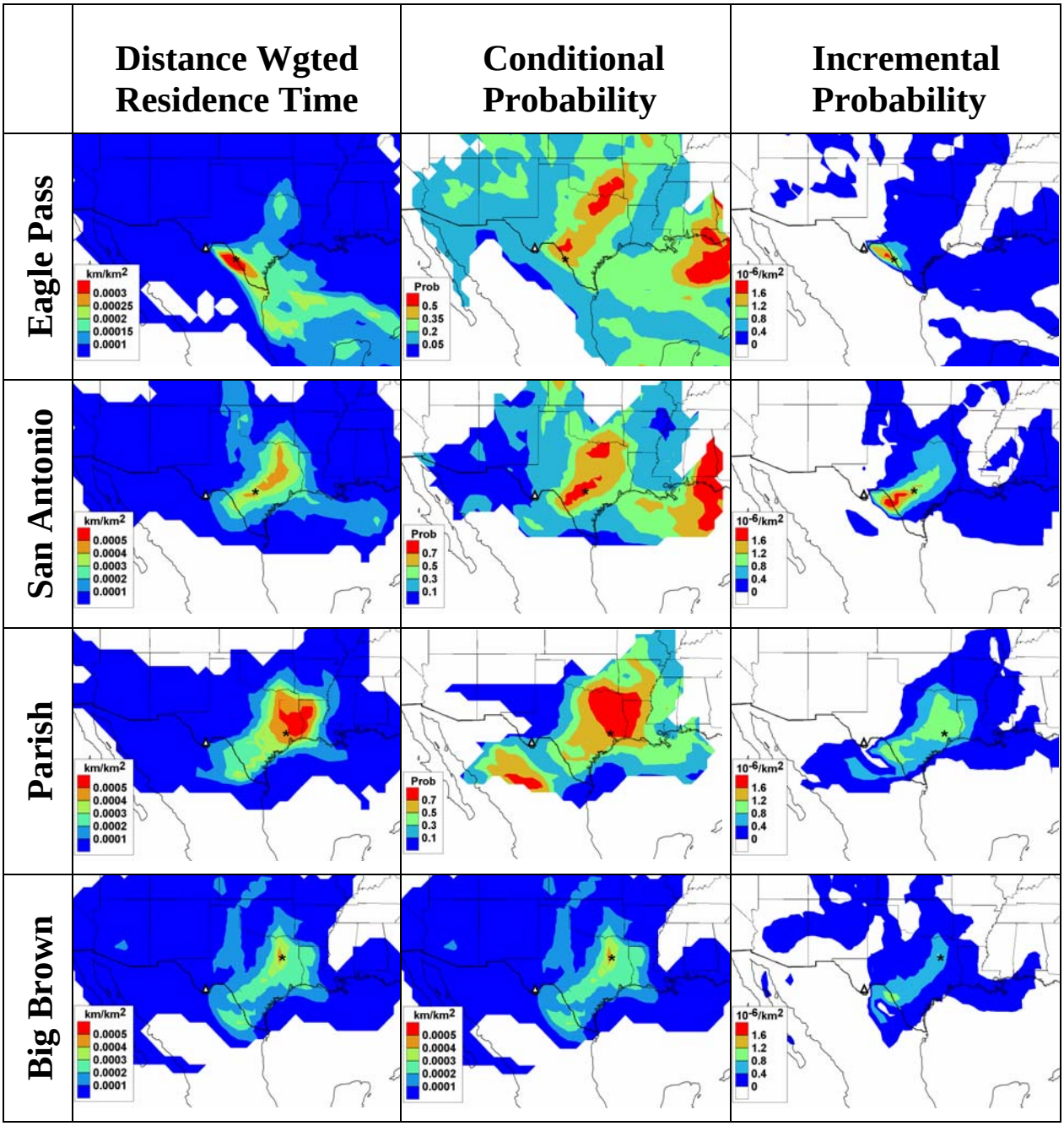

Figure 8-45. The distance weighted residence time analysis, conditional probability, and incremental probability functions for the upper 20th percentiles of the tracer data at Big Bend. These transport probabilities were created using airmass histories generated using the EDAS/FNL meteorological data. The * identifies the location of the tracer release site and the triangle is the location of Big Bend.

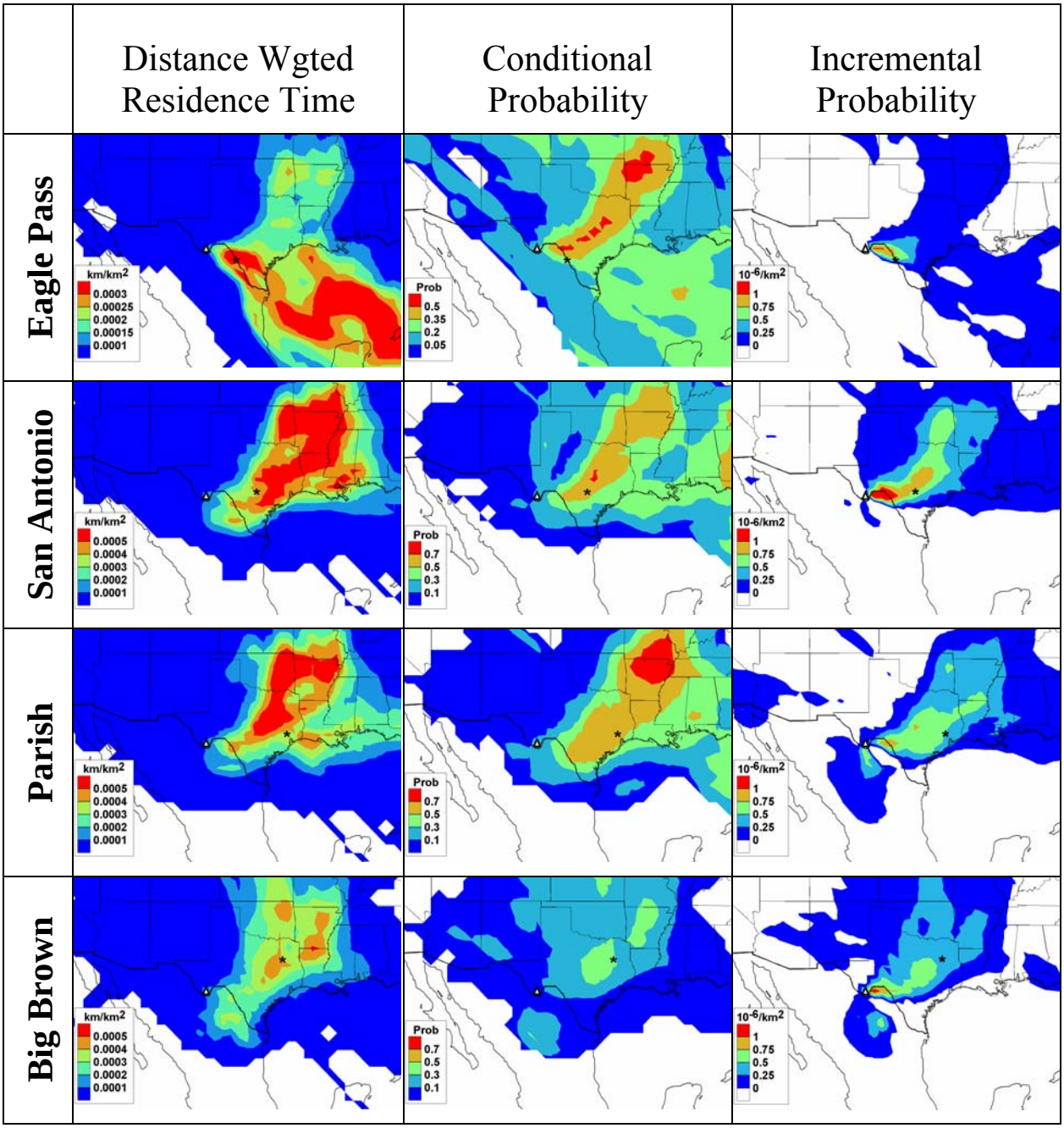

Figure 8-46. The distance weighted residence time analysis, conditional probability, and incremental probability functions for the upper 20th percentiles of the tracer data at Big Bend. These transport probabilities were created using airmass histories generated using the 36 km MM5 meteorological data. The * identifies the location of the tracer release site and the triangle is the location of Big Bend.

8.1.3.3 Airmass Transport to Big Bend, Texas, during the BRAVO Study.

The residence time probability density function and its decomposition for the entire four-month BRAVO study are presented in Figure 8-47. These airmass histories were generated using the Monte Carlo model driven by the EDAS/FNL wind fields. As shown, airmasses en route to Big Bend are most likely to have previously resided southeast of Big Bend, just south of the Mexican-Texas border. This is consistent with airmasses being transported from the Gulf of Mexico along northeastern Mexico to Big Bend. The next highest region of probable transport to Big Bend is over Texas northeast of Big Bend and from the eastern U.S. Airmass transport from west of Big Bend and from southern Mexico infrequently occurred during BRAVO. The airmass transport during BRAVO had two distinct periods. During July to the middle of August airmass histories almost exclusively came from the Gulf of Mexico and up along the Mexican-Texas border to Big Bend. This time period also had the lowest average sulfate concentration and haze during BRAVO (section 4). Airmass transport from Texas and the eastern U.S. was more prevalent after the middle of August, though transport along the Mexican-Texas border still dominated.

The spatial patterns in the residence time PDF are predominantly due to the frequency at which airmass trajectories traverse a given area prior to reaching the receptor. This is seen in Figure 8-47, where the residence time PDF and transport direction frequency plots have similar spatial patterns. The highest accumulation potentials (> 0.15 s/m) exist in a band from northwest Mexico to the Gulf of Mexico and throughout Texas. These are equivalent to effective airmass transport speeds of about 6 m/s. To the north and south of this band the accumulation potential decreases to between 0.1 and 0.15 s/m. The lowest average particle heights (< 1 km) are along the regions with the highest residence times, from the Gulf of Mexico up along the Texas-Mexican border (< 1 km), and throughout Texas (< 1.5 km). West of Big Bend and in the eastern U.S., the airmasses are higher, with average heights above 4 km in Ohio and northwest to Minnesota and in the intra-mountainous western U.S.

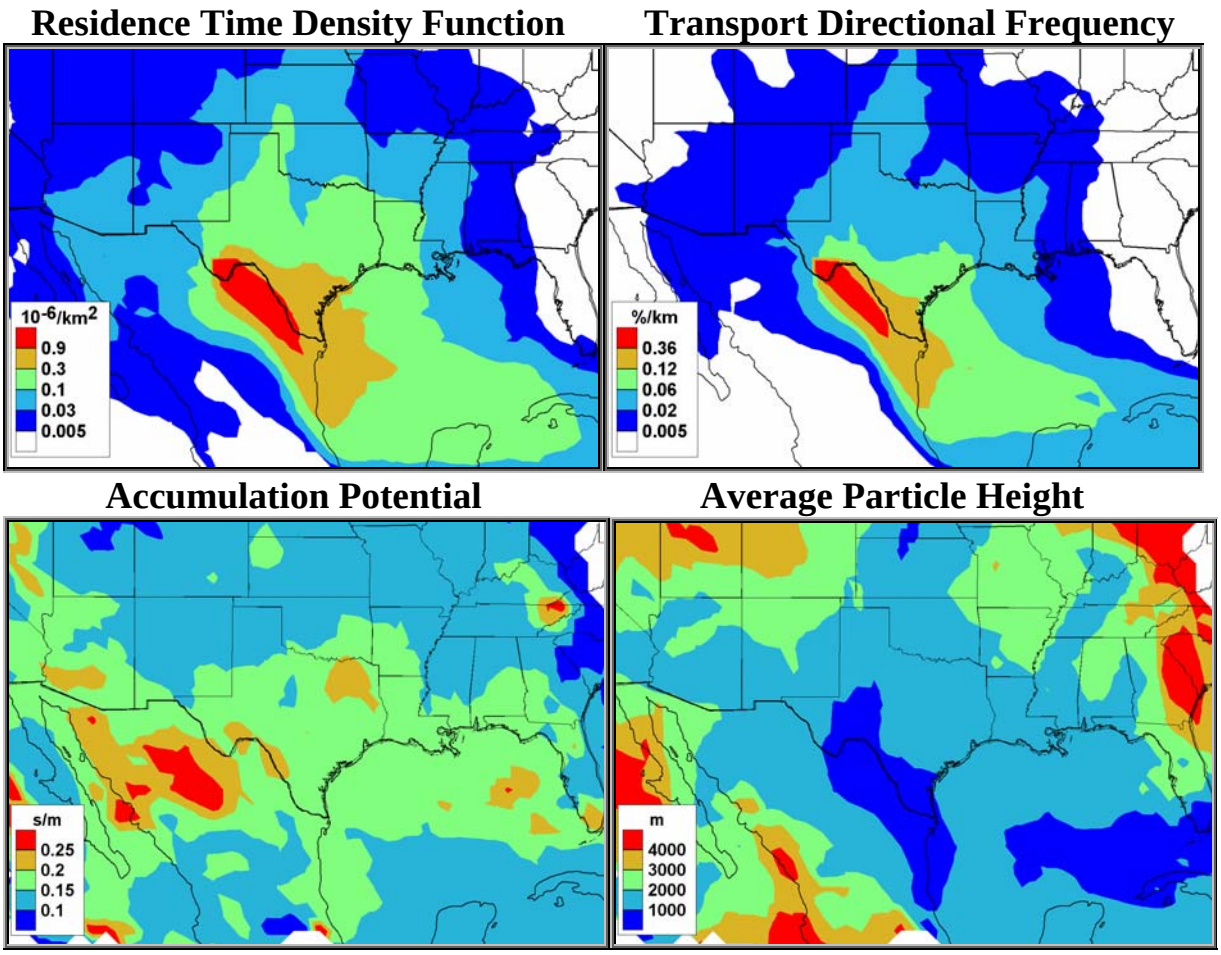

Figure 8-47. The residence time PDF and its decomposition for the entire BRAVO study. The airmass histories were generated using the EDAS/FNL wind fields.

8.1.3.3.1 Airmass Transport during High and Low Particulate Sulfur Days

In order to delineate preferential transport pathways for different particulate sulfur concentrations, the airmass histories were sorted and aggregated according to whether the particulate sulfur was low (below the 20th percentile) or high (above the 80th percentile). The residence time PDF and its decomposition for the high and low sulfur days are presented in Figures 8-48 and 8-49. As shown in Figure 8-48, Big Bend's highest particle sulfur concentrations were primarily associated with prior airmass transport from the southeast, along northeastern Mexico and along the Texas-Mexican border. Airmasses were also likely to have previously resided northeast of Big Bend over eastern Texas and the southeastern U.S. This transport pattern is consistent with airmasses coming from the southeastern U.S. through eastern Texas and up along the Mexican-Texas border to Big Bend. The transport over both northeastern Mexico and eastern Texas had high accumulation potentials (> 0.25 s/m) and low average particle heights (< 2 km). Transport from the industrial Midwestern states did occur, but it was infrequent and had lower accumulation potentials and average heights in excess of 3 km. In fact, over these states no particles were ever below 2 km.

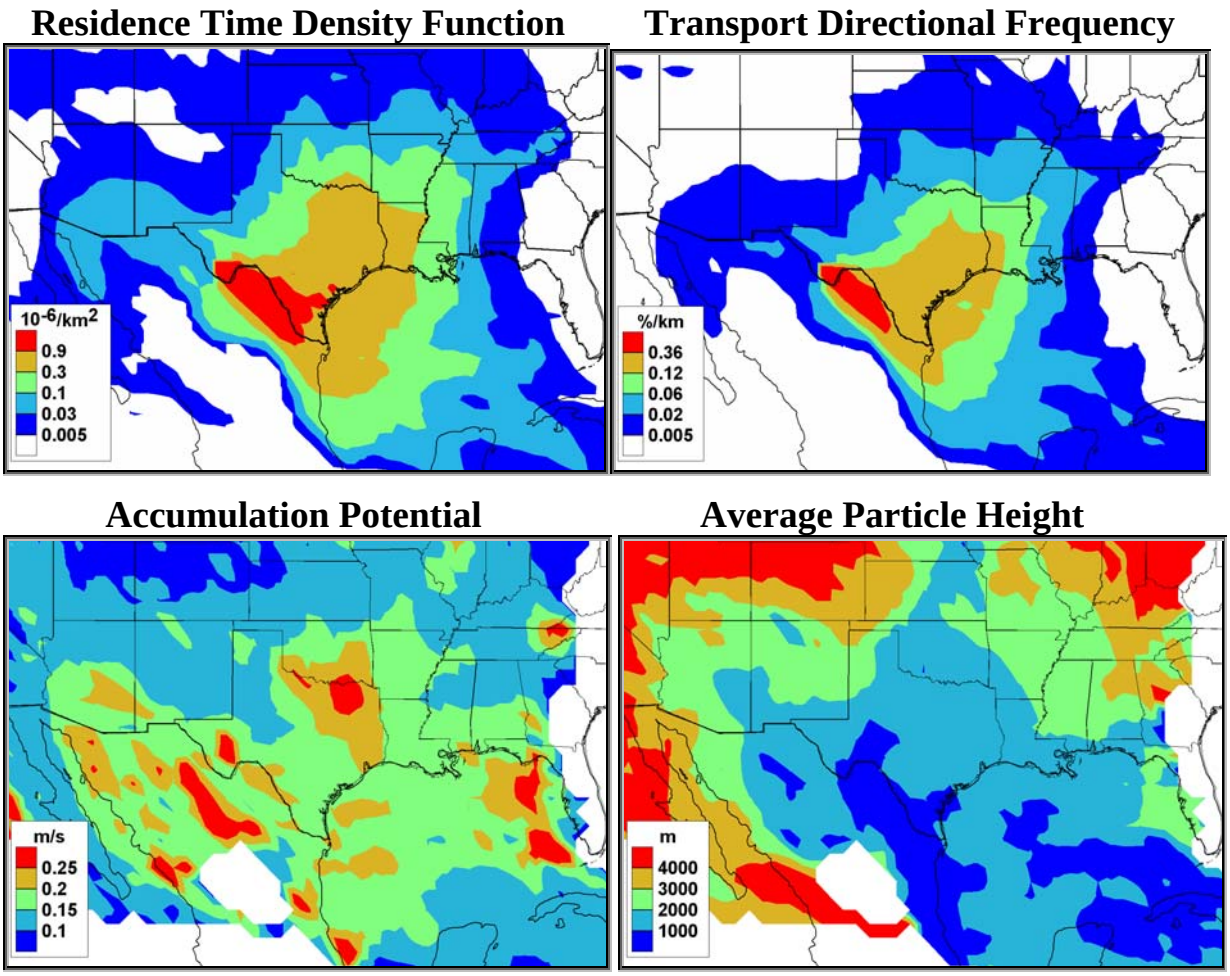

Figure 8-48. The Big Bend NP residence time PDF and its decomposition for the 20% of the days with the highest particulate sulfur. The airmass histories were generated using the EDAS/FNL wind fields.

Transport during the low sulfur days was persistently from the Gulf of Mexico along northeastern Mexico and from the north from the Great Plains states to Big Bend (Figure 8-49). Along these two transport pathways, the airmass histories had low average heights, ~ 1 km, and higher than average transport speeds. Unlike the high sulfur days, almost no transport from eastern Texas or the southeastern U.S. occurs prior to low Big Bend particulate sulfur concentrations. It is interesting that at Big Bend and to its southeast the accumulation potential was large (~ 0.3 s/m) compared to its surroundings, but on the high sulfur days the accumulation potential in this region was small (~0.15 s/m) compared to its surroundings. This is consistent with the fact that Big Bend and its immediate surroundings have few source of sulfur.

The airmass transport pathways to Big Bend NP for individual particulate sulfur episodes were also examined. As shown in Figure 8-50, the three common transport pathways associated with the particulate sulfur episodes were from eastern Texas, the southeastern U.S., and northeastern Mexico. The largest concentrations occurred when transport over several of these regions coincided. For example, the September 1 episode had transport over all three regions and had the highest particle sulfur concentration (3.2 $\mu g/m^3$) during the BRAVO study. Appendix 8c presents the decomposed residence time analysis for all seven Big Bend particulate sulfur episode during BRAVO.

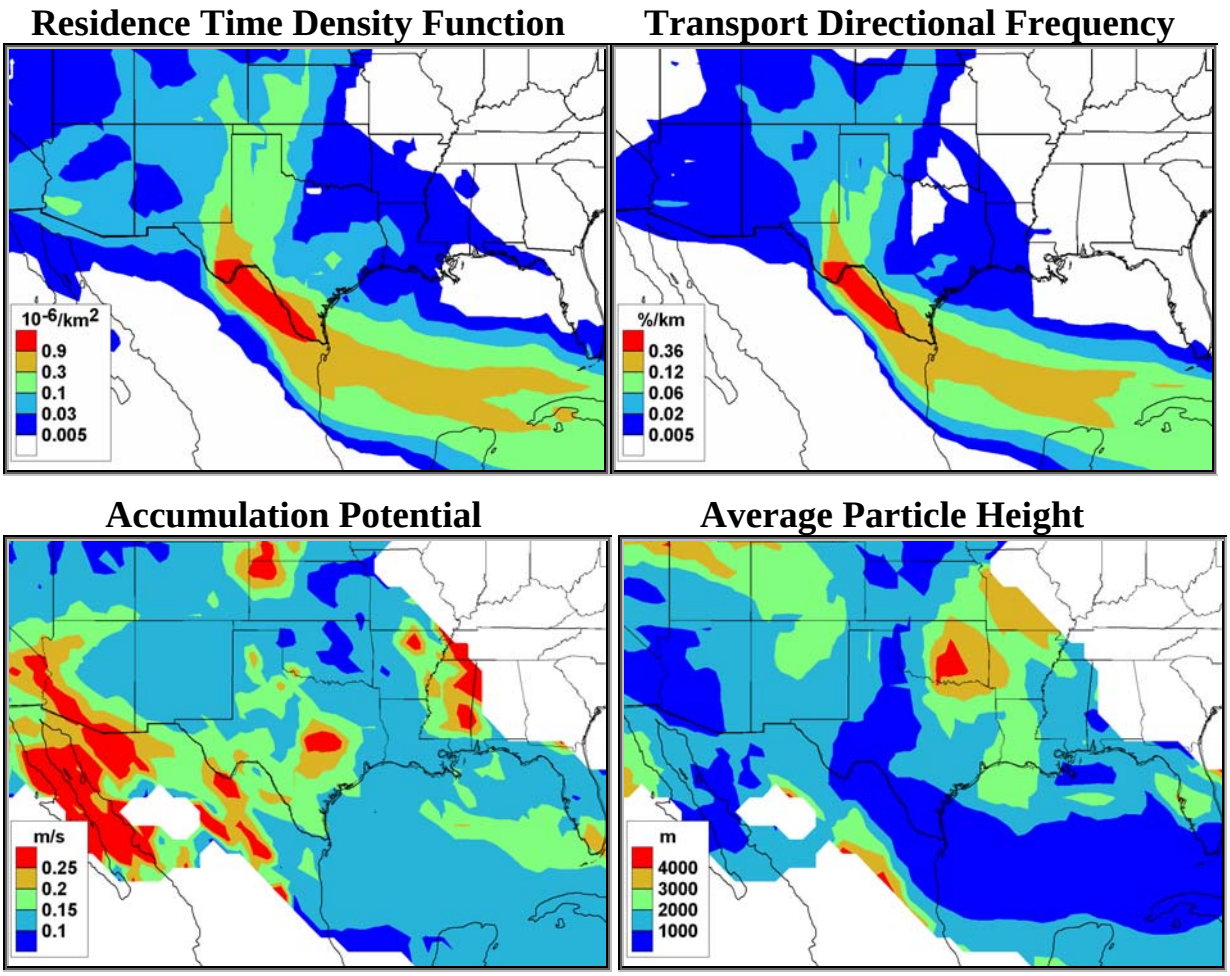

Figure 8-49. The Big Bend NP residence time PDF and its decomposition for the 20% of the days with the lowest particulate sulfur. The airmass histories were generated using the EDAS/FNL wind fields.

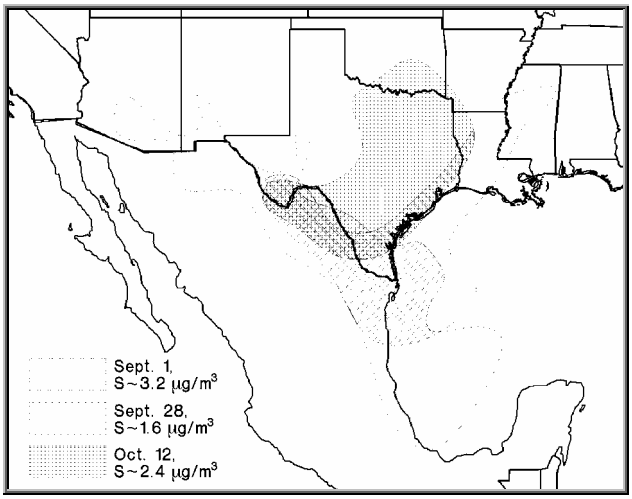

Figure 8-50. Airmass transport pathways to Big Bend NP during three particulate sulfur episodes. Each isopleth shows the most likely pathway the airmass traversed prior to impacting Big Bend. The transport pathways were created using residence time analysis and the contour lines encompass 75% of the residence time hours.

The airmass transport on the high sulfur days using the MM5 meteorological data had some important differences compared to the EDAS/FNL results. As shown in Figure 8-51, both the residence time PDF and transport directional frequency plots show that the likely airmass pathway was from the Mississippi-Louisiana region, down along the Texas coast, and across southern Texas to Big Bend. Therefore the MM5 results indicate a higher likelihood of airmasses traversing the southeastern U.S. and southern Texas en route to Big Bend, compared to the EDAS/FNL results which had a higher likelihood of airmasses traversing eastern Texas and northeastern Mexico. In addition, the MM5 airmass histories had higher transport speeds than those generated with the EDAS/FNL meteorological data. For example, the accumulation potential over Texas varied between 0.1 and 0.17 s/m compared to 0.13 and 0.27 s/m for the EDAS/FNL results. The MM5 and EDAS/FNL airmass histories had similar airmass transport patterns on the low sulfur days.

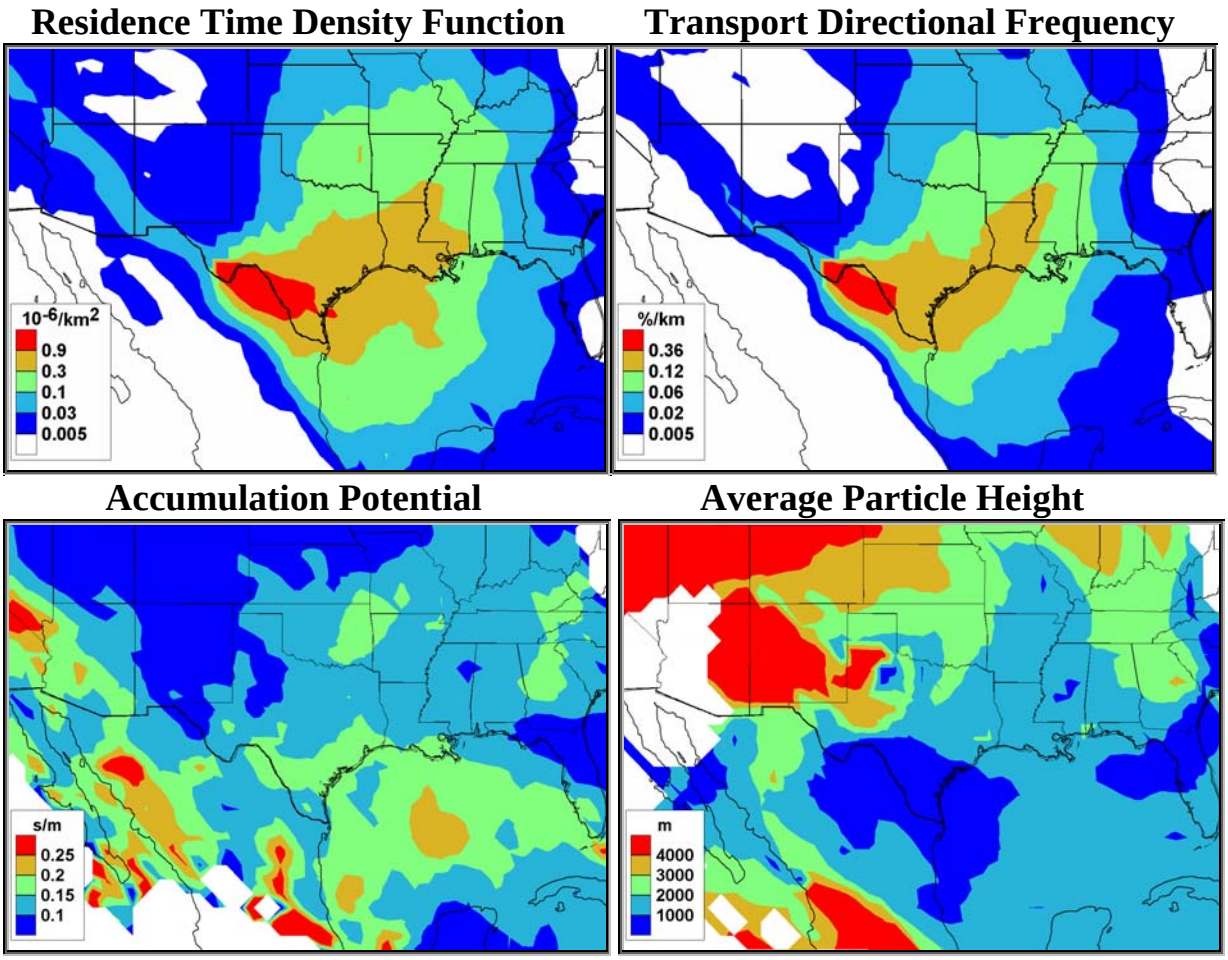

Figure 8-51. The residence time PDF and its decomposition for the 20% of the days with highest particulate sulfur at Big Bend. The airmass histories were generated using the MM5 wind fields.

8.1.3.3.2 Airmass Transport on High Particulate Sulfur Days Compared to Average Days

To better delineate the potential source regions contributing to Big Bend's particulate sulfur, incremental and conditional probability fields for the high sulfur days were examined. As shown in Figure 8-52A, the highest incremental probabilities exist over a broad region in eastern-southeastern Texas and over a region in the vicinity of the Carbón I & II power plants.

Conditional probabilities above 50% encompass a region from eastern Texas to the state of Mississippi. This indicates that, more than half of the time, when airmasses resided over the region they arrived at Big Bend with particulate sulfur concentrations above the 80th percentile. In addition, northeast Texas and eastern Tennessee had conditional probabilities above 70%. Northern Mexico had low conditional and incremental probabilities; however, this was expected since northern Mexico was the most common transport pathway to Big Bend during the entire BRAVO time period (Figure 8-46) and during the high particulate sulfur days (Figure 8-47).

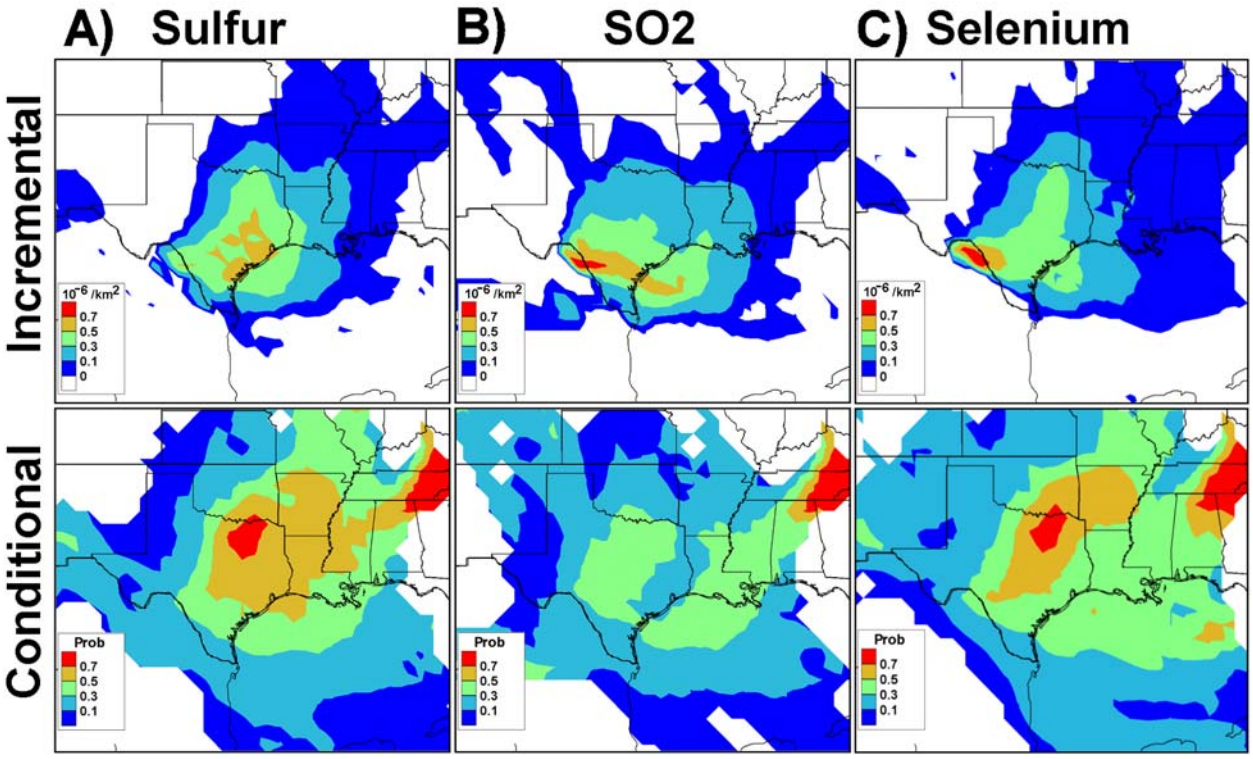

Figure 8-52. The incremental and conditional probabilities for the upper 20th percentiles of the A) fine particulate sulfur, B) sulfur dioxide, and C) fine particle selenium at Big Bend. These transport probabilities were created using airmass histories generated using the EDAS/FNL wind fields.

Incremental and conditional probability fields were also created for the 20% highest sulfur dioxide and selenium concentrations at Big Bend (Figures 8-52B and 8-52C). The highest incremental probabilities for both sulfur dioxide and selenium were in the vicinity of the Carbón I & II power plants. Beyond the Carbón region the airmass transport patterns diverged, with the sulfur dioxide incremental probability high over southern Texas, but for selenium, eastern and southern Texas have about equal incremental probabilities. This indicates a preferred airmass pathway though eastern Texas for the selenium and through southern Texas for sulfur dioxide. The conditional probabilities for sulfur dioxide and selenium do not identify the nearby Carbón region but rather more distant regions in Texas and eastern Tennessee. For eastern Tennessee, there is greater than 70% chance that if an airmass traversed this region it arrived at Big Bend with elevated sulfur dioxide and/or selenium. However, transport from eastern Tennessee was infrequent.

Similar results were found using the MM5 airmass histories, but for sulfur and selenium the incremental probabilities fields showed higher values further south in eastern Texas. In addition, the largest particulate sulfur incremental probability occurred along the Texas-Mexican

border in the vicinity of the Carbón power plants. This is consistent with the observation that during the high sulfur days the MM5 airmass histories had more southerly transport compared to the EDAS/FNL airmass histories.

8.1.3.4 Transport Patterns for 10-Day Airmass Histories

All of the transport analyses were conducted using five-day airmass histories. This was done based on the fact that on average sulfate has an atmospheric lifetime on the order of 3–5 days [*Husar and Husar*, 1978]. However, examination of REMSAD source attribution results indicated longer sulfate lifetimes, and it is known that in non-precipitation airmasses sulfate can have significantly longer lifetimes than 5 days. In addition, even if a 5-day lifetime is correct, after 5 days about one third of the pollutants still exist. In the eastern U.S. the SO_2 emissions are very large and one-third of initial ambient concentration can still be a significant contribution to Texas' and Big Bend's ambient sulfur concentrations. Therefore residence time analyses with longer than 5-day trajectories were conducted.

In order to determine the sensitivity of the airmass history analyses on trajectory length, the residence time analyses were duplicated using 10-day airmass histories. Figure 8-53 presents the decomposed residence time analysis for the ten EDAS/FNL airmass histories. Comparing the results of the 10-day airmass histories to the 5-day (Figure 8-48), it is seen that the largest differences are in the eastern U.S. As shown, the 10-day results show a higher frequency of transport from the eastern U.S., which tends to be at a lower level and slower speed. For example, the accumulation potentials around Georgia increased from ~0.15 s/m to over 0.25 s/m. Also, the average height of the particles along the Ohio River Valley decreased from 3–4 km to about 2 km.

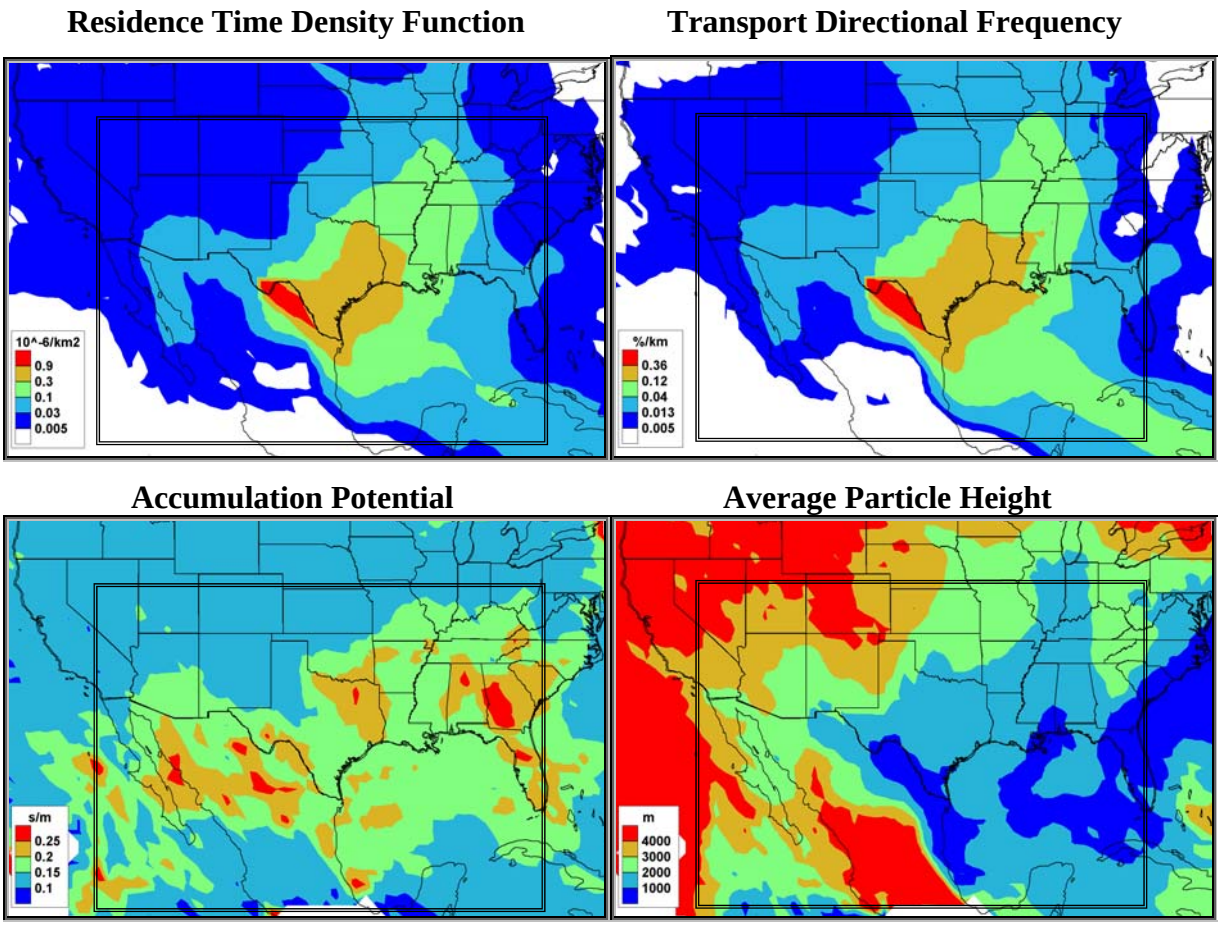

Figure 8-53. The Big Bend NP residence time PDF and its decomposition for the 20% of the days with the highest particulate sulfur. 10-day airmass histories were generated using the EDAS/FNL meteorological data. The box in each plot spans the geographic boundary of the residence time plots in Figure 8-48.

The causes for these changes in the transport conditions from the eastern U.S. due to the increased airmass history length can be seen be examining individual airmass histories. Figure 8-54 presents one of the 10-day airmass histories to Big Bend on September 1. As shown, this airmass was originally composed of elevated and surface level airmasses that converged about four days prior to reaching Big Bend. The elevated airmass traveled from Canada, and five days prior to reaching Big Bend was located 2 to 6 km above the Ohio River Valley. Ten days before reaching Big Bend, the surface level airmass was mostly located over the Midwestern states from Kentucky to Wisconsin. This airmass moved in a counter clockwise direction over this region and 4 to 5 days later was located over Tennessee and Arkansas, at which point it converged with the elevated airmass. Therefore the 5-day airmass histories had only a subset of the airmass trajectories traversing the Ohio River Valley, all of which were elevated and traveling at higher speeds.

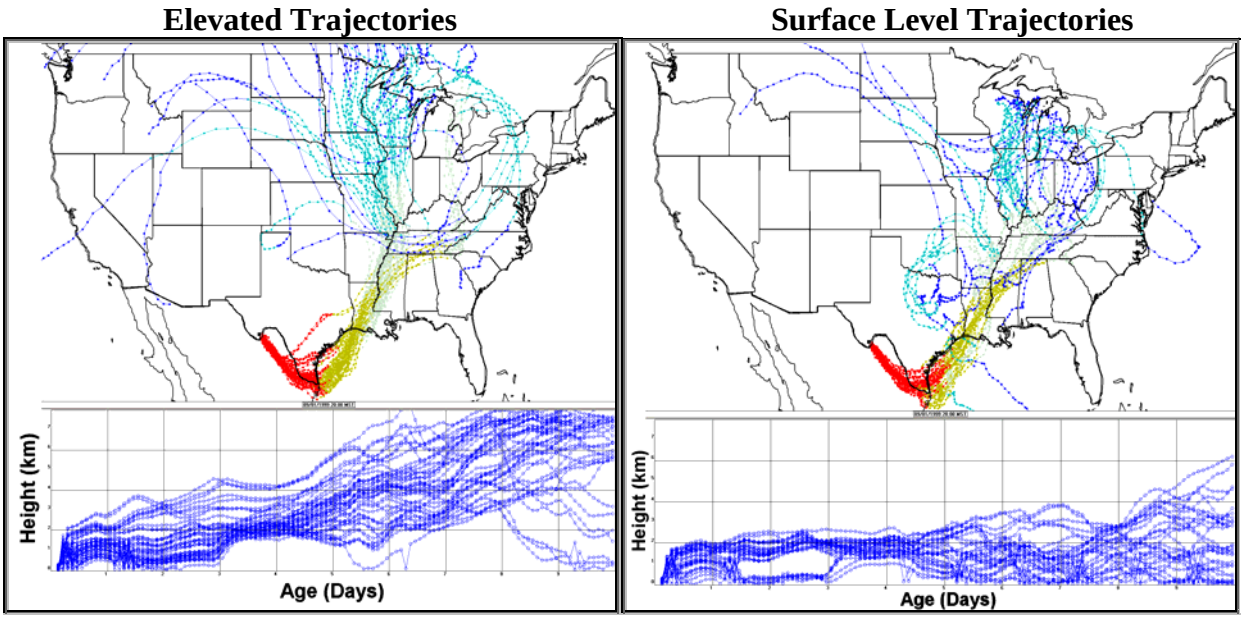

Figure 8-54. Big Bend ten-day airmass history for September 1, 20:00, 1999, generated using the EDAS/FNL data. The airmass history was divided into elevated and surface trajectories. Each color represents two days of transport with the red trajectories 0 to 2 days and blue 8–10 days prior to reaching Big Bend.

The incremental and conditional probabilities for the for the upper 20th percentiles of the particulate sulfur at Big Bend using 10-day airmass histories generated using the EDAS/FNL and MM5 meteorological data are presented in Figure 8-55. As shown, the incremental probabilities are similar to the results using the 5-day airmass histories, but the conditional probabilities show higher probabilities farther from Big Bend into the Great Lakes region. This is consistent with the fact that the incremental probabilities identify more nearby source regions and conditional probabilities tend to identify more distant source regions.

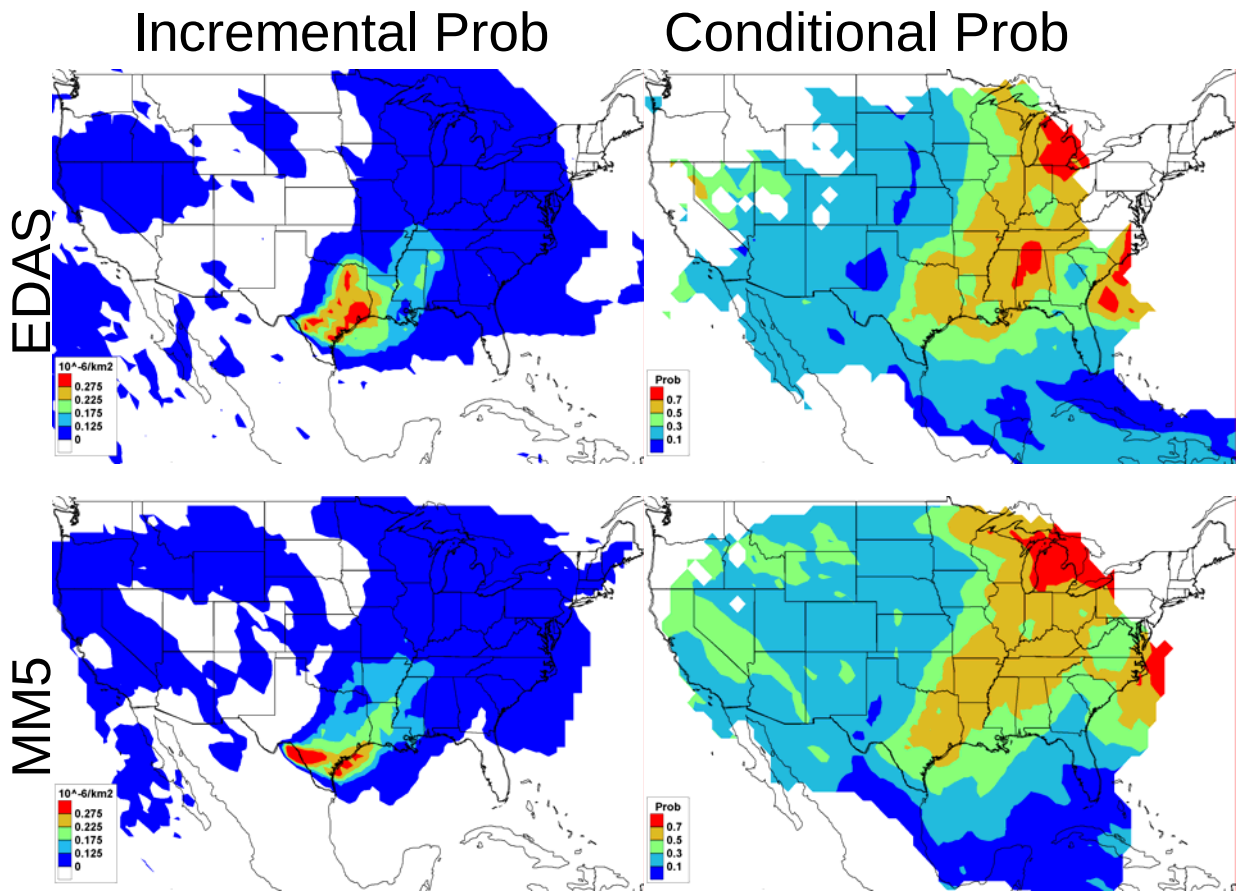

Figure 8-55. The incremental and conditional probabilities for the upper 20th percentiles of the particulate sulfur at Big Bend. These transport probabilities were created using 10-day airmass histories generated using the EDAS/FNL data.

8.1.3.5 Big Bend Climatological Airmass History Analysis

To evaluate the representativeness of the transport meteorology during the BRAVO period, both for other months of the year and for the same months in other years, hourly five-day-long trajectories arriving at Big Bend National Park were calculated with HYSPLIT using EDAS input data for a five-year period (1998 to 2002). Similar analyses for earlier years have been previously reported in *Gebhart et al*. [2000, 2001] and the results are similar.

Figure 8-56 shows the geographic distribution of trajectory residence times for a representative month during each season, aggregated over these years. Histograms of the monthly residence times for different discrete potential source regions in the U.S. and Mexico, showing the same data in a different way, are shown in Figure 8-57. The source areas in Figure 8-57 are the same as those used for TrMB modeling and discussed in chapter 2.

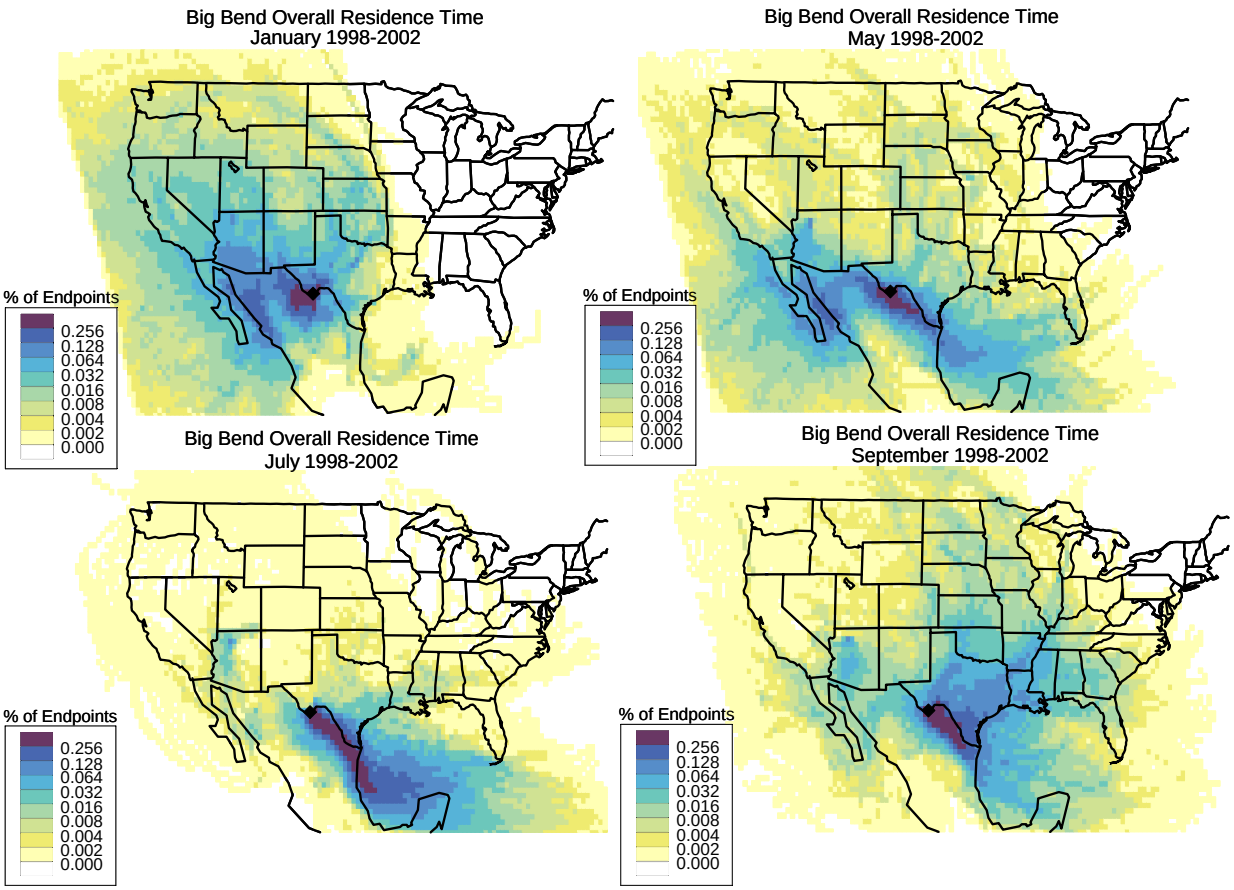

Figure 8-56. Examples of geographic distribution of the fraction of time that air parcels spend during the five days prior to arriving at Big Bend National Park for the months of January, May, July, and September based upon a five-year analysis period (1998 to 2002).

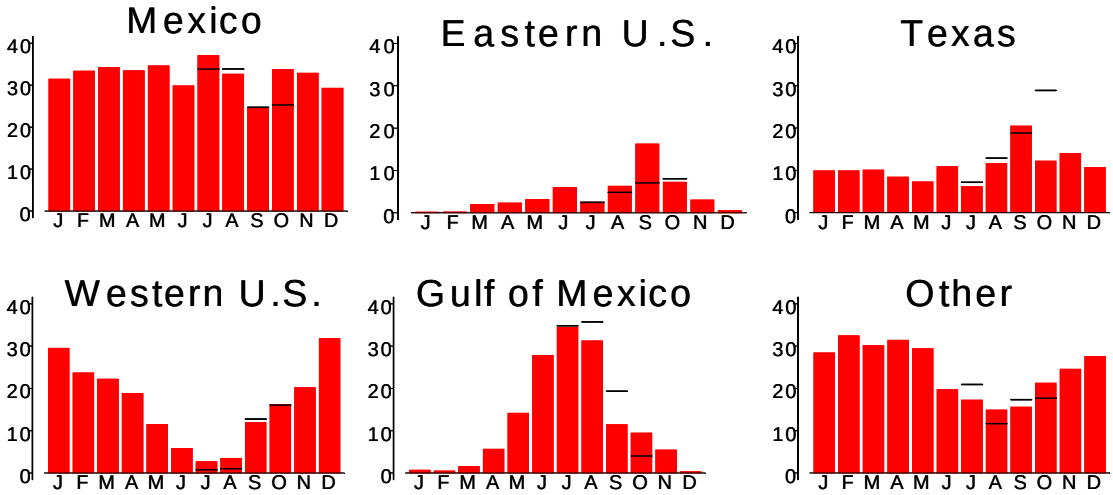

Figure 8-57. Monthly percentages of time that air parcels spend in a region prior to arrival at Big Bend based on 5-day back trajectory calculations for the five-year period from 1998 to 2002. The black lines shown over the months of July through October correspond to the values during the BRAVO study period in 1999. The black line for October was calculated using FNL data rather than EDAS. The plot labeled "Other" represents locations primarily over the Atlantic and Pacific Oceans.

8.1.3.6 Discussion

A fundamental assumption in any airmass history analysis is that the modeled airmass transport is an unbiased simulation of the actual airmass transport. To test this, the airmass histories were validated against measured tracer data using the residence time analysis. The results showed that the CMC model driven by the EDAS/FNL or 36 km MM5 meteorological data was able to properly identify the transport pathways of the tracer data to Big Bend. A similar conclusion was found from the forward simulation of the tracer data using the CMC model in section 5.3. However, there does appear to be a small northerly bias in the transport from the Parish power plant in Houston, Texas. This bias in transport could result in misallocating sulfur attribution to the north of Houston. The results from the conditional and incremental probability analyses highlighted the difficulty in uniquely identifying the tracer source regions using only 1.5 to 4 months of data. For example, transport from San Antonio and Houston to Big Bend often traversed the region where the Carbón power plants reside.

The purpose of this airmass history analysis was to help identify regions with a potential to contribute to the fine particulate sulfur and haze at Big Bend. These results clearly showed that prior to high Big Bend particulate sulfur concentrations, low level and speed transport often occurred over eastern-southeastern Texas and states east of Texas (LA, MS, AL, and AR). In addition, transport over these regions did not often occur prior to low Big Bend sulfur concentrations. These results combined with the fact that eastern Texas and the southeastern U.S. have high sulfur dioxide emissions support the notion that these areas contribute to the sulfate concentrations and haze at Big Bend.

Northeastern Mexico also has large sulfur point and area sources including the Carbón I & II power plants and the Monterrey urban center. However, the association of prior transport over this region with elevated Big Bend sulfur concentrations is inconclusive. The elevated particulate sulfur concentrations at Big Bend were more likely than average to have previously resided over the Carbón I & II plants, but it was found that this region was also a transport corridor for airmasses coming from eastern Texas to Big Bend. Therefore this association may be a coincidence. In addition, prior transport over the Carbón I & II plants and Monterrey regions was associated with low Big Bend particulate sulfur levels. On the other hand, these low particulate sulfur airmasses came directly off the Gulf of Mexico with higher speeds and/or precipitation occurred prior to impacting Big Bend. The higher speeds decrease the possibility of emissions accumulating in the airmass, and the precipitation efficiently removes SO_2 and sulfate particles.

The results using the 5-day airmass histories also showed that higher speeds (> 6 m/s) and elevated transport levels (above 3 km) occurred over the industrial Midwest and eastern Tennessee prior to high sulfur concentrations at Big Bend. The higher speeds and elevation of these airmasses are not conducive for the accumulation of emissions from this region. However, these two regions have some of the highest SO_2 emissions in the U.S. The analysis was redone using 10-day airmass histories. In this case, more frequent, lower level, and lower speed transport over the industrial Midwestern states occurred. These conditions are conducive to bringing emissions from this region to Big Bend, but this is dependent on a long lifetime for the particulate sulfur.

Confidence in the airmass histories and residence time analysis also comes from the examination of the transport patterns for elevated Big Bend concentrations of fine particle sulfur,

sulfur dioxide, and selenium compared to average days. Taken together, these results showed a consistency among the transport pathways that could be explained from known sources and atmospheric lifetimes of each species. Sulfur dioxide is a primary species with an atmospheric lifetime on the order of several days, about half of particulate sulfate's [*Husar et al.*, 1978]. Therefore Big Bend's sulfur dioxide concentration should be influenced by more nearby source regions compared to particulate sulfate. The sulfur dioxide incremental probabilities clearly identified the Carbón I & II power plant region, ~250 km from Big Bend, as a potential source region, while the sulfur incremental probabilities indicated more distant and distributed source regions from the Carbón region to eastern-southeastern Texas. Selenium is a primary fine particle species primarily emitted from coal-fired power plants without wet scrubbers [*Watson et al.*, 2001; *Chow et al.*, 2004]. These results identified the Carbón region as a likely source region as well as the more distant eastern Texas lignite belt which has a number of coal-fired power plants without wet scrubbers.

The robustness of the transport analysis associated with high particulate sulfur was also tested by using the two sets of meteorological data. This resulted in different airmass transport patterns with the EDAS/FNL airmass histories having greater transport from northeastern Texas than the MM5 airmass histories, while the MM5 airmass histories had a higher probability of transport from southeast Texas and states east of Texas. In addition, the MM5 results produced higher speed, thus longer-range airmass transport. These differences do not impact the conclusion from this analysis. However, these differences will result in different source apportionment estimates depending on the meteorological data used in the analysis.

8.1.4 Trajectory Max - Upper Bounds on Source Contribution to Big Bend's Particulate Sulfur

The trajectory max is a simple airmass history technique to place an extreme upper bound on a source region's contribution to Big Bend's particulate sulfur. Trajectory max assumes that if an airmass traversed a source region then the receptor concentration is solely due to emissions from that source region. Therefore the source region in which the receptor resides will have a maximum source contribution of 100%. This technique relies on an unbiased assessment of the average airmass transport from the source regions to the receptor. Section 2.3.1.4 describes the method in detail. This analysis used the same airmass histories generated from the EDAS/FNL and MM5 meteorological data that were used to evaluate the airmass transport to Big Bend National Park in chapter 5 and section 8.1.3.

The results of this analysis using the EDAS/FNL and MM5 airmass histories are presented on a uniform 80 x 80 km grid (Figures 8-58A and 8-59A) and in large source regions (Figures 8-58B and 8-59B) defined in Figure 2-16. As shown, the maximum source contribution patterns are similar to the residence time plots for the 20% highest particulate sulfur days (Figures 8-48 and 8-51). This is expected since the transport patterns on the highest particulate sulfur concentrations will have the largest weights in the source contribution averaging. Also, the maximum source contribution drops off sharply from the receptor to less than 25% past the Mississippi River, west of Texas, and in north Kansas (Figure 8-58A). However, maximum source contributions from the large source regions are above 35% in regions such as the Mid-Atlantic states.

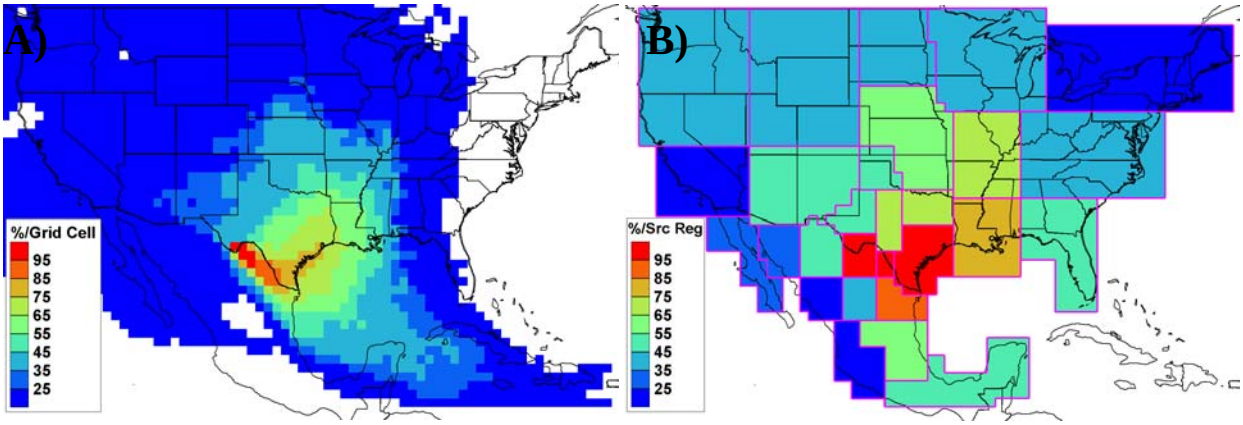

Figure 8-58. The maximum source contributions to Big Bend's particulate sulfur as estimated from EDAS/FNL airmass histories. A) The maximum source contribution for each 80 x 80 km_2 grid cell. B) The maximum source contribution for each source region defined in Figure 2-14.

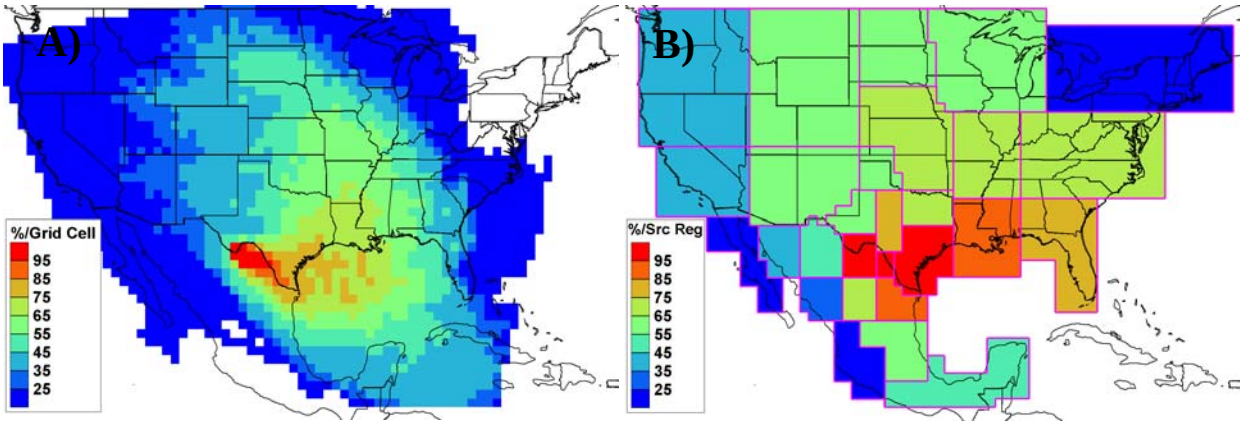

Figure 8-59. The maximum source contributions to Big Bend's particulate sulfur as estimated from MM5 airmass histories. A) The maximum source contribution for each 80 x 80 km_2 grid cell. B) The maximum source contribution for each source region defined in Figure 2-14.

There are two important differences between the EDAS/FNL- and MM5-derived maximum source contributions shown in Figures 8-12 and 8-13. First, the MM5 results have higher source contributions from distant source regions. For example, the MM5-derived maximum source contributions from the Dakotas and western Great Lakes states are 55 to 65% compared to 35 to 45% for the EDAS/FNL results. Second, the MM5 results estimate higher source maximum contributions from the eastern United States from the Ohio River Valley to the Gulf of Mexico with a maximum value of over 85% from the Louisiana region and 75% from Florida.

8.2 Quantitative

8.2.1 Synthesis Inversion – Merging Air Quality Model Source Apportionment Results and Receptor Data

The REMSAD model was employed to predict the sulfate concentrations in most of North America and to estimate the contribution of sulfate from ten major U.S. and Mexican source regions and the model boundary conditions to Big Bend and the other BRAVO monitoring sites. The CMAQ-MADRID model was similarly employed, but predicted sulfate over a smaller region centered on Texas and estimated the sulfate contributions from Texas,

Mexico, western U.S., and eastern U.S. source regions as well as the boundary conditions [*Electric Power Research Institute*, 2004]. The CMAQ-MADRID boundary conditions were generated from the REMSAD-simulated sulfate and SO_2 concentrations which were first nudged to observed data by comparing the REMSAD simulated sulfate and SO_2 concentrations to measured data from the IMPROVE and CASTNet monitoring networks. CMAQ-MADRID also used an upper estimate of the Carbón facilities' SO_2 emissions, 241,000 tons/yr compared to 152,000 tons/yr used by REMSAD. The other Mexican SO_2 emissions in the CMAQ-MADRID domain were doubled compared to what was used in REMSAD. This doubling of emissions was done due to an apparent underestimation in Mexico's contribution to sulfate throughout Texas in the REMSAD model runs.

Both REMSAD and CMAQ-MADRID were run using the 36 km MM5 wind field. CMAQ-MADRID was originally to be used to simulate concentrations on only the MM5 4 and 12 km grids which were nested in the larger 36 km grid. However, for performance reasons, CMAQ-MADRID was run with the 36 km MM5 meteorological data [*EPRI*, 2004]. The emission input fields were only available for the smaller 4 and 12 km domains. Therefore, the CMAQ-MADRID simulation was confined to the smaller 12 km domain.

Overall, REMSAD predicted sulfate across Texas with a 65% gross error, 76 % RMS error, and a bias (difference of averages) of 8%. At Big Bend the gross and RMS errors were 62% and 73%, respectively, and with a bias of -18%. The CMAQ-MADRID model had a gross error of 47%, RMS error of 86%, and bias of 29% for all BRAVO sites, and at Big Bend the gross and RMS errors were 46% and 60%, respectively, and had no bias. These are satisfactory modeling results, but there were spatial and temporal trends in the biases (see section 6.2). For example, REMSAD nearly uniformly underestimated the sulfate concentrations throughout Texas during July and overestimated them in October. The positive bias in eastern Texas was at least partly due to the contributions from the eastern U.S. sources being overestimated.

In order to account for these biases, the REMSAD and CMAQ-MADRID sulfate source attribution results were regressed against the observed sulfate concentrations throughout Texas. The same simulated attribution results are then scaled by the regression coefficients to derive alternative source attribution estimates that, when summed together, better fit the measured data. This approach compensates for some of the systematic errors present in the two simulations of the air quality models and thus should provide more accurate attributions of Big Bend aerosol. The technique is based on the synthesis inversion technique which is fully described in section 2.3.2.3.1 and validated in section 7.2.3. This technique is based upon the equation:

$$c_i = \sum_j G_{ij} s_j + \varepsilon_i = m_i + \varepsilon_i \qquad (2\text{-}33)$$

where c_i is a vector of sulfate observations (the measured fine particulate sulfur concentration multiplied by three.); G_{ij} is a matrix of the source attribution from each source region/time pair to each observation; s_j are the source attribution scaling coefficients; m_i are the modeled concentration values; and ε_i are the errors in c_i. s_j identify spatial or temporal biases in the original REMSAD source attributions due to errors in the emission, transport, chemistry and/or removal process of sulfur. s_j are found by using a constrained least squares regression to invert equation 2-33. In essence, the resulting scaling coefficients partition the underestimated mass back to the source regions and remove overestimated mass from the source regions. The revised predicted sulfate concentrations then best match the measured data in a least square sense. Once

the scaling coefficients are calculated, the synthesized REMSAD source attribution results are estimated by $c_{ij} = G_{ij} s_j$.

8.2.1.1 Spatial and Temporal Variability in the Source Attribution Scaling Coefficients

In general, as more data with varied source attributions are incorporated into the regression analysis, the source attribution scaling coefficients are more stable with smaller errors. Therefore, it is desirable to incorporate data for as long a time period and from as many sites as possible. However, the scaling coefficients compensate for errors in the modeled emissions and physical and chemical processes and will vary in time and space. If data with compensating biases are incorporated into the analysis, then the regression will not be able to account for either bias in the system. The scaling coefficients represent an average bias correction for the spatial and temporal periods used in the analysis. If the biases are large-scale, for example, errors in emissions or underestimation of diffusion, then the scaling coefficients will be applicable to a subset of the monitoring sites and time period used in the analysis. However, if the biases vary in a non-random way over spatial scales of interest, e.g., Texas, and over shorter time periods used in the analysis, then it will be inappropriate to apply these coefficients to a large subset of the monitoring sites or time period used in the analysis. This section examines the spatial and temporal variability to determine the best way to group the observed sulfate observation over the BRAVO monitoring sites and time period. The following uses the REMSAD model source attributions; however, similar results were found using the CMAQ-MADRID source attributions.

8.2.1.1.1 Spatial Variability

The spatial variability was examined by performing the regression analysis using data from each BRAVO monitoring site over the entire BRAVO time period. A constrained regression analysis was used where the coefficient could be within a factor of 4 of the REMSAD source attribution results, e.g., between 0.25 and 4. The regression was performed using all eleven source regions. The results for each monitoring site are presented in Table 8-3. Each regression used a maximum of 112 data points and a minimum of 84 valid data points or a 75% complete time series. Scaling coefficients are also only shown if the source region contributed 6% or more to the receptor site on average as estimated by REMSAD. The four eastern U.S. source regions were aggregated together and the west Texas source region is not shown since it contributed 6% or more too only two receptor sites.

Table 8-3. Source attribution scaling coefficients and standard errors resulting from the regression of the REMSAD source attributions against the particulate sulfur data measured at each BRAVO monitoring site over the entire time period. The monitoring sites needed 75% or 84 valid data points for the regression to be conducted. Regression coefficients are shown only if the source region contributed 6% or more to the receptor site on average as estimated by REMSAD. The West Texas source region is not shown because it rarely contributed 6% of the sulfate to any site. The four eastern U.S. source regions were aggregated together. Source regions with a regression coefficient more than a factor of two of the average standard error away from the average coefficients across all sites are bolded.

			Source Attribution Scaling Coefficients						
Monitoring Site	**Bias (%)**	**r**	**Carbón**	**Rest Mex.**	**NE TX**	**SE TX**	**E U.S.**	**W U.S.**	**Bndy Cnd**
K-Bar 24-hour	-10	0.57	1.9 ± 0.4	2.6 ± 0.6		1.4 ± 1.1	0.7 ± 0.5	0.3 ± 1.1	1.5 ± 1.7
San Vicente	-10	0.57	2.0 ± 0.5	2.7 ± 0.7		1.2 ± 1.1	0.7 ± 0.5	0.3 ± 1.1	
Persimmon Gap	-7	0.56	2.5 ± 0.5	1.8 ± 0.8		2.3 ± 0.8	0.5 ± 0.4	0.3 ± 1.0	1.8 ± 1.5
Marathon	-7	0.54	2.5 ± 0.5	1.7 ± 0.8		2.0 ± 0.7	0.4 ± 0.4	0.3 ± 0.9	1.7 ± 1.4
Fort Stockton	-7	0.56	2.1 ± 0.5	1.6 ± 0.8		2.2 ± 0.6	0.4 ± 0.4	0.3 ± 0.8	1.9 ± 1.2

Monahans Sandhills	-7	0.64	1.6 ± 0.6			**2.7 ± 0.6**	0.6 ± 0.3	0.3 ± 0.9	2.6 ± 1.1
Esperanza	-3	0.54	1.9 ± 0.3	1.3 ± 0.3		1.0 ± 0.5	0.4 ± 0.4	0.3 ± 0.4	3.7 ± 0.8
McDonald Obs.	-8	0.55	2.4 ± 0.4	0.8 ± 0.4		1.5 ± 0.5	0.5 ± 0.4	0.3 ± 0.5	2.3 ± 1.0
Presidio	-10	0.50	1.5 ± 0.4	1.4 ± 0.5	0.3 ± 1.0	0.6 ± 0.9	0.7 ± 0.5	0.3 ± 0.8	2.6 ± 1.5
LBJ NHS	-8	0.64			0.3 ± 0.6	1.5 ± 0.2	0.6 ± 0.2		0.5 ± 1.0
Fort McKavett	-5	0.71			0.3 ± 0.4	1.6 ± 0.3	0.6 ± 0.2	0.3 ± 0.8	1.2 ± 0.9
Lake Colorado City	-3	0.73			0.3 ± 0.3	1.7 ± 0.3	0.6 ± 0.2	0.3 ± 0.5	2.3 ± 0.7
Fort Lancaster	-7	0.54	1.1 ± 0.7		0.3 ± 0.6	2.3 ± 0.5	0.4 ± 0.3	0.3 ± 1.0	2.3 ± 1.1
Sanderson	-8	0.45	1.7 ± 0.7			2.3 ± 0.6	0.3 ± 0.4	0.3 ± 1.3	
Langtry	-9	0.59	1.5 ± 0.7			2.2 ± 0.5	0.6 ± 0.3	0.3 ± 1.2	
Amistad	-10	0.64	**0.3 ± 0.6**			2.3 ± 0.5	0.6 ± 0.3	0.3 ± 1.2	1.3 ± 1.3
Brackettville	-11	0.65			0.3 ± 0.7	2.0 ± 0.4	0.6 ± 0.2	0.3 ± 1.3	1.0 ± 1.2
Eagle Pass	-15	0.51			0.3 ± 0.8	1.7 ± 0.5	0.5 ± 0.2	0.3 ± 1.5	0.9 ± 1.4
Laredo	-14	0.61			0.3 ± 0.7	1.0 ± 0.7	0.7 ± 0.2		1.9 ± 1.4
Falcon Dam	-14	0.58		**4.0 ± 0.7**	0.3 ± 0.8	0.7 ± 1.0	0.5 ± 0.2		2.7 ± 1.2
Laguna Atascosa	-24	0.63			0.3 ± 1.2	**0.3 ± 0.8**	0.7 ± 0.2		3.5 ± 1.4
Lake Corpus Christi	-13	0.67			0.3 ± 0.7	0.6 ± 0.5	0.7 ± 0.2		2.1 ± 1.1
Pleasanton	-15	0.69			0.3 ± 0.8	0.9 ± 0.3	0.8 ± 0.2		0.8 ± 1.3
Everton Ranch	-16	0.71			0.3 ± 0.7	1.2 ± 0.4	0.6 ± 0.2		1.7 ± 1.3
Hagerman	-2	0.71			0.7 ± 0.4	2.1 ± 0.5	0.6 ± 0.1	0.3 ± 0.6	2.6 ± 0.7
Purtis Creek	-7	0.71			0.4 ± 0.3	1.7 ± 0.4	0.8 ± 0.1	0.0 ± 0.0	2.5 ± 0.7
Stephenville	-6	0.61			0.6 ± 0.6	1.3 ± 0.4	0.7 ± 0.2	0.3 ± 1.0	2.3 ± 0.9
Stillhouse Lake	-8	0.64			0.3 ± 0.5	1.1 ± 0.2	0.7 ± 0.1		2.2 ± 0.9
Somerville Lake	-8	0.66			0.3 ± 0.3	1.1 ± 0.2	0.7 ± 0.1		2.0 ± 0.9
Aransas	-14	0.71			0.3 ± 0.7	**0.3 ± 0.5**	0.8 ± 0.1		2.0 ± 1.1
San Bernard	-13	0.73				**0.3 ± 0.4**	0.7 ± 0.1		3.3 ± 1.0
Big Thicket	-6	0.74				1.6 ± 0.3	0.6 ± 0.1		2.1 ± 0.8
Center	-4	0.69				1.8 ± 0.4	0.6 ± 0.1		1.8 ± 0.7
Wright Patman	-0.5	0.67			0.8 ± 0.4		0.5 ± 0.1		2.4 ± 0.8
Guadalupe Mtn	Not Enough Data								
Wichita Mtn	Not Enough Data								
Padre Island	Not Enough Data								
Avg Coef ± Avg Err	-9	0.61	1.8 ± 0.5	2 ± 0.6	0.3 ± 0.7	1.45 ± 0.55	0.6 ± 0.3	0.3 ± 1	2.1 ± 1.1
Standard Deviation			0.6	1	0.17	0.7	0.13	0	0.75

As shown in Table 8-3, the scaling coefficients over most source regions are within the average standard error across all sites. The southeast Texas source region is an exception where half of the coefficients are more than one standard error from the average. Only six of the scaling coefficients are greater than the average by more than a factor of 2 of the average standard error. This occurs for the southeast Texas source region at the three Texas Gulf Coast sites, San Bernard, Aransas, and Laguna Atascosa, and Monahans Sandhills located in western Texas. The Carbón scaling coefficient for Amistad, Texas, is also significantly smaller than average. Amistad is about 70 km from the Carbón power plants. Last, the Rest of Mexico source region is significantly greater than average for Falcon Dam which is located along the Texas/Mexican

border. The correlation coefficient (r) for each inversion varied between 0.45 and 0.74 and was 0.57 at Big Bend.

8.2.1.1.2 Temporal Variability

The temporal variability in the source attribution scaling coefficients was examined by performing the regression analysis using data from all monitoring sites for five consecutive days which gave a maximum of 185 data values. The scaling coefficients were again constrained to be between 0.25 and 4. To give each monitoring site equal weight in the regression analysis, the observed data and REMSAD source attributions for each monitoring site were normalized by the monitoring site's average observed sulfate concentration. A moving five-day window was used over the entire time period and the scaling coefficients were attributed to the center day resulting in daily coefficients from July 9–October 28, 1999.

The daily variability of the regression coefficients are presented in Figure 8-60 and their averages over the BRAVO time period are presented in Table 8-4. As shown in Table 8-4, the average coefficients over Texas and the eastern U.S. are ~1, and 1.9 for Mexico. In general, the standard deviations of the coefficients over time are greater than they were over space, indicating greater temporal variability in time than in space. This is also evident in Figure 8-60, where the coefficients in most regions fluctuate between the lower bound of 0.25 and 3. The coefficients also show temporal trends with coefficients greater than 1 during July and early August and below 1 in October. This is expected due to the monthly biases in the REMSAD modeling results (see section 6.2).

Table 8-4. Synthesized REMSAD daily source attribution scaling coefficients and their standard error averaged over the entire BRAVO period for each source regions. The standard deviation of the scaling coefficients is also provided.

Source Region	Average Scaling Coef.	Average Std Error	Scaling Coef Std Dev
Carbón	1.44	0.41	0.90
Rest of Mexico	2.36	1.15	1.54
NE Texas	0.85	0.89	0.65
SE Texas	0.95	0.25	0.55
West Texas	1.36	2.06	1.52
Louisiana	1.16	1.20	1.16
East Central	1.08	3.92	1.25
MO/AR/IL	0.56	3.57	0.62
Rest of Eastern U.S.	1.01	1.02	1.11
Western U.S.	0.70	6.83	1.13
Boundary Cond.	3.26	2.33	1.09
Texas	1.05	1.07	1.03
Mexico	1.90	0.78	1.34
Eastern U.S.	0.95	2.43	1.09

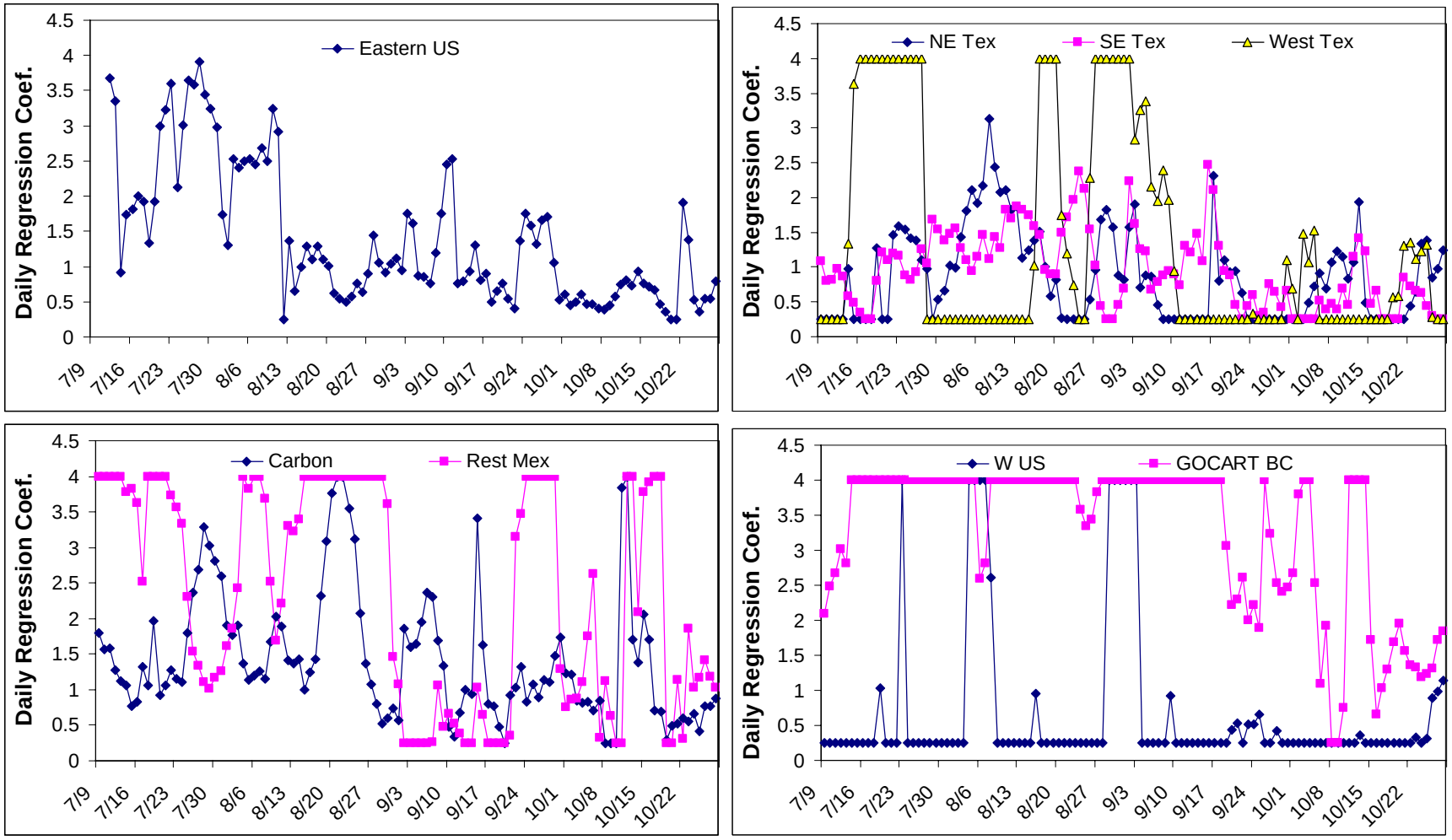

Figure 8-60. Synthesized REMSAD daily source attribution scaling coefficients using all sites and a 5-day moving window. The four eastern U.S. source regions were aggregated together because of high collinearities between these source regions.

Instabilities in the regression coefficients for several regions are also evident. The coefficients for the western Texas and western U.S. source regions fluctuate between the constraints 0.25 and 4. Both source regions had small contributions to the predicted sulfate in Texas and the regression analysis was most likely unable to resolve them due to the errors in the system. This is also reflected in the fact that most of these coefficients were not significantly different from 0 or 1 as defined by the standard error. Eastern U.S. sources also demonstrated instabilities during July and early August when they had little influence on the simulated sulfate. Last, the boundary conditions also illustrate instabilities particularly from July 14–September 20. During this period the boundary conditions were highly collinear with the other source regions.

The performance of the regression analysis is presented in Table 8-5 where the observed sulfur concentrations are compared to the predicted sulfate concentrations for each site, using the temporally varying regression coefficients. As shown, the correlation coefficients vary between 0.64 and 0.88 and have a relative RMS error between 33 and 65% and a bias between -25 and 13%. At the Big Bend monitoring site at K-Bar, r = 0.79 and the RMS error was 47%. For all monitoring sites the correlation coefficients are larger and the RMS errors are smaller compared to the results for the spatially varying regression coefficients (Table 8-3).

Table 8-5. The performance statistics for each BRAVO monitoring site using the temporally varying source attribution scaling coefficients derived from Synthesized REMSAD.

		Average				
Monitoring Site	**# Obs**	**Observation**	**Prediction**	**Bias (%)**	**RMS Error (%)**	**r**
K-Bar	109	2.47	2.11	-15	47	0.79
San Vicente	104	2.58	2.14	-17	44	0.81
Persimmon Gap	106	2.72	2.29	-16	42	0.81
Marathon	110	2.54	2.30	-9	40	0.80
Fort Stockton	112	2.51	2.41	-4	38	0.80
Monahans Sandhills	110	2.95	2.66	-10	38	0.83
Esperanza	91	1.95	2.06	6	38	0.68
McDonald Obs.	94	2.11	2.18	3	34	0.81
Presidio	94	2.30	2.18	-5	46	0.70
LBJ NHS	108	3.07	3.11	1	39	0.83
Fort McKavett	111	2.59	2.64	2	38	0.86
Lake Colorado City	97	2.80	2.95	5	35	0.85
Fort Lancaster	96	3.05	2.83	-7	46	0.68
Sanderson	110	3.01	2.58	-14	49	0.64
Langtry	102	3.46	2.88	-17	42	0.80
Amistad	110	3.05	2.80	-8	39	0.81
Brackettville	103	3.01	2.58	-14	40	0.84
Eagle Pass	101	2.75	2.58	-6	48	0.73
Laredo	108	2.88	2.58	-10	55	0.69
Falcon Dam	94	3.04	2.64	-13	43	0.75
Laguna Atascosa	108	2.87	2.14	-25	57	0.72
Lake Corpus Christi	81	3.13	3.00	-4	47	0.72
Pleasanton	101	3.18	3.05	-4	41	0.85
Everton Ranch	84	3.54	3.37	-5	45	0.78
Hagerman	93	4.07	3.78	-7	33	0.88
Purtis Creek	89	4.28	3.83	-11	35	0.83
Stephenville	91	3.55	3.35	-6	36	0.86

Stillhouse Lake	111	3.54	3.36	-5	36	0.86
Somerville Lake	101	3.58	3.59	0	39	0.81
Aransas	86	3.66	3.23	-12	43	0.81
San Bernard	97	3.94	3.62	-8	47	0.77
Big Thicket	88	4.18	3.98	-5	38	0.80
Center	96	4.00	4.19	5	36	0.84
Wright Patman	95	4.39	4.70	7	40	0.82
Guadalupe Mtns						
Wichita Mtns						
Padre Island						
Average	97	3.14	2.93	-7	42	0.79

8.2.1.2 The Optimum Synthesized REMSAD

It is evident from the above results that the regression coefficients vary more in time than in space over Texas, and the regression performance improved for the temporally varying coefficients over the spatially varying coefficients. Therefore the model is better able to account for the spatial variability in the observed sulfate, but does not capture the day-to-day variability.

Based on these results, the synthesis inversion was used to calculate spatially invariant but temporally variable source attribution scaling coefficients. This was done by incorporating data from most BRAVO monitoring sites and performing the inversion for each day. To better account for random spatial errors in the model biases and incorporate as much data as possible in each regression, multiple days were included in the analysis. Therefore errors such as the temporal displacements of a frontal passage by a day or so would be averaged out. The source contributions from the eastern U.S. were found to be collinear, so these four source regions were combined into a single eastern U.S. source region.

The constrained least square regression used in the previous analysis has several shortcomings. First, the constraints of 0.25 and 4 were subjective, and when the regression coefficients hit the constraint boundary, the standard errors are not the true standard error of the analysis. Second, the regression coefficients for source regions such as the western U.S. displayed large instabilities, indicating the analysis was unable to resolve their contribution, which could result in other biases in the system. To overcome these shortcomings, a Bayesian least square regression technique was used [*Enting,* 2002]. This technique incorporates into the regression analysis prior estimates of the source attribution scaling coefficients and an assumed normally distributed error for these coefficients. This *a-prior* information results in more stable regression coefficients for source regions that are poorly resolved in the constrained regression and has meaningful standard errors for all coefficients. The equation for the Bayesian least square regression is:

$$J(s) = \Sigma_{jk} (y_i - \Sigma_u G_{iu} s_u) X_{jk} (y_k - \Sigma_v G_{kv} s_v) + \Sigma_{uv} (s_u - z_u) W_{uv} (s_v - z_v) \quad (8\text{-}1)$$

where y is a vector of the observed values ($\mu g/m^3$), G is a matrix of the source attribution from each source region/time pair to each observation y_i ($\mu g/m^3$), X is a diagonal matrix of the observation variances $(\mu g/m^3)^2$, s is the source attribution scaling coefficient, z is a vector of the prior source attribution scaling coefficients, and W is a diagonal matrix of the prior source attribution scaling coefficients variances $(\mu g/m^3)^2$.

In this analysis the priors (z) were assumed to be 1, i.e. an unbiased model, and the variances were estimated from comparisons of the model results to IMPROVE and CASTNet measured sulfate data which were not used in this analysis. The comparison with the measured data showed that the REMSAD simulation of eastern U.S. sulfate could be a factor of three higher than the measured sulfate (see chapter 6). No observed data were available for Mexico, but it is known that the Mexican SO_2 emissions had large uncertainties compared to those in the U.S. Therefore the prior variances for the Mexican and eastern U.S. source regions were set to 4, or an error of 2. The variances for the two eastern Texas source regions were set to 2. A variance of 4 was not used since this resulted in some large negative coefficients. The variances for the West Texas, western U.S., and boundary condition source regions were set to 0.5. This smaller variance helped to constrain these coefficients to be around 1, minimizing the instabilities identified in the constrained regression analysis. The regression analyses occasionally resulted in small negative source attribution scaling coefficients and these coefficients were set to 0.

In section 8.2.1.1.1, it was shown that the source attribution scaling coefficients derived for each monitoring site using all data generally did not vary significantly in space. However, there were several monitoring sites that had significantly different coefficients. The inclusion of the data from these monitoring sites could result in scaling coefficients that were not directly applicable to the Big Bend data. To better identify the monitoring sites and time periods which had significantly different biases compared to Big Bend, the synthesis inversion was applied to each monitoring site over three different time periods: July 9–August 5, August 6–September 19, and September 20–October 28. Each of these time periods displayed distinct airmass transport patterns to Big Bend with transport primarily from east-southeast of Big Bend from July 9–August 5, transport primarily from northeast-southeast of Big Bend from August 6–September 19, and transport from any direction after September 20. The scaling coefficients and their errors for the Texas, Mexican, and eastern U.S. source regions are presented in Table 8-6. Note that some of the scaling coefficient had large negative number, < -1. These values mostly occurred for the NE Texas source region when this source region had a small (< 10%) average contribution to the receptor site.

A t-test was used to determine if the scaling coefficient for a given monitoring site was statistically different from Big Bend's. If a scaling coefficient for a monitoring site had a t value greater than 3 and the source region contributed 10% or more to the monitoring site on average, then it was excluded from the analysis. This is a conservative cut off, but was chosen to minimize any false positives and the exclusion of valid data. All bolded coefficients in Tables 8-6a, b, and c failed the hypothesis test and these data were excluded from the analysis. As shown, data from all monitoring sites were used from July 9–August 5 and September 20–October 28. However, data from 19 of the 37 sites were not used in the analysis from August 6–September 19.

Table 8-6a. Source attribution scaling coefficients and standard errors resulting from the regression of the REMSAD source attribution estimates against the particulate sulfate data measured at each BRAVO monitoring site from July 9–August 5. The source attribution scaling coefficients for each monitoring site were compared to the Big Bend values using Student t statistics. Source regions that contributed more than 10% of the sulfate as estimated by REMSAD are underlined and if they also had a t value greater than 3 they are bolded. The scaling coefficients for the West Texas, the western U.S., and boundary conditions are not shown.

Source Regions	Carbón	Rest of Mexico	NE Texas	SE Texas	Eastern U.S.
Big Bend (K-Bar)	1.7 ± 0.6	2.2 ± 0.5	1.1 ± 1.0	1.4 ± 1.0	2.0 ± 0.7
San Vicente	2.0 ± 0.6	2.0 ± 0.5	1.2 ± 1.0	1.6 ± 0.9	2.4 ± 0.7
Persimmon Gap	2.1 ± 0.5	1.5 ± 0.6	1.1 ± 1.0	1.3 ± 0.8	1.6 ± 0.6
Marathon	2.5 ± 0.5	1.5 ± 0.6	0.8 ± 1.0	1.2 ± 0.8	1.2 ± 0.6
Fort Stockton	2.3 ± 0.5	1.5 ± 0.6	0.8 ± 1.0	1.2 ± 0.7	1.5 ± 0.6
Monahans Sandhills	1.7 ± 0.6	1.3 ± 0.7	1.0 ± 1.0	1.6 ± 0.7	1.6 ± 0.5
Esperanza	2.0 ± 0.8	1.1 ± 0.5	1.0 ± 1.0	0.8 ± 0.9	0.9 ± 0.8
McDonald Obs	2.0 ± 0.7	0.8 ± 0.5	1.0 ± 1.0	1.6 ± 0.9	1.8 ± 0.7
Presidio	0.9 ± 0.7	1.1 ± 0.5	1.0 ± 1.0	0.9 ± 1.0	1.1 ± 0.8
LBJ	1.0 ± 1.0	1.0 ± 1.0	1.1 ± 1.0	1.4 ± 0.2	1.1 ± 0.4
Fort McKavett	1.4 ± 1.0	2.7 ± 0.8	1.0 ± 1.0	1.1 ± 0.4	1.0 ± 0.6
Lake Colorado City	1.2 ± 0.8	1.9 ± 0.8	0.7 ± 0.9	1.5 ± 0.6	0.8 ± 0.6
Fort Lancaster	2.0 ± 0.7	2.1 ± 0.8	1.1 ± 1.0	1.5 ± 0.7	0.2 ± 0.6
Sanderson	2.4 ± 0.5	3.0 ± 0.8	1.0 ± 1.0	1.3 ± 0.6	1.8 ± 0.5
Langtry	3.0 ± 0.5	1.6 ± 0.8	1.0 ± 1.0	1.5 ± 0.5	1.8 ± 0.5
Amistad	1.7 ± 0.5	2.2 ± 0.8	1.1 ± 1.0	1.1 ± 0.6	2.3 ± 0.5
Brackettville	0.2 ± 1.0	2.3 ± 0.8	1.1 ± 1.0	0.6 ± 0.5	2.5 ± 0.5
Eagle Pass	0.0 ± 1.0	3.1 ± 0.7	1.0 ± 1.0	1.1 ± 0.8	2.0 ± 0.5
Laredo	1.0 ± 1.0	3.5 ± 0.7	0.9 ± 1.0	0.8 ± 1.0	2.1 ± 0.4
Falcon Dam	1.0 ± 1.0	3.2 ± 0.9	1.0 ± 1.0	1.2 ± 1.0	1.8 ± 0.5
Laguna Atascosa	1.0 ± 1.0	1.0 ± 1.0	0.7 ± 1.0	1.0 ± 1.0	1.3 ± 0.3
North Padre Island	1.0 ± 1.0	1.4 ± 1.0	0.9 ± 1.0	1.3 ± 1.0	2.7 ± 0.3
Lake Corpus Christi	1.0 ± 1.0	1.0 ± 1.0	1.0 ± 1.0	2.1 ± 0.9	0.4 ± 0.3
Pleasanton	1.0 ± 1.0	1.6 ± 1.0	0.8 ± 1.0	1.0 ± 0.3	1.7 ± 0.3
Everton Ranch	1.0 ± 1.0	0.9 ± 1.0	1.2 ± 1.0	2.7 ± 0.8	2.0 ± 0.3
Hagerman	1.0 ± 1.0	1.0 ± 1.0	0.9 ± 0.8	1.3 ± 0.4	0.8 ± 0.1
Purtis Creek	1.0 ± 1.0	1.0 ± 1.0	1.2 ± 0.7	1.4 ± 0.6	1.1 ± 0.1
Stephenville	1.0 ± 1.0	1.0 ± 1.0	1.5 ± 0.8	1.5 ± 0.3	0.9 ± 0.2
Stillhouse Lake	1.0 ± 1.0	1.1 ± 1.0	1.9 ± 0.7	0.8 ± 0.2	1.1 ± 0.2
Somerville Lake	1.0 ± 1.0	1.0 ± 1.0	1.0 ± 1.0	1.0 ± 0.2	1.1 ± 0.2
Aransas	1.0 ± 1.0	0.9 ± 1.0	0.9 ± 1.0	0.9 ± 1.0	1.6 ± 0.3
San Bernard	1.0 ± 1.0	1.0 ± 1.0	1.0 ± 1.0	1.2 ± 0.5	1.4 ± 0.4
Big Thicket	1.0 ± 1.0	1.0 ± 1.0	2.0 ± 0.9	1.7 ± 0.3	0.6 ± 0.1
Center	1.0 ± 1.0	1.0 ± 1.0	1.3 ± 0.5	1.4 ± 0.3	0.7 ± 0.1
Wright Patman Lake	1.0 ± 1.0	1.1 ± 1.0	1.1 ± 0.3	2.1 ± 0.5	0.6 ± 0.1
Guadalupe Mtns					
Wichita Mtns					

Table 8-6b. Source attribution scaling coefficients and standard errors resulting from the regression of the REMSAD source attribution estimates against the particulate sulfate data measured at each BRAVO monitoring site from August 6–September 19. The source attribution scaling coefficients for each monitoring site were compared to the Big Bend values using Student t statistics. Source regions that contributed more than 10% of the sulfate as estimated by REMSAD are underlined and if they also had a t value greater than 3 they are bolded. The scaling coefficients for the West Texas, the western U.S., and boundary conditions are not shown.

Source Regions	Carbón	Rest of Mexico	NE Texas	SE Texas	Eastern U.S.
Big Bend (K-Bar)	1.4 ± 0.4	1.9 ± 0.9	1.9 ± 1.3	2.4 ± 0.8	1.3 ± 0.2
San Vicente	1.4 ± 0.4	2.4 ± 0.9	1.9 ± 1.3	2.1 ± 0.8	1.3 ± 0.2
Persimmon Gap	2.1 ± 0.4	2.1 ± 1.0	1.7 ± 1.3	2.9 ± 0.6	0.9 ± 0.1
Marathon	2.1 ± 0.5	1.5 ± 1.0	0.6 ± 1.2	2.8 ± 0.6	0.8 ± 0.1
Fort Stockton	1.7 ± 0.5	0.9 ± 0.9	1.4 ± 1.0	2.4 ± 0.5	0.8 ± 0.1
Monahans Sandhills	2.2 ± 0.6	0.6 ± 1.0	-0.2 ± 0.6	3.4 ± 0.5	1.1 ± 0.1
Esperanza	1.4 ± 0.5	1.5 ± 0.8	1.2 ± 1.4	2.3 ± 1.0	0.4 ± 0.3
McDonald Obs	2.3 ± 0.5	1.0 ± 0.8	1.5 ± 1.5	2.0 ± 0.7	0.8 ± 0.2
Presidio	1.3 ± 0.4	1.8 ± 0.7	2.5 ± 1.4	1.6 ± 0.9	1.1 ± 0.2
LBJ	1.1 ± 2.0	4.9 ± 1.8	-0.7 ± 0.6	1.1 ± 0.2	**0.8 ± 0.1**
Fort McKavett	-1.1 ± 1.8	0.8 ± 1.1	0.1 ± 0.3	2.3 ± 0.3	1.0 ± 0.1
Lake Colorado City	-0.6 ± 1.0	2.4 ± 1.5	0.2 ± 0.3	1.5 ± 0.3	1.2 ± 0.1
Fort Lancaster	1.5 ± 0.6	2.0 ± 0.9	0.3 ± 0.5	2.4 ± 0.4	**0.4 ± 0.1**
Sanderson	1.9 ± 0.6	1.9 ± 1.1	1.9 ± 0.8	2.3 ± 0.5	**0.2 ± 0.1**
Langtry	-0.3 ± 0.6	3.2 ± 1.1	-0.9 ± 0.7	2.6 ± 0.4	1.0 ± 0.1
Amistad	-0.2 ± 0.5	3.8 ± 1.0	-2.1 ± 0.7	2.7 ± 0.4	0.8 ± 0.1
Brackettville	3.4 ± 1.5	5.1 ± 1.2	-0.5 ± 0.6	2.1 ± 0.3	**0.7 ± 0.1**
Eagle Pass	1.1 ± 1.6	2.1 ± 1.0	-0.8 ± 0.8	1.2 ± 0.4	**0.5 ± 0.1**
Laredo	1.2 ± 2.0	2.7 ± 0.9	-1.3 ± 0.9	2.2 ± 0.6	**0.3 ± 0.1**
Falcon Dam	1.1 ± 2.0	3.5 ± 0.6	-3.7 ± 1.1	3.6 ± 1.0	**0.4 ± 0.1**
Laguna Atascosa	1.4 ± 2.0	5.8 ± 1.9	0.2 ± 1.3	0.8 ± 0.8	**0.4 ± 0.1**
North Padre Island	1.3 ± 2.0	0.6 ± 2.0	2.3 ± 1.9	1.6 ± 1.4	**0.5 ± 0.1**
Lake Corpus Christi	1.3 ± 2.0	3.2 ± 1.9	-0.4 ± 0.8	1.7 ± 0.5	**0.7 ± 0.1**
Pleasanton	1.5 ± 2.0	6.6 ± 1.7	-1.1 ± 0.7	1.2 ± 0.2	**0.8 ± 0.1**
Everton Ranch	1.8 ± 2.0	6.7 ± 1.8	-2.6 ± 0.7	1.5 ± 0.3	**0.7 ± 0.1**
Hagerman	1.6 ± 2.0	4.1 ± 1.9	-0.7 ± 0.3	3.2 ± 0.3	1.0 ± 0.1
Purtis Creek	1.5 ± 2.0	4.5 ± 1.9	0.1 ± 0.3	2.5 ± 0.4	**0.8 ± 0.1**
Stephenville	1.1 ± 2.0	4.8 ± 1.8	0.5 ± 0.4	1.0 ± 0.3	1.0 ± 0.1
Stillhouse Lake	1.6 ± 2.0	4.7 ± 1.9	-1.1 ± 0.5	1.6 ± 0.2	0.7 ± 0.1
Somerville Lake	1.5 ± 2.0	4.4 ± 1.9	-2.2 ± 0.8	1.1 ± 0.2	**0.7 ± 0.1**
Aransas	1.7 ± 2.0	5.1 ± 1.9	-1.0 ± 0.9	1.1 ± 0.6	**0.7 ± 0.1**
San Bernard	1.6 ± 2.0	4.0 ± 1.9	-0.6 ± 0.7	0.6 ± 0.3	**0.7 ± 0.1**
Big Thicket	1.9 ± 2.0	5.4 ± 1.9	1.3 ± 1.1	1.3 ± 0.2	**0.5 ± 0.1**
Center	1.5 ± 2.0	4.5 ± 1.9	1.2 ± 0.4	1.7 ± 0.3	**0.7 ± 0.0**
Wright Patman Lake	1.7 ± 2.0	3.8 ± 1.9	1.1 ± 0.3	3.1 ± 0.6	**0.4 ± 0.0**
Guadalupe Mtns	1.8 ± 0.7	0.9 ± 0.9	-0.4 ± 1.5	3.3 ± 0.9	**0.3 ± 0.2**
Wichita Mtns	0.6 ± 2.0	1.4 ± 2.0	2.8 ± 0.6	0.2 ± 0.4	0.7 ± 0.1

Table 8-6c. Source attribution scaling coefficients and standard errors resulting from the regression of the REMSAD source attribution estimates against the particulate sulfate data measured at each BRAVO monitoring site from September 20–October 28. The source attribution scaling coefficients for each monitoring site were compared to the Big Bend values using Student t statistics. Source regions that contributed more than 10% of the sulfate as estimated by REMSAD are underlined and if they also had a t value greater than 3 they are bolded. The scaling coefficients for the West Texas, the western U.S., and boundary conditions are not shown.

Source Regions	Carbón	Rest of Mexico	NE Texas	SE Texas	Eastern U.S.
Big Bend (K-Bar)	1.6 ± 0.5	2.4 ± 0.6	-0.1 ± 0.7	0.9 ± 0.7	0.6 ± 0.2
San Vicente	1.7 ± 0.5	2.5 ± 0.6	-0.2 ± 0.7	1.0 ± 0.7	0.6 ± 0.2
Persimmon Gap	1.8 ± 0.6	2.1 ± 0.7	-0.1 ± 0.7	0.4 ± 0.7	0.7 ± 0.2
Marathon	1.9 ± 0.6	2.2 ± 0.7	0.5 ± 0.8	0.1 ± 0.7	0.6 ± 0.2
Fort Stockton	2.0 ± 0.6	2.0 ± 0.7	0.8 ± 0.8	-0.1 ± 0.7	0.4 ± 0.2
Monahans Sandhills	2.0 ± 0.5	1.6 ± 0.8	1.3 ± 0.7	-0.1 ± 0.8	0.4 ± 0.2
Esperanza	1.4 ± 0.8	2.0 ± 0.8	1.0 ± 0.8	0.6 ± 0.7	0.3 ± 0.3
McDonald Obs	0.8 ± 0.7	1.4 ± 0.7	1.1 ± 0.7	0.0 ± 0.7	0.5 ± 0.3
Presidio	1.1 ± 0.5	1.7 ± 0.6	0.9 ± 0.7	0.4 ± 0.7	0.4 ± 0.2
LBJ	0.7 ± 1.0	1.2 ± 1.0	-0.1 ± 0.3	1.2 ± 0.3	0.4 ± 0.1
Fort McKavett	1.9 ± 0.9	3.0 ± 0.8	1.1 ± 0.5	0.7 ± 0.4	0.3 ± 0.1
Lake Colorado City	1.2 ± 0.5	2.0 ± 0.8	1.3 ± 0.6	0.5 ± 0.7	0.2 ± 0.2
Fort Lancaster	2.0 ± 0.4	2.2 ± 0.8	1.6 ± 0.6	0.3 ± 0.7	0.4 ± 0.2
Sanderson	2.4 ± 0.5	2.3 ± 0.7	0.5 ± 0.7	-0.4 ± 0.7	0.6 ± 0.2
Langtry	2.6 ± 0.4	2.0 ± 0.7	1.3 ± 0.6	-0.2 ± 0.6	0.6 ± 0.1
Amistad	1.1 ± 0.4	2.1 ± 0.7	1.0 ± 0.5	0.9 ± 0.6	0.5 ± 0.1
Brackettville	0.2 ± 0.5	4.0 ± 0.7	0.8 ± 0.5	1.1 ± 0.4	0.4 ± 0.1
Eagle Pass	0.4 ± 0.5	4.0 ± 0.7	1.4 ± 0.5	1.9 ± 0.5	0.3 ± 0.1
Laredo	0.5 ± 0.4	3.7 ± 0.7	1.1 ± 0.3	1.1 ± 0.5	0.4 ± 0.1
Falcon Dam	0.3 ± 0.8	3.1 ± 0.6	0.1 ± 0.5	1.6 ± 0.5	0.4 ± 0.1
Laguna Atascosa	0.9 ± 0.9	1.4 ± 0.9	-0.7 ± 0.4	1.5 ± 0.4	0.5 ± 0.1
North Padre Island	1.0 ± 1.0	1.5 ± 1.0	-1.0 ± 0.4	3.0 ± 0.5	0.4 ± 0.1
Lake Corpus Christi	0.7 ± 0.8	1.1 ± 1.0	0.2 ± 0.3	1.0 ± 0.4	0.5 ± 0.1
Pleasanton	0.9 ± 0.6	1.9 ± 1.0	0.7 ± 0.3	0.8 ± 0.3	0.4 ± 0.1
Everton Ranch	1.0 ± 0.9	1.3 ± 1.0	0.3 ± 0.3	0.9 ± 0.3	0.4 ± 0.1
Hagerman	1.0 ± 1.0	1.2 ± 1.0	1.6 ± 0.3	2.1 ± 0.4	0.4 ± 0.1
Purtis Creek	0.9 ± 1.0	1.2 ± 1.0	0.6 ± 0.3	1.6 ± 0.4	0.5 ± 0.1
Stephenville	1.4 ± 1.0	2.1 ± 0.9	0.8 ± 0.5	1.9 ± 0.3	0.2 ± 0.1
Stillhouse Lake	0.9 ± 1.0	1.4 ± 1.0	0.9 ± 0.3	1.0 ± 0.2	0.3 ± 0.1
Somerville Lake	0.9 ± 1.0	1.2 ± 1.0	0.6 ± 0.2	1.0 ± 0.2	0.5 ± 0.0
Aransas	0.7 ± 1.0	1.3 ± 1.0	-0.4 ± 0.3	0.7 ± 0.4	0.6 ± 0.0
San Bernard	1.1 ± 1.0	1.3 ± 1.0	0.1 ± 0.5	0.2 ± 0.3	0.6 ± 0.0
Big Thicket	0.9 ± 1.0	1.2 ± 1.0	0.9 ± 0.6	2.7 ± 0.8	0.6 ± 0.0
Center	0.9 ± 1.0	1.1 ± 1.0	0.8 ± 0.4	1.2 ± 0.8	0.5 ± 0.0
Wright Patman Lake	0.9 ± 1.0	1.1 ± 1.0	0.7 ± 0.4	1.4 ± 0.6	0.4 ± 0.0
Guadalupe Mtns	1.6 ± 0.9	1.5 ± 0.9	0.8 ± 0.9	0.6 ± 0.8	0.4 ± 0.3
Wichita Mtns	1.2 ± 1.0	1.4 ± 1.0	0.3 ± 0.9	0.5 ± 0.6	1.0 ± 0.4

The analysis was conducted using a number of different moving window widths. It was found that the average source attributions over the four-month BRAVO study period were not sensitive to the window width producing similar results for windows from 21 days to 1 day in width, but the regression performance did diminish as the window width increased. The source attribution results for some of the individual sulfate episodes at Big Bend were sensitive to the width of the window. This was most severe for the aggregation windows using 1 day and more than 15 days compared to the others. A 3-day window was chosen as the optimum aggregation window. This produced the best balance between stable scaling coefficients and model performance. Also, this captured the variability in the REMSAD model simulation due to synoptic forcing which is on the order of 3–5 days, and airmasses typically resided over Texas for less than three days. Last, the Big Bend sulfate episode duration was typically 5 days or longer so the 3-day window was able to capture variations in the biases across the episodes.

8.2.1.2.1 The Optimum Synthesized REMSAD Results

The overall Big Bend average source attributions and performance statistics are presented in Table 8-7 and Figure 8-61. Figure 8-62 presents the absolute and relative daily source attributions and compares the predicted and observed sulfate time series. As shown in Figure 8-62, the regressed REMSAD results properly reproduce the general temporal pattern in Big Bend's sulfate, particularly in July and August, and the overall correlation coefficient is 0.85 with an RMS error of 42%. In September and October the peak sulfate days are underestimated, leading to an overall average underestimation of 18%. Comparing these results to the original REMSAD simulation (chapter 6), the synthesized REMSAD has a higher correlation coefficient, and smaller bias and RMS error. In addition, REMSAD systematically underestimated the July and August sulfate at Big Bend by a factor of 2, while the synthesized REMSAD underestimated the observed by 13% in these months (Figure 8-62). Also, the synthesized REMSAD captured the September 28 episode which REMSAD missed and the October 12 episode, but the peak sulfate concentrations are still underestimated by nearly a factor of two.

Table 8-7. The optimum synthesized REMSAD average source attribution scaling coefficients and the average standard errors, and the source attribution and standard error for the entire BRAVO time period (7/9–10/28/1999). The regression performance statistics are also provided. The relative contributions are the ratios of average predicted absolute values and are reported as percents.

Source Region	Avg Scaling Coeff. and Avg Std Error	Absolute Source Contribution ($\mu g/m^3$)	Relative Source Contribution (%)	Original REMSAD Source Contribution (%)
Carbón	1.52 ± 1	0.46 ± 0.04	23 ± 1.8	14
Rest of Mexico	1.66 ± 1.6	0.32 ± 0.03	16 ± 1.4	10
NE Texas	0.85 ± 1	0.09 ± 0.02	5 ± 0.8	5
SE Texas	1.12 ± 0.8	0.19 ± 0.02	10 ± 1.0	9
West Texas	0.92 ± 0.7	0.03 ± 0.01	1 ± 0.3	2
Eastern U.S.	0.95 ± 0.3	0.65 ± 0.02	32 ± 1.2	42
Western U.S.	0.87 ± 0.6	0.12 ± 0.02	6 ± 0.7	9
Boundary Condition	1.07 ± 0.7	0.14 ± 0.01	7 ± 0.5	7
Texas	0.97 ± 0.05	0.31 ± 0.03	16 ± 1.2	16
Mexico	1.59 ± 1	0.78 ± 0.05	39 ± 2.3	23
Eastern U.S.	0.95 ± 0.3	0.65 ± 0.02	32 ± 1.2	42
Western U.S.	0.87 ± 0.6	0.12 ± 0.02	6 ± 0.7	9

Regression Performance statistics

r	0.85
Average Observation ($\mu g/m^3$)	2.58
Average Prediction ($\mu g/m^3$)	2.1
Bias (%)	-18
RMS Error (%)	42

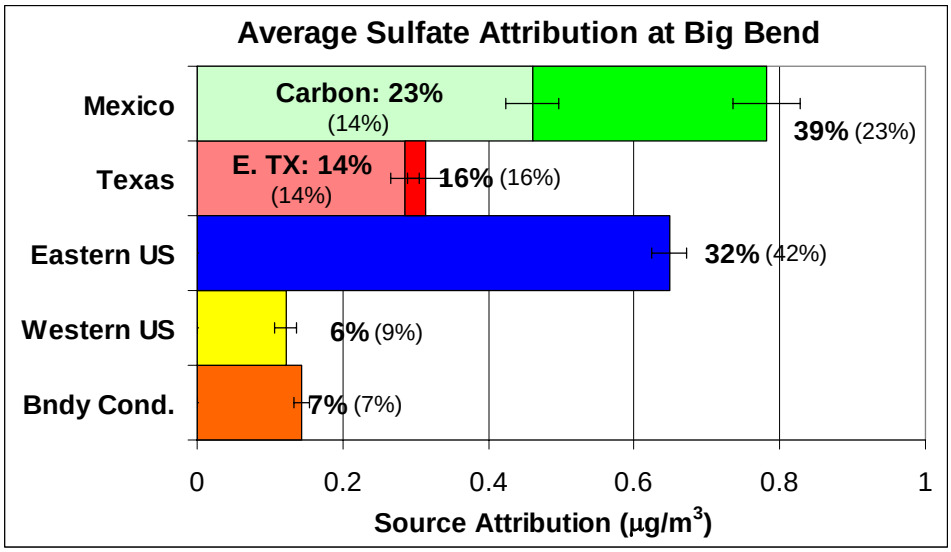

Figure 8-61. The optimum synthesized REMSAD average source attribution and standard errors to Big Bend's predicted sulfate for the entire BRAVO time period (7/9–10/28/1999). The bolded labels are the relative contributions, i.e., the ratios of average absolute values. The values in parentheses are the original REMSAD source attribution estimates.

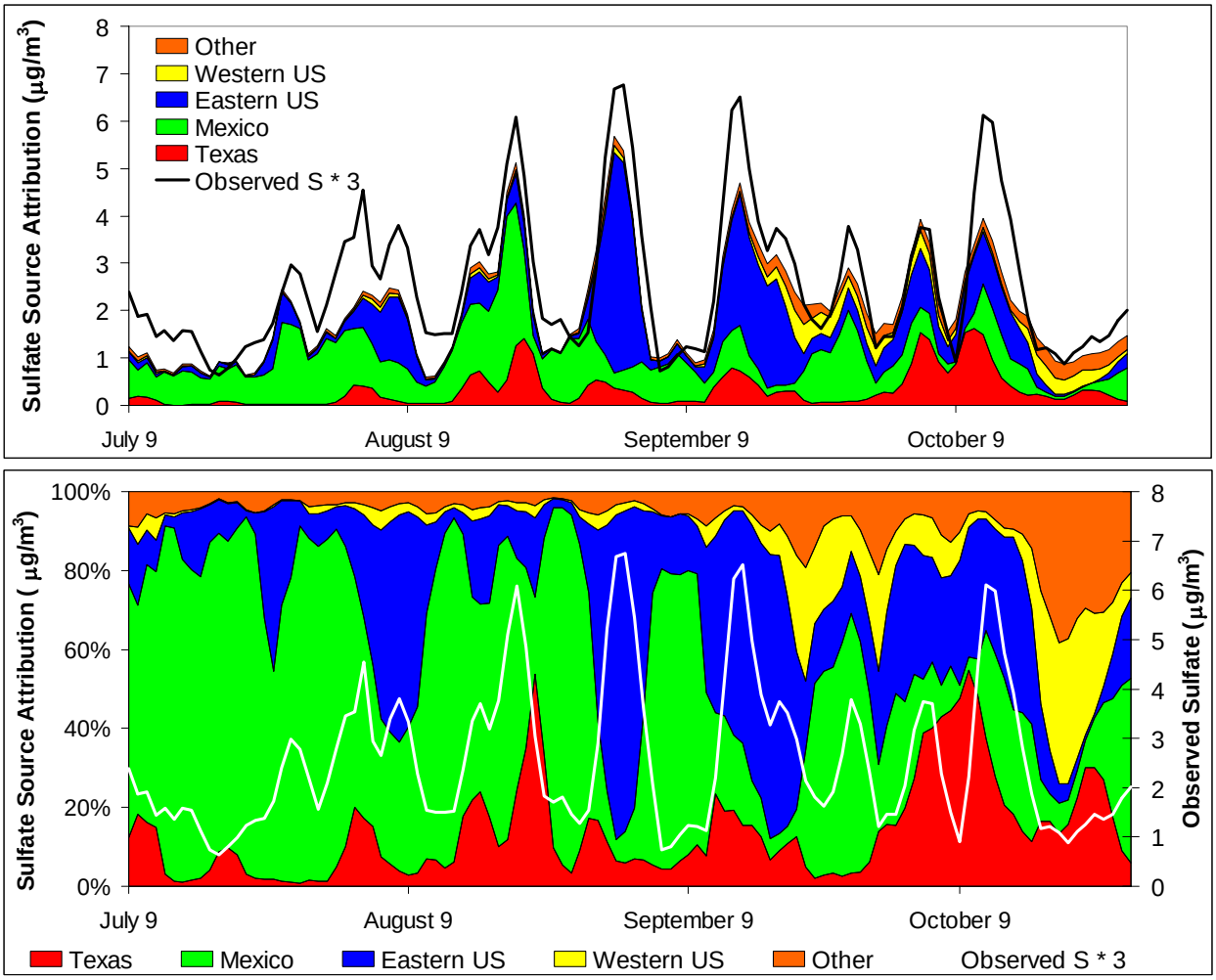

Figure 8-62. The optimum synthesized REMSAD absolute and relative source attribution to the predicted sulfate at Big Bend.

Although the synthesized REMSAD bias is smaller than the original results, it still underestimates the observed Big Bend concentrations by nearly 20%. This large underestimation has two potential causes. First, it is at least partially due to biases in the regression analysis. As equation 2-33 is written, the modeled source regions account for all sulfate at Big Bend. Therefore there is not a constant coefficient, i.e. intercept, in the regression analysis. The source attributions comprising the design matrix can have large errors, but these errors were not accounted for in the analysis. In such a case, it can be shown that the regression analysis will always underestimate the average concentrations. Future analyses will incorporate the errors in the source attributions to minimize this regression analysis bias. The second potential cause of the bias is due to spatial variability in the source attribution scaling coefficients. The original simulated concentrations generally had higher concentrations, relative to the measured data, in eastern Texas than western Texas and around Big Bend. The regression analysis will find a balance between all sites in Texas, so it is quite possible that Big Bend concentrations will be underestimated while the eastern Texas sites will be overestimated. This is supported by the results in Table 8-4, where the biases at the eastern Texas sites are generally smaller than those in western Texas and around Big Bend. However, note that the predicted average sulfate at most sites is underestimated due to the systematic bias in the regression analysis.

The average source attribution scaling factors are presented in Table 8-7. The overall average for the eastern U.S. and Texas is about 1 while for Mexico it is 2. Consequently, over the BRAVO time period, the original REMSAD eastern U.S. and Texan source contributions to the Texas monitoring sites are unbiased while the Mexican contributions are underestimated on average by a factor of two. This can be due to underestimation in Mexican emissions or a systematic bias in the modeled transport, chemistry, or removal processes. It is interesting that the scaling factor for Carbón is 1.52. The REMSAD model was run with the lower Carbón SO_2 emission rate of 152,000 tons/yr which is a factor 1.58 lower than the upper estimate of 241,000 tons/yr. The scaling factors for all three regions had a trend in time with the highest factors in July and the lowest in October. For example, the average scaling factor for the eastern U.S. was 1.2 in July and August, but 0.7 in September and October.

The average source attributions for each region are also reported in Table 8-7 and Figure 8-61 as well as the original REMSAD results. Mexico is the largest average contributor at 39% while the eastern U.S. contributes 32% and Texas 16%. In Mexico, the Carbón I & II power plants contributed 23% and in Texas, east Texas contributed 14%, or 90% of Texas' total contribution. Comparing these results to the original REMSAD source attribution it is seen that the Mexican contribution increased by 70% and the eastern U.S. contribution decreased by about 25% over the original REMSAD source attributions. Texas' contribution remained about the same.

As shown in Figure 8-62, each source region's contribution has unique trends over the four month period. Mexico's contributions dominate the predicted sulfate concentrations in July and August, contributing from 0.5 to 1.5 $\mu g/m^3$ of sulfate every day, and occasionally exceeding 2 $\mu g/m^3$. In September and October, the contribution from Mexico to Big Bend's sulfate decreased typically less than 1 $\mu g/m^3$ per day. The Texas source regions have little contribution in July and the largest contribution in October. The Texas sources also tend to have the largest absolute contribution (>1 $\mu g/m^3$) during the highest sulfate days. The eastern U.S. source regions' contributions are episodic, also occurring during Big Bend sulfate episodes where they exceeded 4 $\mu g/m^3$ during the September 1 episode. The western U.S. contributions are near zero until late September and October.

Table 8-8 and Figure 8-63 present the source attributions for each Big Bend sulfate episode. As shown, Mexico, the eastern U.S., and Texas all contribute 24% or more of the predicted sulfated in two or more of the episodes. Mexico is the dominant contributor for the July 22, August 18, and September 28 episodes at 79, 56, and 49%, respectively. The eastern U.S. is the dominant contributor for the August 30, September 12, and October 3 and 11 episodes at 62, 49, 37, and 38%, respectively. Texas contributes about 25% of the predicted sulfate to both the October 3 and 11 episodes.

Table 8-8. The optimum synthesized REMSAD relative source attribution and standard error to the predicted sulfate for each Big Bend sulfate episode. The relative contributions are the ratios of average predicted absolute values.

	Big Bend Fine Particulate Sulfur Episodes						
Source Region	**7/22-7/31**	**8/16-8/23**	**8/30-9/4**	**9/12-9/17**	**9/25-9/28**	**10/3-10/7**	**10/11-10/16**
Carbón	24 ± 5.3	51 ± 6.3	10 ± 4.5	13 ± 5.9	6 ± 3.9	14 ± 8.3	19 ± 4.1
Rest of Mexico	54 ± 10.5	4 ± 1.5	3 ± 2.2	4 ± 2.3	55 ± 7.3	6 ± 3.9	8 ± 3.0
NE Texas	0 ± 0.0	3 ± 3.0	2 ± 0.8	0 ± 0.8	0 ± 0.6	15 ± 6.9	13 ± 2.8
SE Texas	1 ± 0.2	21 ± 3.3	7 ± 2.9	16 ± 5.0	1 ± 1.0	16 ± 6.7	17 ± 3.4
West Texas	1 ± 0.1	0 ± 0.1	1 ± 0.2	1 ± 0.3	2 ± 1.2	3 ± 1.1	1 ± 0.4
Eastern U.S.	17 ± 3.2	15 ± 2.5	72 ± 4.3	58 ± 7.1	15 ± 2.1	31 ± 3.4	34 ± 2.3
Western U.S.	1 ± 0.4	2 ± 0.7	3 ± 0.8	3 ± 1.2	15 ± 5.4	9 ± 3.8	2 ± 1.5
Bndy Cond.	3 ± 0.7	3 ± 0.9	4 ± 1.0	5 ± 1.6	6 ± 1.9	6 ± 2.1	7 ± 1.4
Texas	17 ± 3.2	15 ± 2.5	72 ± 4.3	58 ± 7.1	15 ± 2.1	31 ± 3.4	34 ± 2.3
Mexico	1 ± 0.2	25 ± 4.4	9 ± 3.0	17 ± 5.1	4 ± 1.6	34 ± 9.7	31 ± 4.5
Eastern U.S.	78 ± 11.8	55 ± 6.5	13 ± 5.0	17 ± 6.4	60 ± 8.3	20 ± 9.1	27 ± 5.1
Western U.S.	1 ± 0.4	2 ± 0.7	3 ± 0.8	3 ± 1.2	15 ± 5.4	9 ± 3.8	2 ± 1.5

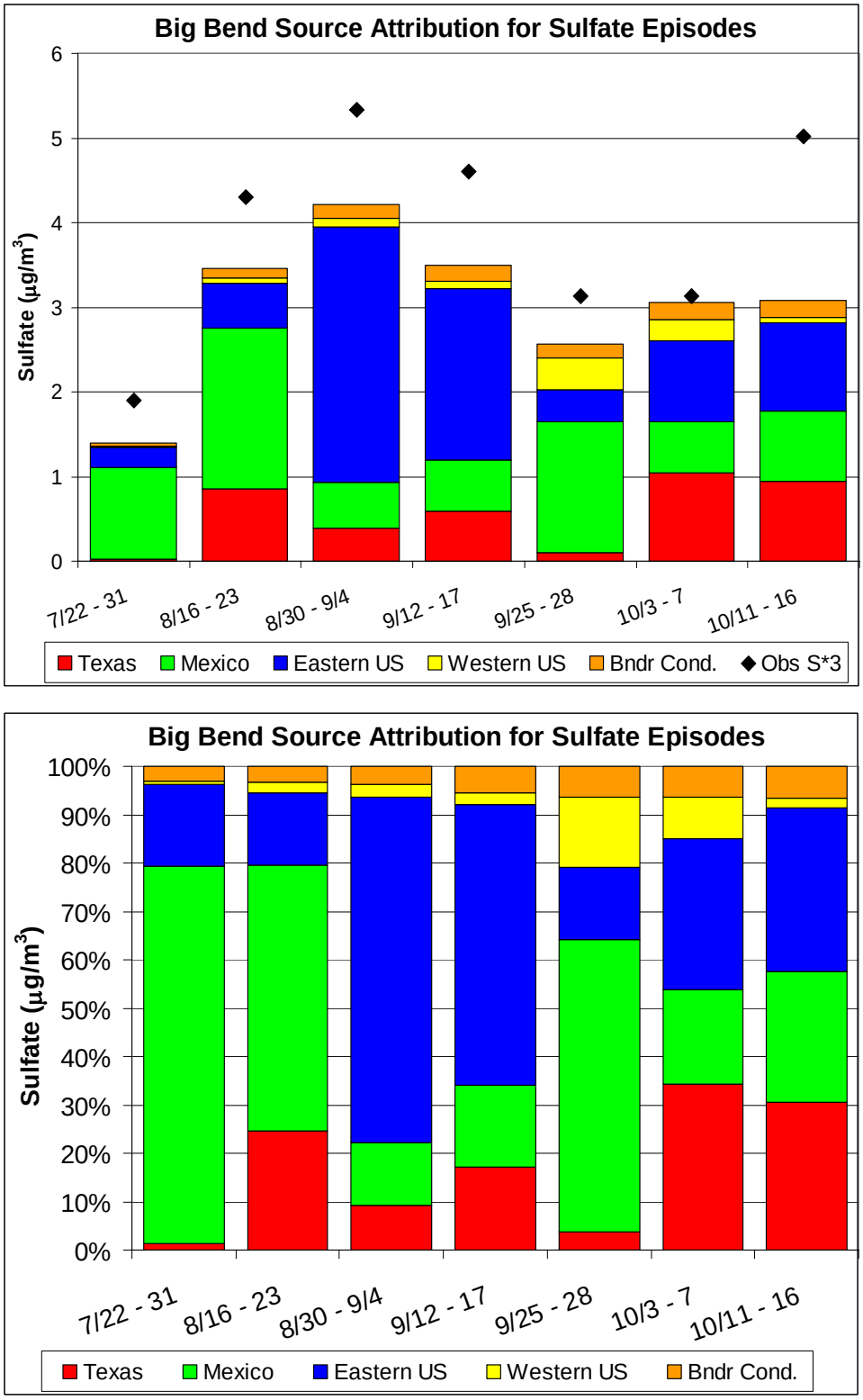

Figure 8-63. The optimum synthesized REMSAD average source attribution and standard error to Big Bend's predicted sulfate for each Big Bend sulfate episode.

As shown in Figure 8-62, Mexico is the largest contributor to Big Bend's sulfate during the days with the lowest sulfate concentrations. This is particularly so from July–September when the Mexican sulfate often accounted for more than 80% of Big Bend's sulfate concentrations when the overall concentrations were below 2 μg/m^3. In October, the western U.S. and boundary condition source regions also were major contributors to the lowest sulfur days, together accounting for 60–80% of the sulfur from October 19–24.

8.2.1.3 The Optimum Synthesized CMAQ Results

The same approached used in the synthesized REMSAD analysis was applied to the CMAQ-MADRID source attribution estimates. In the Bayesian regression analysis, the prior estimate of the five source attribution scaling coefficients was 1 and their variance was also set to 1. These variances are smaller than those used in the REMSAD synthesis approach. This was done because the original CMAQ-MADRID simulation had addressed eastern U.S. and Mexican biases by nudging the REMSAD boundary conditions to measured data and increasing the Mexican emissions. This resulted in CMAQ-MADRID having larger Mexican and smaller eastern U.S. contributions and the simulated sulfate concentrations compared better to the observed concentrations than REMSAD. The sensitivity of the results on the *a-prior* variances was explored. It was found that larger variances did not appreciably change the results, but did occasionally result in negative coefficients. Table 8-9 presents the result of the synthesis inversion applied to each monitoring site and identifies which site's data were not used and when in the regression analysis since their scaling coefficients were significantly different from Big Bend's.

Table 8-9. Source attribution scaling coefficients and standard errors resulting from the regression of the CMAQ-MADRID source attribution estimates against the particulate sulfate data measured at each BRAVO monitoring site for three time periods. The source attribution scaling coefficients for each monitoring site were compared to the Big Bend values using Student t statistics. Source regions with a t value greater than 3 and which contributed more than 10% to the receptor sites concentration as estimated by CMAQ-MADRID are bolded. The scaling coefficients for the western U.S. and boundary conditions are not shown.

Time Period	**7/9–8/5/1999**			**8/6–9/19/1999**			**9/20–10/28/1999**		
Source Region	**Mexico**	**Texas**	**E U.S.**	**Mexico**	**Texas**	**E U.S.**	**Mexico**	**Texas**	**E U.S.**
Big Bend (K-Bar)	1.6 ± 0.2	0.7 ± 0.6	0.8 ± 0.5	0.7 ± 0.2	1.1 ± 0.3	0.8 ± 0.1	0.6 ± 0.2	0.0 ± 0.3	1.2 ± 0.2
San Vicente	1.6 ± 0.3	0.9 ± 0.6	1.4 ± 0.5	0.9 ± 0.2	0.8 ± 0.3	0.7 ± 0.1	0.9 ± 0.2	0.0 ± 0.3	0.9 ± 0.2
Persimmon Gap	1.4 ± 0.3	0.5 ± 0.5	0.9 ± 0.5	0.9 ± 0.2	1.0 ± 0.3	0.7 ± 0.1	0.7 ± 0.2	0.0 ± 0.3	1.2 ± 0.3
Marathon	1.6 ± 0.2	0.3 ± 0.5	0.7 ± 0.4	1.1 ± 0.2	1.0 ± 0.2	0.6 ± 0.1	0.7 ± 0.2	0.1 ± 0.3	1.0 ± 0.3
Fort Stockton	1.2 ± 0.2	0.1 ± 0.5	0.8 ± 0.4	0.5 ± 0.1	1.5 ± 0.2	0.5 ± 0.1	0.7 ± 0.2	0.1 ± 0.3	0.9 ± 0.3
Monahans Sandhills	1.0 ± 0.2	0.5 ± 0.5	1.1 ± 0.4	0.8 ± 0.2	1.7 ± 0.2	0.7 ± 0.1	0.7 ± 0.2	0.6 ± 0.4	0.7 ± 0.3
Esperanza	1.7 ± 0.5	1.0 ± 0.7	1.1 ± 0.6	0.8 ± 0.2	1.1 ± 0.3	0.6 ± 0.2	1.1 ± 0.4	0.8 ± 0.4	0.1 ± 0.4
McDonald Obs	1.0 ± 0.3	1.2 ± 0.6	1.4 ± 0.5	1.0 ± 0.2	1.2 ± 0.3	0.5 ± 0.1	0.4 ± 0.3	0.4 ± 0.4	0.7 ± 0.3
Presidio	0.7 ± 0.3	0.9 ± 0.6	0.7 ± 0.5	0.8 ± 0.2	0.7 ± 0.3	0.9 ± 0.1	0.6 ± 0.2	0.4 ± 0.4	0.6 ± 0.3
LBJ	1.4 ± 0.7	1.4 ± 0.2	0.1 ± 0.3	1.6 ± 0.6	0.3 ± 0.1	0.8 ± 0.1	0.9 ± 0.5	0.7 ± 0.2	**0.3 ± 0.1**
Fort McKavett	1.7 ± 0.3	0.6 ± 0.4	0.7 ± 0.4	0.9 ± 0.5	0.9 ± 0.2	0.8 ± 0.1	1.6 ± 0.3	0.8 ± 0.2	**0.2 ± 0.1**
Lake Colorado City	1.2 ± 0.3	0.7 ± 0.5	0.9 ± 0.4	0.4 ± 0.3	1.0 ± 0.2	0.9 ± 0.1	0.5 ± 0.1	1.1 ± 0.3	**0.0 ± 0.2**
Fort Lancaster	1.3 ± 0.2	1.0 ± 0.4	0.1 ± 0.4	1.3 ± 0.2	1.8 ± 0.2	**0.2 ± 0.1**	0.8 ± 0.1	1.0 ± 0.3	**0.1 ± 0.2**
Sanderson	1.8 ± 0.2	0.4 ± 0.5	0.6 ± 0.4	1.1 ± 0.2	1.6 ± 0.2	**0.1 ± 0.1**	0.8 ± 0.2	0.3 ± 0.3	0.6 ± 0.2
Langtry	1.4 ± 0.1	0.5 ± 0.5	0.9 ± 0.3	0.5 ± 0.2	1.1 ± 0.2	0.8 ± 0.1	0.9 ± 0.1	1.1 ± 0.2	**0.2 ± 0.1**
Amistad	0.9 ± 0.1	0.6 ± 0.5	1.2 ± 0.3	0.5 ± 0.1	0.7 ± 0.2	0.8 ± 0.1	0.4 ± 0.1	**1.2 ± 0.2**	**0.2 ± 0.1**
Brackettville	2.0 ± 0.5	0.6 ± 0.5	1.2 ± 0.3	2.4 ± 0.4	0.7 ± 0.1	0.7 ± 0.1	0.4 ± 0.1	0.9 ± 0.2	**0.3 ± 0.1**
Eagle Pass	0.9 ± 0.1	1.0 ± 0.6	0.9 ± 0.3	0.7 ± 0.2	0.5 ± 0.2	**0.4 ± 0.1**	0.4 ± 0.1	**1.2 ± 0.2**	**0.1 ± 0.1**

Laredo	1.7 ± 0.3	0.8 ± 0.7	1.3 ± 0.3	1.1 ± 0.3	0.3 ± 0.2	**0.5 ± 0.1**	0.6 ± 0.1	0.6 ± 0.1	**0.3 ± 0.1**
Falcon Dam	2.5 ± 0.4	0.9 ± 0.7	0.4 ± 0.4	1.0 ± 0.2	0.0 ± 0.2	0.5 ± 0.1	0.9 ± 0.2	0.5 ± 0.1	**0.4 ± 0.1**
Laguna Atascosa	1.5 ± 0.7	0.8 ± 0.7	0.8 ± 0.2	3.2 ± 0.6	0.1 ± 0.2	**0.4 ± 0.0**	2.5 ± 0.5	0.5 ± 0.1	0.4 ± 0.0
North Padre Island	1.2 ± 0.7	1.0 ± 0.7	1.7 ± 0.2	1.4 ± 0.7	0.1 ± 0.3	**0.5 ± 0.0**	1.9 ± 0.7	0.7 ± 0.1	**0.4 ± 0.0**
Lake Corpus Christi	1.2 ± 0.7	0.6 ± 0.6	0.3 ± 0.2	1.4 ± 0.7	**0.2 ± 0.1**	**0.4 ± 0.0**	0.6 ± 0.5	0.5 ± 0.1	**0.3 ± 0.0**
Pleasanton	2.1 ± 0.6	1.1 ± 0.5	0.6 ± 0.2	1.9 ± 0.5	0.3 ± 0.1	0.7 ± 0.1	1.4 ± 0.4	0.7 ± 0.1	**0.3 ± 0.1**
Everton Ranch	1.3 ± 0.7	1.9 ± 0.4	0.2 ± 0.2	1.7 ± 0.7	**0.0 ± 0.1**	0.8 ± 0.1	1.6 ± 0.6	0.5 ± 0.1	0.5 ± 0.1
Hagerman	1.0 ± 0.7	0.7 ± 0.3	1.0 ± 0.2	1.1 ± 0.7	1.0 ± 0.1	1.0 ± 0.1	1.0 ± 0.6	0.7 ± 0.1	0.5 ± 0.1
Purtis Creek	1.0 ± 0.7	0.3 ± 0.1	0.9 ± 0.1	1.1 ± 0.7	0.9 ± 0.1	0.8 ± 0.0	1.4 ± 0.7	0.5 ± 0.1	0.4 ± 0.0
Stephenville	1.0 ± 0.7	1.1 ± 0.4	0.7 ± 0.2	1.2 ± 0.6	0.7 ± 0.2	0.9 ± 0.1	1.6 ± 0.4	0.9 ± 0.2	**0.2 ± 0.1**
Stillhouse Lake	1.3 ± 0.7	0.5 ± 0.2	0.9 ± 0.1	1.8 ± 0.7	0.3 ± 0.1	1.0 ± 0.1	1.9 ± 0.7	0.4 ± 0.1	0.5 ± 0.1
Somerville Lake	1.0 ± 0.7	0.5 ± 0.2	0.7 ± 0.2	1.3 ± 0.7	0.4 ± 0.1	0.7 ± 0.1	1.3 ± 0.7	0.5 ± 0.1	0.5 ± 0.0
Aransas	1.0 ± 0.7	0.7 ± 0.7	0.8 ± 0.2	1.7 ± 0.7	**0.0 ± 0.1**	0.7 ± 0.0	0.7 ± 0.6	0.3 ± 0.1	0.4 ± 0.0
San Bernard	1.0 ± 0.7	0.2 ± 0.2	0.8 ± 0.2	1.4 ± 0.7	**0.0 ± 0.1**	0.7 ± 0.0	1.6 ± 0.7	0.3 ± 0.1	0.4 ± 0.0
Big Thicket	1.0 ± 0.7	0.4 ± 0.1	0.6 ± 0.1	1.2 ± 0.7	0.9 ± 0.1	**0.5 ± 0.0**	1.2 ± 0.7	1.1 ± 0.3	0.5 ± 0.0
Center	1.0 ± 0.7	0.4 ± 0.1	0.7 ± 0.1	1.0 ± 0.7	0.9 ± 0.1	0.7 ± 0.0	1.1 ± 0.7	0.6 ± 0.2	**0.4 ± 0.0**
Wright Patman Lake	1.0 ± 0.7	0.6 ± 0.1	0.9 ± 0.1	1.1 ± 0.7	0.8 ± 0.1	0.6 ± 0.0	1.0 ± 0.7	0.4 ± 0.1	**0.4 ± 0.0**
Guadalupe Mtns				0.9 ± 0.3	1.5 ± 0.3	0.5 ± 0.2	0.9 ± 0.4	0.7 ± 0.4	0.4 ± 0.4
Wichita Mtns				0.8 ± 0.6	0.6 ± 0.2	1.0 ± 0.1	1.3 ± 0.6	1.1 ± 0.6	1.0 ± 0.6

The source attribution results are presented in Tables 8-10 and 8-11 and Figures 8-64 through 8-67. The synthesis inversion improved the comparison of Big Bend's predicted sulfate to the observed sulfate with a correlation coefficient of 0.89 compared to 0.72 and the RMS error of 36% compared to 61% (Table 8-10). However, the synthesis inversion had a bias of -16% compared to no bias for the original CMAQ-MADRID results. This bias is most notable during July and the sulfate episodes (Figure 8-66). These statistics are similar to those found for the synthesized REMSAD (Table 8-6), and the potential causes for the bias are the same as those discussed for the synthesized REMSAD results.

Table 8-10. The optimum synthesized CMAQ average source attribution scaling coefficients and the average standard errors, and the source attributions and standard errors for the entire BRAVO time period (7/9–10/28/1999). The regression performance statistics are also provided. The relative contributions are the ratios of average predicted absolute values.

Source Region	Avg Scaling Coeff and Avg Std Error	Absolute Source Contribution ($\mu g/m^3$)	Relative Source Contribution (%)	Original CMAQ Source Contribution (%)
Texas	0.75 ± 0.5	0.37 ± 0.03	16.9 ± 1.3	19.4
Mexico	1.1 ± 0.5	0.82 ± 0.04	38 ± 1.7	31.7
Eastern U.S.	0.73 ± 0.4	0.65 ± 0.03	30.1 ± 1.2	38.5
Western U.S.	1.1 ± 0.9	0.18 ± 0.02	8.5 ± 0.8	5.9
Boundary Condition	1.2 ± 1	0.14 ± 0.01	6.4 ± 0.6	4.7

Regression Performance statistics

	Synthesized CMAQ	Original CMAQ-MADRID
r	0.89	0.72
Average Observation ($\mu g/m^3$)	2.58	2.58
Average Prediction ($\mu g/m^3$)	2.17	2.58
Bias (%)	-16	0
RMS Error (%)	36	61

Table 8-11. The optimum synthesized CMAQ relative source attributions and standard errors to the predicted sulfate for each Big Bend sulfate episode. The relative contributions are the ratios of average predicted absolute values.

	Big Bend Fine Particulate Sulfur Episodes						
Source Region	**7/22–7/31**	**8/16–8/23**	**8/30–9/4**	**9/12–9/17**	**9/25–9/28**	**10/3–10/7**	**10/11–10/16**
Texas	1 ± 0.8	32 ± 3.7	13 ± 3.2	17 ± 4.4	2 ± 0.9	28 ± 9.2	46 ± 6.8
Mexico	85 ± 6.3	33 ± 5.4	6 ± 3.8	25 ± 4.7	49 ± 8.7	32 ± 9.	18 ± 4.3
Eastern U.S.	9 ± 2.	27 ± 2.6	73 ± 5.3	49 ± 6.4	9 ± 2.9	26 ± 4.2	30 ± 3.4
Western U.S.	1 ± 0.6	5 ± 1.4	1 ± 0.6	4 ± 1.2	35 ± 6.3	10 ± 3.9	5 ± 2.7
Bndy. Cond.	5 ± 1.2	4 ± 1.2	6 ± 1.5	5 ± 1.4	6 ± 2.4	4 ± 1.6	1 ± 0.4

The daily source attribution scaling coefficients are presented in Figure 8-64 and the average coefficients over the four month period in Table 8-10. Both Texas and the eastern U.S. are less than 1 at 0.77 and 0.7, respectively, indicating that these source regions were biased high on average over all of the BRAVO monitoring sites and time periods. The average scaling coefficients for the Mexican, western U.S., and boundary condition source regions were about 1, indicating unbiased average source contributions. The synthesized REMSAD average scaling coefficients for Carbón and Rest of Mexico were 1.5 and 1.7, respectively. These coefficients are similar to the amount that the Carbón and Rest of Mexico emissions were increased in the CMAQ-MADRID run compared to REMSAD.

Comparing the synthesized CMAQ source attribution of Big Bend's sulfate to the synthesized REMSAD results, it is seen that they produced similar average and daily source attributions, and so will not be discussed in detail. However, some differences occurred during the sulfate episodes. For example, during the August 20 episode, the synthesized REMSAD results predicted that the Mexican sources contributed more than 50% to Big Bend's sulfate (Figure 8-63), while synthesized CMAQ had Mexico, Texas, and the eastern U.S. each contributing about 30% of the sulfate (Figure 8-67). Also, during the October 13 sulfate episodes, the synthesized CMAQ estimated Texas' contribution to be almost 50% on average and up to 60% on an individual day during these two episodes (Figure 8-67) compared to a 30% average contribution using the synthesized REMSAD results (Figure 8-63).

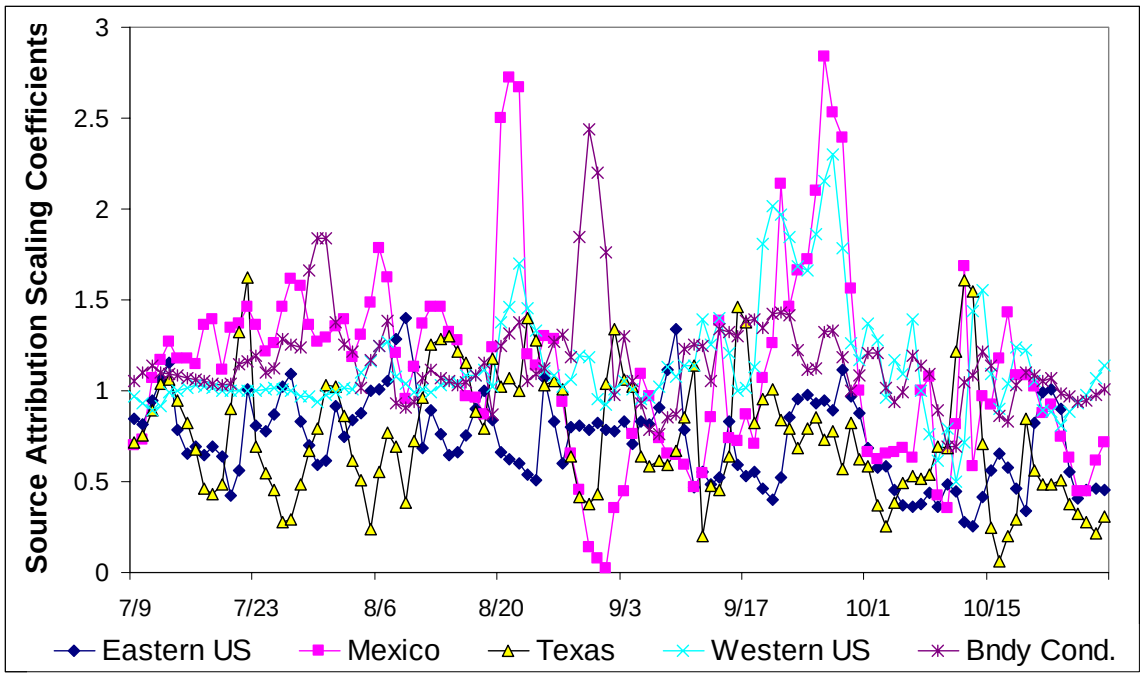

Figure 8-64. The optimum synthesized CMAQ daily source attribution scaling coefficients.

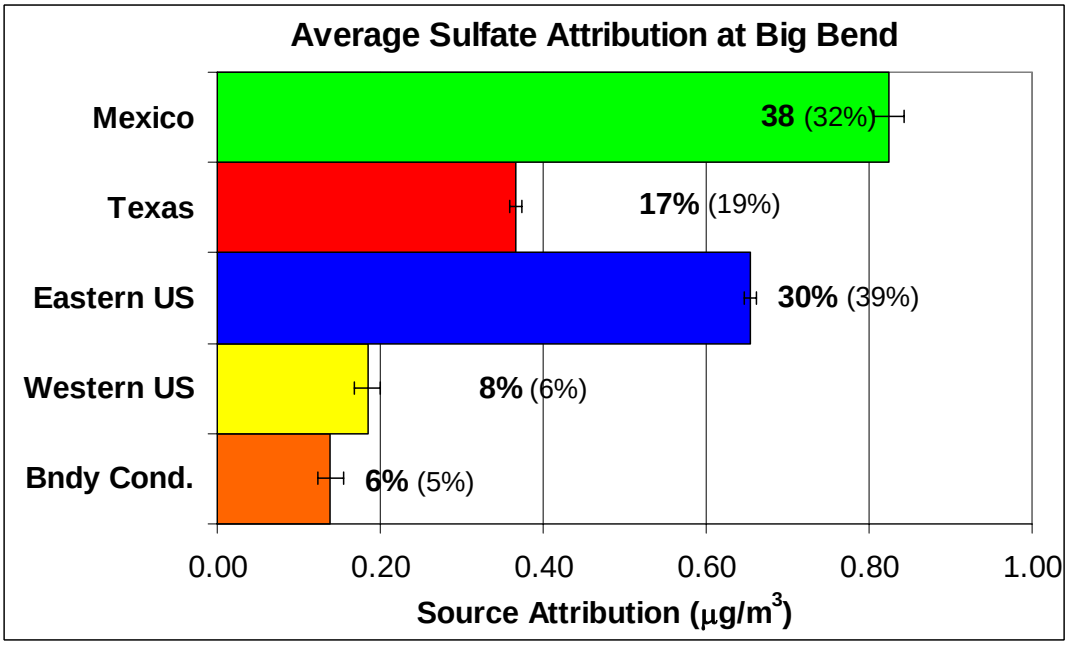

Figure 8-65. The optimum synthesized CMAQ average source attributions and standard errors to Big Bend's predicted sulfate for the entire BRAVO time period (7/9–10/28/1999). The bolded labels are the relative contributions, i.e. the ratios of average absolute values. The values in parentheses are the original CMAQ-MADRID source attribution estimates.

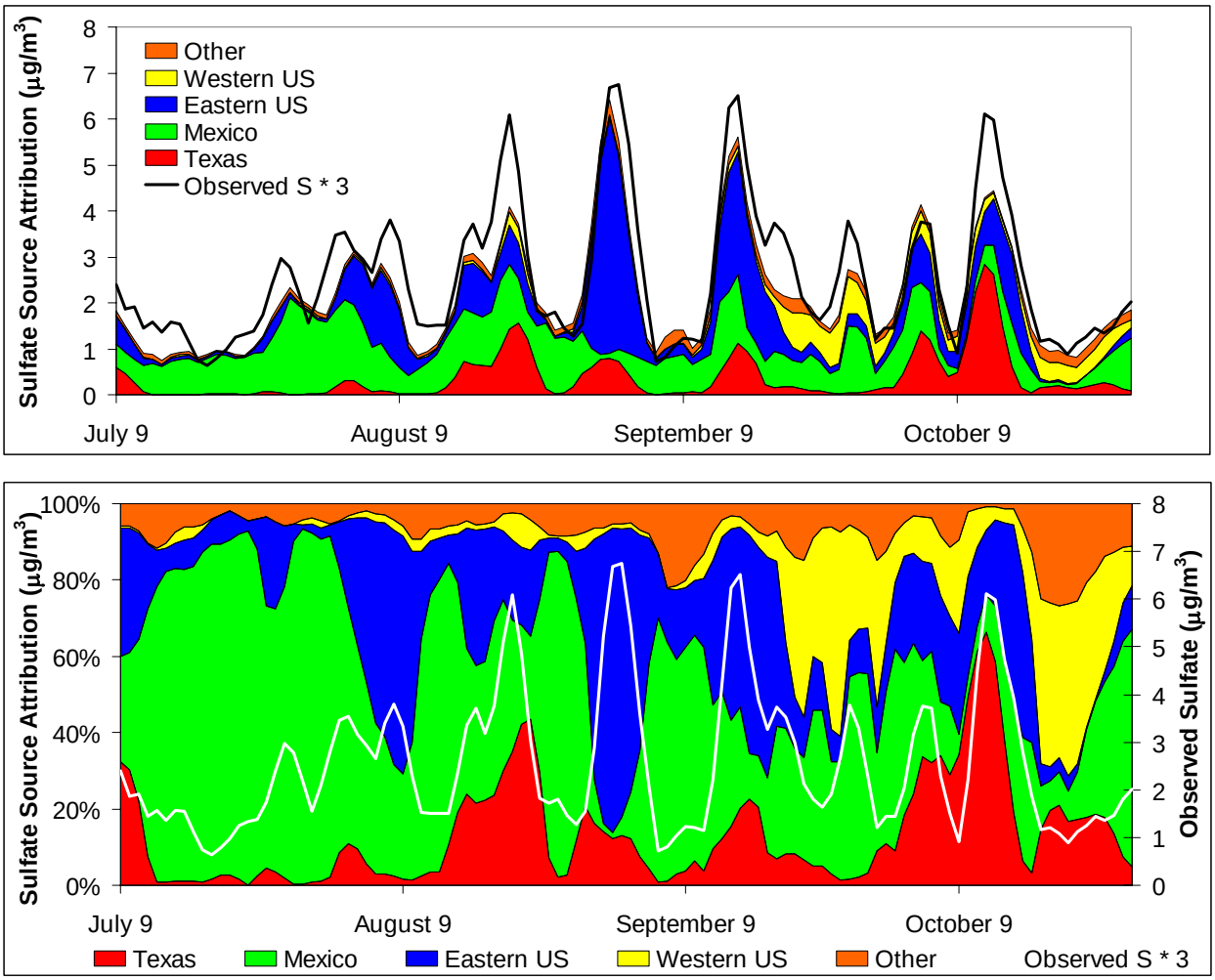

Figure 8-66. The optimum synthesized CMAQ daily absolute and relative source attributions to the predicted sulfate at Big Bend. The daily source attributions were smoothed using a three-day moving average.

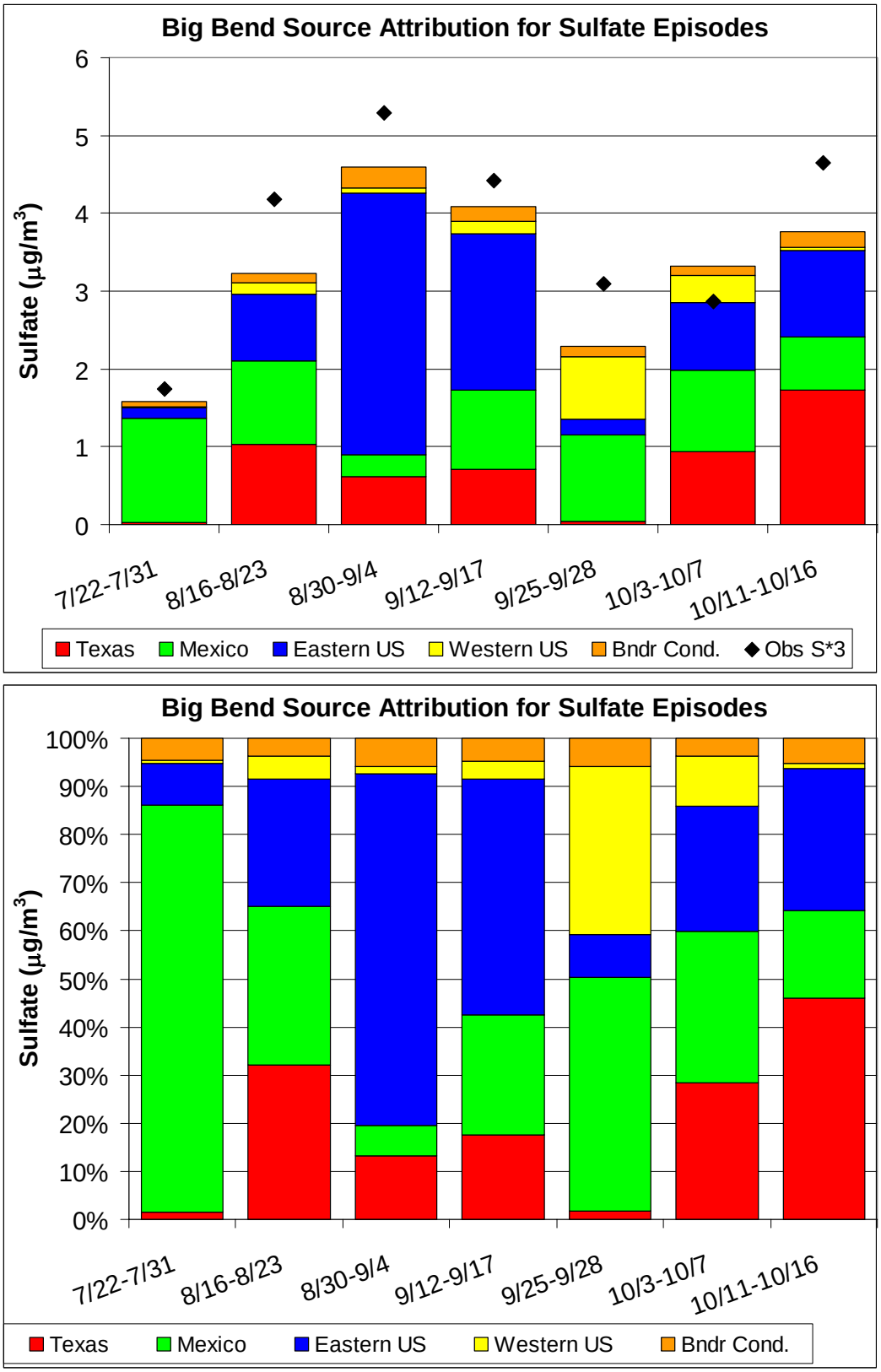

Figure 8-67. The optimum synthesized CMAQ average source attributions and standard errors to Big Bend's predicted sulfate for each Big Bend sulfate episode.

8.2.1.4 Summary and Discussion

In order to account for potential biases in the REMSAD and CMAQ-MADRID source attributions of Big Bend's sulfate, the model results were merged with the observed sulfate concentrations measured throughout Texas. The method is based on the synthesis inversion of the conservation of mass equation to derive source attribution scaling coefficients that varied in time but were fixed in space. In essence, these scaling coefficients partitioned the underestimated mass back to the source regions and removed overestimated mass from the source regions so that the predicted sulfate concentrations over Texas better matched the measured data.

The REMSAD and CMAQ synthesis inversions produced similar average contributions to Big Bend's sulfate, with Mexico having the largest contribution at 38%, while the eastern U.S. contributed about 30% and Texas 15%. The notable subregions from the REMSAD analysis were the Carbón I & II power plants, which contributed 23%, and east Texas, which contributed 14%, or 90% of the total Texas contribution. Comparing these results to the original model source attribution results, the Mexican contributions increased by 70% and 20% for the synthesized REMSAD and CMAQ results, respectively. The eastern U.S. contribution decreased by about 25% and the contributions from Texas remained about the same for both analyses.

Examining the seven largest sulfate episodes at Big Bend it was found that Mexico, eastern U.S., and Texas source regions were all large contributors during two or more episodes accounting for more than 30% of Big Bend's sulfate. The REMSAD and CMAQ-MADRID models completely missed the September 25–28 Big Bend sulfate episode and had temporal shifts in the October 11–16 episode. Therefore the synthesis inversion results for these two episodes need to be viewed with caution.

It is reassuring that the two synthesis inversions produced similar results. However, there were some differences on a higher time resolution, particularly during the Big Bend sulfur episodes. While neither result is truly correct, the synthesized CMAQ results are likely more trustworthy. The CMAQ-MADRID model was run using the REMSAD results for its boundary conditions, but these results were modified by the IMPROVE and CASTNet observed particulate sulfur and SO_2 concentrations. This reduced the eastern U.S. bias found in REMSAD. In the CMAQ-MADRID simulation, the Mexican emissions were increased by a factor of 2 within the CMAQ-MADRID domain and the upper bound on the Carbón emissions was used. This was done to address the underestimation from the Mexican sources. The resulting CMAQ-MADRID simulated sulfate concentrations at Big Bend compared better to the observed data than REMSAD results and had no bias. Therefore the synthesis inversion technique needed to correct for smaller biases.

8.2.2 Trajectory Mass Balance (TrMB)

The Trajectory Mass Balance (TrMB) Model (see section 2.3.2.1) is a receptor model in which measured concentrations at a receptor are assumed to be linearly related to the frequencies of airmass transport from several source regions to that receptor. TrMB is used to estimate the 4-month average contributions to fine particulate sulfur measured at Big Bend National Park from several source regions during July–October 1999.

8.2.2.1 Input and Modeling Details

Fine (< 2.5 μm diameter) 24-hour average particulate elemental sulfur concentrations (see chapter 3) measured at Big Bend by the IMPROVE sampler were originally used as the

dependent variable. However, there are two minor problems with this data set. First, data are missing for several days, including July 9–11, 23–25, 29, 31, August 1, and October 26–28. Since there are other measurements of fine sulfur and sulfate at Big Bend, it is possible to substitute other measurements for these missing concentrations. Other measurements at K-Bar include 24-hour averages of IMPROVE 12- and 24-hour sulfate and 6-, 12-, and 24-hour sulfur and the URG sampler's 24-hour sulfate concentrations. Once per week the URG sampler obtained replicate samples. Therefore there were from one to seven 24-hour averages of fine particulate sulfur or sulfate for each day. As shown in Figure 8-68, on some days the range of measured values was quite large. Days of particular interest are September 1, 14–15, and October 12, which, because they have high measured concentrations, are influential points in the TrMB regressions. On September 1 and 15 in particular, the IMPROVE 24-hour sulfur concentrations are at the maximum of a relatively large range of values.

Therefore, rather than use this single measurement for sulfur, the final source attribution for BRAVO was done using the daily median of all available 24-hour average sulfur concentrations for each day from July 5 through October 29. Although there are measured concentrations both before and after these dates, these are the time limits of what can be modeled using the BRAVO MM5 wind fields, so for consistency all model runs were for only these days. This gives a total of 117 days for the TrMB modeling. The final sulfur time series was within the measurement error of the sulfur measured by the URG sampler.

Source areas were chosen based on several criteria and are discussed in detail in section 2.3.2.5.

Back trajectories were started from Big Bend National Park (29.3 deg N Lat, 103.18 deg W Lon) and traced backwards in time for 5, 7, and 10 days. Original TrMB modeling for BRAVO utilized only 5-day back trajectories, but early results from REMSAD (section 2.2 and chapter 6) showed that, in general, REMSAD predicted more sulfate from distant source areas and less from closer source areas than did the back trajectory techniques. A possible reason for this result is that the lifetime of sulfur in the atmosphere was longer than 5 days on average or on a significant number of days during BRAVO. Trajectory lengths were therefore increased to determine if this alone would cause the TrMB results to more closely resemble the REMSAD results.

Three models, HYSPLIT version 4.5, the CAPITA Monte Carlo (CMC) model, and ATAD were used to generate back trajectories. All models were run with at least two input wind fields, the Mesoscale Meteorological Model (MM5) on a 36 km grid scale and EDAS when available with the lower resolution FNL when EDAS was missing. EDAS data were missing for the entire month of October and for several days in July. ATAD was also run with its traditional input of raw rawinsonde data. Sections 2.1.3 and 2.2 describe the details and differences between the wind fields and models. ATAD cannot generate trajectories longer than 5 days without significant code changes, so 7- and 10-day trajectories were not generated with this model.

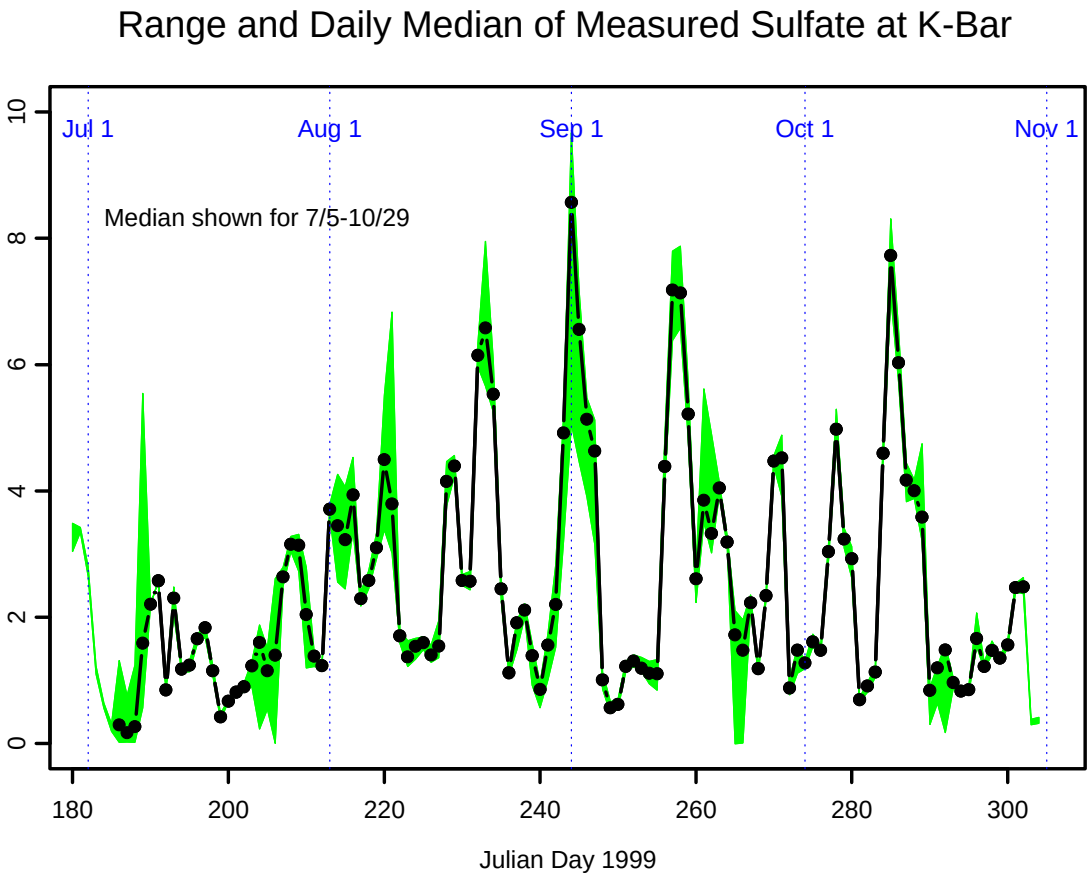

Figure 8-68. Range (in green) and daily median of IMPROVE and URG 24-hour averaged sulfur and sulfate measurements at K-Bar (in black).

HYSPLIT was started at heights of 100, 200, 500, and 1000 m above ground. An airmass location or "endpoint" was calculated hourly for each height. The number of endpoints in each source area was aggregated over these start heights. The CMC model released 20 particles every 2 hours with the position of each particle or endpoint calculated once every two hours for the EDAS/FNL data and once per hour for the MM5 data. Thus the total number of endpoints associated with a single 24-hour sulfur concentration for 5-day back trajectories is 11520 for HYSPLIT, 14400 for CMC with MM5, 28800 for CMC with EDAS/FNL and 160 for ATAD with any input.

All model/wind field combinations were tested with known attributions of the tracer data (section 7.1.1) and simulated sulfate from the REMSAD model (section 7.2.1). Based on the results of these tests HYSPLIT/MM5, CMC/EDAS/FNL, and ATAD/EDAS/FNL were dropped from consideration due to their poor performance. In addition, tests of biases in the wind fields (chapter 4) show that ATAD with raw rawinsonde data as input generates back trajectories that are too southerly, probably due to the sparse data in Mexico and the Gulf of Mexico. This leaves only the input combinations of HYSPLIT/EDAS/FNL and CMC/MM5 with 5-, 7-, and 10-day trajectories and ATAD/MM5 with 5-day trajectories for use in the measured sulfur attributions at Big Bend.

8.2.2.2 Results and Discussion

A summary of the TrMB results for measured fine particulate sulfur at K-BAR is shown in Table 8-12. The table includes the relative percent attributions and uncertainties. Also included are some statistics on goodness of fit between predicted and observed sulfur and number of observations.

Table 8-12. Relative attributions of median 24-hour sulfur at Big Bend to each source region by each model/wind field combination. Uncertainties are based on the standard errors of the regression coefficients. Model statistics are shown in the last 4 rows.

Percent Attribution of Sulfate to Each Source Area	**CAPITA MC with MM5**			**HYSPLIT with EDAS & FNL start heights 100–1000 m AGL**			**ATAD with MM5**
Trajectory Length (days)	5	7	10	5	7	10	5
North Central States (4)	0±3	0±4	0±5	0±2	0±3	0±4	0±2
Northeast (5)	0±2	1±2	1±4	2±1	3±1	0±3	0±1
MO/IL/AR (10)	5±3	9±4	10±5	0±3	0±6	0±9	5±2
East Central States (11)	1±3	5±6	9±7	1±2	4±3	6±4	0±2
LA/MS (20)	17±6	11±9	4±9	4±5	7±6	10±8	17±5
FL/GA (21)	0±3	0±4	0±4	0±2	0±3	0±4	0±2
Eastern U.S (4,5,10,11,20,21)	**23%**	**26%**	**24%**	**7%**	**14%**	**16%**	**17%**
Pacific Northwest (1)	3±3	3±3	5±4	0±3	0±3	0± 3	2±2
Northern Rockies (2)	0±4	0±4	0±5	0±6	1±6	0±7	0±3
Dakotas (3)	3±4	0±5	3±6	3±3	5±4	4±5	0±2
Southern California (6)	0±3	0±3	0±5	0±2	0±2	2±3	1±2
AZ/NM (7)	5±9	3±9	7±10	4±7	2±9	0±12	0±4
Central Plains (9)	3±10	15±11	10±12	1±7	0±6	0±8	0±5
Western U.S (1,2,3,6,7,9).	**14%**	**21%**	**25%**	**8%**	**8%**	**6%**	**3%**
Texas Panhandle (8)	0±4	0±5	0±5	0±6	0±7	5±8	0±2
West Texas (15)	0±5	3±5	0±5	1±7	0±8	0±10	1±3
North Central Texas (16)	2±5	0±5	0±5	4±5	1±6	1±7	9±5
Northeast Texas (17)	4±4	0±4	0±4	5±3	6±3	6±6	2±2
Southeast Texas (19)	13±10	9±11	12±11	35±8	29±10	18±12	8±8
Texas (8,15,16,17,19)	**19%**	**12%**	**12%**	**45%**	**36%**	**30%**	**20%**
Baja California (12)	0±3	1±4	0±6	1±3	0±5	0±6	No Ends
Northwest Mexico (13)	1±4	0±5	0±7	2±7	4±10	5±8	0±1
North Central Mexico (14)	0±4	0±4	1±5	0±3	0±3	0±4	2±4
Carbón I & II (18)	23±12	24±12	22±11	24±10	21±11	22±12	33±10
West Central Mexico (22)	1±5	1±5	1±5	0±3	4±4	6±4	0±2
Central Mexico (23)	0±3	0±3	0±3	0±3	0±3	0±4	0±2
Monterrey Region, MX (24)	5±10	0±9	0±9	4±7	5±8	7±8	6±6
SW Coast of Mexico (25)	0±2	0±1	0±1	1±1	0±2	1±3	0±1
Mexico City & Volcano (26)	9±6	8±6	10±6	7±4	8±4	6±5	10±5
S. Mexico/ Yucatan (27)	6±5	7±5	6±5	0±4	0±5	1±5	1±4
Mexico (12,13,14,18,22,23,24,25,26,27)	**45%**	**41%**	**40%**	**39%**	**42%**	**48%**	**50%**
Mean observed S (ng/m^3)	835.7	835.7	835.7	835.7	835.7	835.7	835.7
Mean predicted S (ng/m^3)	832.7	833.1	834.6	807.7	795.9	786.9	823.3
R^2	0.622	0.669	0.689	0.478	0.500	0.459	0.585
Number of observations	117	117	117	117	117	117	117

Detailed results and measures of model performance for each model and wind field combination are shown in Tables 8-13 through 8-19. Because of the different number of total endpoints for each combination, the regression coefficients with units of (ng/m^3 S/endpoint) are not directly comparable between cases. However, the predicted sulfur and percentages of sulfur attributed to the receptor from each source area are comparable.

Tables 8-13 through 8-19 also give indications of how well the model determined the regression coefficients. The coefficients and their standard errors are shown in column 2, the T statistic (coefficient/standard error) in column 3, the p value (probability that the coefficient could be zero) in column 4, and Variance Inflation Factor (VIF) in column 5. A T statistic of 2 corresponding to a p value of 0.05 is significant at the 95% confidence level with lower T statistics and higher p values being less significant.

The VIF is an indication of the collinearity of the source area with all other source areas. Source areas with VIFs of 10 and higher are considered to have significant collinearity with some linear combination of other regions. The more collinear a source region is with another region or a combination of other regions, the more difficulty in precisely determining the regression coefficient, resulting in higher standard errors for the coefficients, lower T statistics, higher p values, higher VIFs, and more uncertainty in the source attribution. With one exception (CMC MM5 10-day trajectories, E. Central States) VIFs greater than 10 occurred for source areas to the west and/or north from which airmasses usually arrived infrequently and from which the attributed sulfur is expected to be low.

Some source regions have negative coefficients indicating that the area is a net sink rather than a net source of sulfur. A negative coefficient would be likely to result if the daily endpoint counts in an area are inversely correlated with the sulfur concentrations or, in other words, the more air that arrives from that area the lower the sulfur concentrations at Big Bend. There were no negative coefficients that were statistically significant at the 95% level and all negative coefficients were small. Negative regression coefficients could be eliminated by restricting them to be zero or greater. This will probably be considered in future analyses.

Attribution results vary somewhat depending on the trajectory model/wind field combination used, though for most of the 27 smaller source regions the differences between combinations are within the uncertainties due to the standard errors of the regression coefficients.

In general, when comparing results between model runs, all combinations give approximately the same total attribution to Mexico. Values range from 39–50% with a median of 42%. With MM5 input in the CMC model, longer trajectories result in somewhat less attribution to Mexico, while the reverse is true for HYSPLIT with EDAS/FNL input for which longer trajectories result in slightly more sulfur being attributed to Mexico.

The biggest disagreement between model/wind field combinations is in the mean relative percent of sulfur attributed to Texas. HYSPLIT with EDAS/FNL input attributes approximately twice the percent of sulfur (30–45%) to Texas as is predicted from MM5 input modeled with ATAD (20%) or CMC (12–19%). Both HYSPLIT and CMC trajectory models attribute lower fractions of sulfur to Texas as the trajectory length increases.

MM5 input in both ATAD and CMC models results in a larger attribution (17–26%) to the eastern U.S. than HYSPLIT with EDAS/FNL (7–16%). The longer the HYSPLIT trajectories, the larger the fraction of sulfur attributed to the eastern U.S. The greatest percentage

attributed to the eastern U.S. by the CMC model was with the 7-day trajectories, with both 5- and 10-day lengths resulting in a lower percentage from this region.

For all model/wind field combinations the smallest relative attribution to any of the four large source regions was to the western U.S., though the percentages attributed by HYSPLIT/EDAS/FNL (6–8%) were only about half what was attributed by CMC/MM5 (14–25%). ATAD/MM5 had the lowest relative attribution to the western U.S. at just 3%. Longer HYSPLIT/EDAS/FNL trajectories caused slightly less relative attribution to the western U.S., while longer CMC/MM5 trajectories resulted in higher relative attributions to the western U.S.

Comparisons of these results with the results from the regional air quality model REMSAD show that TrMB predicts that larger fractions of sulfur arrive from Mexico and the western U.S. and a smaller fraction arrives from the eastern U.S. than is predicted by REMSAD. This is true for all input model/wind field combinations. Both CMC with MM5 and ATAD with MM5 give approximately the same average attribution to Texas as REMSAD, while HYSPLIT/EDAS/FNL attributes much more to Texas than REMSAD. Since REMSAD used the MM5 wind field as input, it is expected that TrMB modeling with the EDAS/FNL wind fields will be more different than with the MM5 input.

Reasons for the differences could include collinearities between TrMB source areas, inaccurate locations of the back trajectories, failure of the linearity assumptions, or any of many problems with the deterministic model including input data or parameterization of the physics and chemistry within the model. Model reconciliation is discussed in more detail in chapter 9.

The 7th column of Tables 8-13 through 8-19 gives the daily average fine elemental particulate sulfur (ng/m^3) attributed to each source area. These are calculated by multiplying the regression coefficient by the number of endpoints in the area for each day and then taking the mean, or equivalently by multiplying average number of endpoints per source area per day, shown in column 6, by the regression coefficient. Unlike the coefficients themselves, these values and the values in all columns to the right can be compared between tables. The uncertainty in the average predicted sulfur is calculated by multiplying the mean number of endpoints by the standard error of the coefficient. The raw percent attribution, shown in column 8, is 100% times the mean predicted sulfur attributed to the area divided by the total predicted sulfur. Column 9 is relative percent attribution and is the percent attribution that is usually reported and is shown in Table 8-12. It is calculated by setting the negative attributions to zero and then forcing the remaining positive values to sum to 100%. The uncertainties for these values are assumed to be the same as for the raw attributions, though this is likely an underestimate.

The final column in Tables 8-13 through 8-19 is the number of days when there were airmasses arriving at the receptor from each source area, and so is a measure of the frequency of impact of the source area on Big Bend. It is also of statistical interest since it is the number of days used to determine the regression coefficient. A single endpoint in a source region is enough to have the day count as a "hit" for that region, so trajectory models with fewer total endpoints will indicate that a source area impacted Big Bend on fewer days. As the trajectory lengths increase, the number of days with a potential impact also increases. Maximum possible number of days is 117.

Table 8-13. TrMB regression details for particulate sulfur at Big Bend and CAPITA MC MM5 5-day trajectory endpoints.

Source Area	Coef.±SE	T	P	VIF	Mean Ends/ day	Pred S (ng/m^3) ± unc	% Pred S	Relative % ± unc	No. days hit
North Central States (4)	-0.099±0.111	-0.89	0.38	2.0	204.8	-20±23	-2	0±3	50
Northeast (5)	1.117±3.559	0.31	0.75	2.1	3.9	4±14	1	0±2	13
MO/IL/AR (10)	0.110±0.061	1.82	0.07	2.0	434.0	48±26	6	5±3	58
East Central States (11)	0.125±0.243	0.52	0.61	2.6	93.5	12±23	1	1±3	40
LA/MS (20)	0.255±0.076	3.34	0.00	4.2	678.9	173±52	21	17±6	63
FL/GA (21)	-0.150±0.104	-1.44	0.16	1.7	240.5	-36±25	-4	0±3	72
Pacific Northwest (1)	0.273±0.229	1.19	0.24	5.3	96.8	26±22	3	3±3	33
Northern Rockies (2)	-0.169±0.124	-1.37	0.17	4.2	241.8	-41±30	-5	0±4	48
Dakotas (3)	0.140±0.151	0.92	0.36	4.5	227.1	32±34	4	3±4	43
Southern California (6)	-0.321±0.610	-0.53	0.60	5.9	37.3	-12±23	-1	0±3	26
AZ/NM (7)	0.283±0.407	0.70	0.49	30.7	188.1	53±77	6	5±9	41
Central Plains (9)	0.055±0.134	0.41	0.68	10.3	600.0	33±80	4	3±10	57
Texas Panhandle (8)	-0.022±0.456	-0.05	0.96	4.6	80.5	-2±37	-0	0±4	45
West Texas (15)	-0.030±0.231	-0.13	0.90	7.4	178.9	-5±41	-1	0±5	49
North Central Texas (16)	0.053±0.140	0.38	0.70	5.5	325.7	17±46	2	2±5	56
Northeast Texas (17)	0.201±0.169	1.19	0.24	3.3	194.3	39±33	5	4±4	60
Southeast Texas (19)	0.147±0.102	1.44	0.15	7.0	844.7	125±86	15	13±10	86
Baja California (12)	-0.183±1.520	-0.12	0.91	6.2	14.8	-3±22	-0	0±3	17
Northwest Mexico (13)	0.182±0.909	0.20	0.84	25.1	37.3	7±34	1	1±4	22
N Central Mexico (14)	-0.138±0.376	-0.37	0.72	6.7	91.1	-13±34	-2	0±4	32
Carbón I & II (18)	0.204±0.093	2.20	0.03	4.2	1112.2	227±103	27	23±12	98
W Central Mexico (22)	0.136±1.016	0.13	0.89	29.9	41.4	6±42	1	1±5	21
Central Mexico (23)	-0.203±0.229	-0.89	0.38	3.4	125.3	-25±29	-3	0±3	49
Monterrey Reg., MX (24)	0.052±0.091	0.57	0.57	5.9	890.9	46±81	6	5±10	90
SW Coast Mexico (25)	-0.220±1.051	-0.21	0.83	4.6	12.2	-3±13	-0	0±2	6
Mex City, Volcano (26)	0.195±0.119	1.63	0.11	3.8	443.3	86±53	10	9±6	66
S Mexico/ Yucatan (27)	0.116±0.077	1.52	0.13	2.4	500.5	58±39	7	6±5	60

Table 8-14. TrMB regression details for particulate sulfur at Big Bend and HYSPLIT EDAS/FNL 5-day trajectory endpoints.

Source Area	Coef.±SE	T	P	VIF	Mean Ends/ day	Pred S (ng/m^3) ± unc	% Pred S	Relative % ± unc	No. days hit
North Central States (4)	-0.159±0.273	-0.58	0.56	2.1	58.9	-9±16	-1	0±2	16
Northeast (5)	61.710±20.149	3.06	0.00	1.4	0.4	22±8	3	2±1	3
MO/IL/AR (10)	-0.250±0.188	-1.33	0.19	2.0	136.6	-34±26	-4	0±3	35
East Central States (11)	1.155±1.844	0.63	0.53	2.1	8.8	10±16	1	1±2	10
LA/MS (20)	0.114±0.123	0.93	0.36	2.9	347.3	40±43	5	4±5	53
FL/GA (21)	-0.282±0.190	-1.49	0.14	1.3	89.6	-25±17	-3	0±2	42
Pacific Northwest (1)	-0.568±0.972	-0.59	0.56	3.2	28.9	-16±28	-2	0±3	22
Northern Rockies (2)	-0.155±0.425	-0.36	0.72	4.7	108.4	-17±46	-2	0±6	31
Dakotas (3)	0.250±0.214	1.17	0.25	3.0	102.4	26±22	3	3±3	19
Southern California (6)	-0.080±0.397	-0.20	0.84	3.3	34.3	-3±14	-0	0±2	15
AZ/NM (7)	0.149±0.251	0.59	0.55	13.4	235.9	35±59	4	4±7	30
Central Plains (9)	0.042±0.184	0.23	0.82	5.5	306.5	13±56	2	1±7	44
Texas Panhandle (8)	-0.375±0.519	-0.72	0.47	8.5	101.1	-38±52	-5	0±6	32
West Texas (15)	0.038±0.239	0.16	0.87	9.2	237.4	9±57	1	1±7	32
North Central Texas (16)	0.153±0.142	1.08	0.29	3.4	283.3	43±40	5	4±5	42
Northeast Texas (17)	0.288±0.169	1.70	0.09	2.5	154.1	44±26	5	5±3	47
Southeast Texas (19)	0.295±0.060	4.91	0.00	2.8	1142.3	337±69	42	35±8	95
Baja California (12)	0.264±0.611	0.43	0.67	4.9	45.1	12±28	1	1±3	13
Northwest Mexico (13)	0.325±0.894	0.36	0.72	12.6	64.6	21±58	3	2±7	16
N Central Mexico (14)	0.031±0.234	0.13	0.90	2.6	87.0	3±20	0	0±3	24
Carbón I & II (18)	0.137±0.048	2.87	0.01	2.0	1711.0	235±82	29	24±10	99
W Central Mexico (22)	-0.149±2.275	-0.07	0.95	4.3	10.4	-2±24	-0	0±3	12
Central Mexico (23)	-0.487±0.604	-0.81	0.42	1.9	36.8	-18±22	-2	0±3	31
Monterrey Reg., MX (24)	0.045±0.065	0.69	0.50	2.5	898.2	40±58	5	4±7	85
SW Coast Mexico (25)	28.897±17.658	1.64	0.11	1.2	0.4	10±7	1	1±1	3
Mex City, Volcano (26)	0.384±0.163	2.36	0.02	1.8	187.1	72±30	9	7±4	47
S Mexico/ Yucatan (27)	-0.010±0.122	-0.08	0.94	1.7	246.4	-2±30	-0	0±4	51

Table 8-15. TrMB regression details for particulate sulfur at Big Bend and ATAD with MM5 input 5-day trajectory endpoints.

Source Area	Coef.±SE	T	P	VIF	Mean Ends/ day	Pred S (ng/m^3) ± unc	% Pred S	Relative % ± unc	No. days hit
North Central States (4)	-0.039±1.240	-0.03	0.98	1.5	12.1	0±15	-0	0±2	19
Northeast (5)	37.966±74.343	0.51	0.61	2.2	0.1	4±7	0	0±1	2
MO/IL/AR (10)	3.091±1.327	2.33	0.02	1.4	13.4	42±18	5	5±2	27
East Central States (11)	0.584±2.724	0.21	0.83	2.4	7.1	4±19	1	0±2	16
LA/MS (20)	6.839±1.876	3.65	0.00	3.6	22.7	155±43	19	17±5	35
FL/GA (21)	-0.119±2.425	-0.05	0.96	1.6	7.9	-1±19	-0	0±2	26
Pacific Northwest (1)	11.430±8.531	1.34	0.18	3.2	1.8	21±15	3	2±2	6
Northern Rockies (2)	-1.069±4.633	-0.23	0.82	4.9	4.8	-5±22	-1	0±3	13
Dakotas (3)	0.904±4.005	0.23	0.82	2.0	4.3	4±17	0	0±2	11
Southern California (6)	1.761±4.350	0.41	0.69	3.0	3.1	6±13	1	1±2	5
AZ/NM (7)	0.394±4.665	0.08	0.93	12.0	6.5	3±30	0	0±4	8
Central Plains (9)	-2.477±2.702	-0.92	0.36	5.7	15.1	-38±41	-5	0±5	24
Texas Panhandle (8)	-15.576±9.078	-1.72	0.09	3.8	1.9	-30±17	-4	0±2	10
West Texas (15)	1.795±4.870	0.37	0.71	4.4	5.2	9±25	1	1±3	17
North Central Texas (16)	8.975±4.741	1.89	0.06	7.3	9.2	83±44	10	9±5	26
Northeast Texas (17)	2.615±2.539	1.03	0.31	1.5	6.1	16±15	2	2±2	19
Southeast Texas (19)	2.596±2.249	1.15	0.25	5.3	29.6	77±67	9	8±8	67
Baja California (12)	NA	NA	NA	NA	0.0	0±0	0	0±0	0
Northwest Mexico (13)	-0.611±9.148	-0.07	0.95	4.1	1.2	-1±11	-0	0±1	3
N Central Mexico (14)	6.507±11.791	0.55	0.58	12.5	2.8	18±33	2	2±4	9
Carbón I & II (18)	8.268±2.205	3.75	0.00	3.7	36.6	303±81	37	33±10	95
W Central Mexico (22)	-8.373±23.453	-0.36	0.72	4.5	0.7	-6±16	-1	0±2	4
Central Mexico (23)	-0.846±3.177	-0.27	0.79	3.1	5.6	-5±18	-1	0±2	17
Monterrey Reg., MX (24)	1.716±1.491	1.15	0.25	2.8	34.4	59±51	7	6±6	71
SW Coast Mexico (25)	-4.108±17.338	-0.24	0.81	1.6	0.3	-1±5	-0	0±1	1
Mex City, Volcano (26)	5.367±2.270	2.37	0.02	2.7	17.5	94±40	11	10±5	44
S Mexico/ Yucatan (27)	0.738±1.717	0.43	0.67	1.9	17.4	13±30	2	1±4	43

Table 8-16. TrMB regression details for particulate sulfur at Big Bend and CAPITA MC MM5 input 7-day trajectory endpoints.

Source Area	Coef.±SE	T	P	VIF	Mean Ends/ day	Pred S (ng/m^3) ± unc	% Pred S	Relative % ± unc	No. days hit
North Central States (4)	-0.068±0.090	-0.76	0.45	2.4	333.8	-23±30	-3	0±4	62
Northeast (5)	0.373±0.566	0.66	0.51	3.7	35.6	13±20	2	1±2	36
MO/IL/AR (10)	0.164±0.056	2.98	0.00	2.6	623.9	102±34	12	9±4	64
East Central States (11)	0.207±0.172	1.21	0.23	7.0	271.4	56±47	7	5±6	56
LA/MS (20)	0.142±0.088	1.61	0.11	9.0	849.8	120±75	14	11±9	74
FL/GA (21)	-0.111±0.073	-1.53	0.13	1.8	449.0	-50±33	-6	0±4	82
Pacific Northwest (1)	0.226±0.157	1.44	0.15	5.0	159.9	36±25	4	3±2	53
Northern Rockies (2)	-0.175±0.094	-1.85	0.07	3.8	375.5	-66±35	-8	0±4	62
Dakotas (3)	-0.001±0.153	-0.01	1.00	5.5	295.3	0±45	-0	0±5	62
Southern California (6)	-0.139±0.422	-0.33	0.74	7.3	68.7	-10±29	-1	0±3	38
AZ/NM (7)	0.128±0.290	0.44	0.66	24.7	257.2	33±75	4	3±9	48
Central Plains (9)	0.224±0.126	1.78	0.08	11.5	726.5	163±92	20	15±11	64
Texas Panhandle (8)	-0.497±0.415	-1.20	0.23	4.7	95.0	-47±39	-6	0±5	53
West Texas (15)	0.188±0.218	0.86	0.39	7.5	197.4	37±43	4	3±5	52
North Central Texas (16)	-0.063±0.124	-0.51	0.61	4.8	347.7	-22±43	-3	0±5	59
Northeast Texas (17)	-0.102±0.153	-0.67	0.51	3.9	240.4	-25±37	-3	0±4	66
Southeast Texas (19)	0.112±0.103	1.08	0.28	8.8	901.9	101±93	12	9±11	89
Baja California (12)	0.326±1.006	0.32	0.75	8.0	31.8	10±32	1	1±4	27
Northwest Mexico (13)	0.016±0.780	0.02	0.98	29.5	58.0	1±45	0	0±5	29
N Central Mexico (14)	-0.180±0.309	-0.58	0.56	7.0	115.2	-21±36	-2	0±4	38
Carbón I & II (18)	0.236±0.086	2.73	0.01	4.1	1128.0	267±97	32	24±12	99
W Central Mexico (22)	0.156±0.750	0.21	0.84	30.4	56.2	9±42	1	1±5	26
Central Mexico (23)	-0.031±0.199	-0.16	0.88	3.1	136.3	-4±27	-1	0±3	50
Monterrey Reg., MX (24)	-0.007±0.084	-0.09	0.93	5.6	905.6	-7±76	-1	0±9	92
SW Coast Mexico (25)	-0.351±0.386	-0.91	0.37	3.3	26.4	-9±10	-1	0±1	13
Mex City, Volcano (26)	0.201±0.114	1.77	0.08	4.5	460.6	93±53	11	8±6	73
S Mexico/ Yucatan (27)	0.132±0.072	1.85	0.07	2.7	565.2	75±41	9	7±5	67

Table 8-17. TrMB regression details for particulate sulfur at Big Bend and HYSPLIT EDAS/FNL input 7-day trajectory endpoints.

Source Area	Coef.±SE	T	P	VIF	Mean Ends/ day	Pred S (ng/m^3) ± unc	% Pred S	Relative % ± unc	No. days hit
North Central States (4)	-0.147±0.114	-1.29	0.20	2.0	179.8	-26±20	-3	0±3	32
Northeast (5)	37.790±15.233	2.48	0.02	1.6	0.7	28±11	3	3±1	5
MO/IL/AR (10)	-0.163±0.140	-1.16	0.25	3.2	325.2	-53±46	-7	0±6	47
East Central States (11)	1.208±0.764	1.58	0.12	2.2	31.7	38±24	5	4±3	24
LA/MS (20)	0.134±0.079	1.69	0.09	3.4	588.9	79±47	10	7±6	57
FL/GA (21)	-0.132±0.112	-1.17	0.24	1.4	208.7	-28±23	-3	0±3	54
Pacific Northwest (1)	-0.216±0.334	-0.65	0.52	2.1	71.5	-15±24	-2	0±3	37
Northern Rockies (2)	0.043±0.240	0.18	0.86	3.4	192.6	8±46	1	1±6	44
Dakotas (3)	0.359±0.194	1.85	0.07	3.2	153.2	55±30	7	5±4	38
Southern California (6)	-0.020±0.331	-0.06	0.95	3.4	48.8	-1±16	-0	0±2	19
AZ/NM (7)	0.087±0.247	0.35	0.73	17.6	294.6	26±73	3	2±9	33
Central Plains (9)	-0.091±0.118	-0.77	0.44	4.0	436.9	-40±52	-5	0±6	55
Texas Panhandle (8)	0.040±0.507	0.08	0.94	9.3	113.9	5±58	1	0±7	36
West Texas (15)	-0.124±0.241	-0.51	0.61	10.5	264.9	-33±64	-4	0±8	34
North Central Texas (16)	0.023±0.141	0.16	0.87	3.9	318.3	7±45	1	1±6	49
Northeast Texas (17)	0.243±0.110	2.21	0.03	2.6	246.1	60±27	8	6±3	51
Southeast Texas (19)	0.252±0.066	3.83	0.00	3.7	1242.4	313±82	39	29±10	96
Baja California (12)	-0.218±0.544	-0.40	0.69	6.5	70.7	-15±38	-2	0±5	18
Northwest Mexico (13)	0.491±0.884	0.56	0.58	22.9	86.1	42±76	5	4±10	18
N Central Mexico (14)	0.016±0.220	0.07	0.94	2.6	99.2	2±22	0	0±3	25
Carbón I & II (18)	0.127±0.048	2.64	0.01	1.8	1753.1	223±84	28	21±11	99
W Central Mexico (22)	1.388±1.071	1.30	0.20	6.6	28.4	39±30	5	4±4	13
Central Mexico (23)	-1.291±0.567	-2.28	0.03	2.0	44.2	-57±25	-7	0±3	32
Monterrey Reg., MX (24)	0.057±0.066	0.85	0.40	2.4	912.4	52±60	7	5±8	88
SW Coast Mexico (25)	0.284±1.898	0.15	0.88	2.9	8.1	2±15	0	0±2	8
Mex City, Volcano (26)	0.437±0.174	2.50	0.01	2.1	197.7	86±34	11	8±4	50
S Mexico/ Yucatan (27)	-0.002±0.105	-0.02	0.99	2.0	342.4	-1±36	-0	0±5	55

Table 8-18. TrMB regression details for particulate sulfur at Big Bend and CAPITA MC MM5 input 10-day trajectory endpoints.

Source Area	Coef.±SE	T	P	VIF	Mean Ends/ day	Pred S (ng/m^3) ± unc	% Pred S	Relative % ± unc	No. days hit
North Central States (4)	-0.058±0.087	-0.66	0.51	3.7	461.5	-27±40	-3	0±5	69
Northeast (5)	0.085±0.362	0.24	0.82	7.0	85.9	7±31	1	1±4	53
MO/IL/AR (10)	0.155±0.057	2.73	0.01	3.4	741.2	115±42	14	10±5	70
East Central States (11)	0.252±0.150	1.68	0.10	10.8	400.8	101±60	12	9±7	65
LA/MS (20)	0.049±0.075	0.66	0.51	7.8	981.7	48±74	6	4±9	79
FL/GA (21)	-0.122±0.060	-2.03	0.05	1.8	603.4	-74±36	-9	0±4	85
Pacific Northwest (1)	0.232±0.153	1.52	0.13	6.4	232.5	54±36	6	5±4	64
Northern Rockies (2)	-0.118±0.089	-1.33	0.19	4.0	499.4	-59±44	-7	0±5	70
Dakotas (3)	0.110±0.152	0.72	0.47	6.0	349.0	38±53	5	3±6	69
Southern California (6)	-0.311±0.361	-0.86	0.39	9.8	120.4	-37±43	-4	0±5	56
AZ/NM (7)	0.236±0.250	0.94	0.35	24.6	337.6	80±84	10	7±10	59
Central Plains (9)	0.140±0.122	1.14	0.26	12.1	796.9	111±97	13	10±12	71
Texas Panhandle (8)	-0.155±0.405	-0.38	0.70	4.9	108.9	-17±44	-2	0±5	62
West Texas (15)	-0.004±0.208	-0.02	0.99	7.2	216.2	-1±45	-0	0±5	62
North Central Texas (16)	-0.067±0.120	-0.56	0.58	5.1	368.6	-25±44	-3	0±5	68
Northeast Texas (17)	-0.051±0.142	-0.36	0.72	3.9	262.7	-13±37	-2	0±4	69
Southeast Texas (19)	0.146±0.099	1.48	0.14	8.3	939.3	137±93	16	12±11	90
Baja California (12)	-0.207±0.838	-0.25	0.81	16.2	62.2	-13±52	-2	0±6	46
Northwest Mexico (13)	0.002±0.658	0.00	1.00	28.7	83.0	0±55	0	0±7	42
N Central Mexico (14)	0.069±0.265	0.26	0.80	6.8	147.6	10±39	1	1±5	50
Carbón I & II (18)	0.222±0.080	2.78	0.01	4.0	1139.0	253±91	30	22±11	99
W Central Mexico (22)	0.110±0.612	0.18	0.86	27.3	72.9	8±45	1	1±5	34
Central Mexico (23)	-0.115±0.190	-0.61	0.55	3.2	147.1	-17±28	-2	0±3	58
Monterrey Reg., MX (24)	-0.015±0.081	-0.19	0.85	4.8	920.6	-14±75	-2	0±9	93
SW Coast Mexico (25)	-0.538±0.327	-1.65	0.10	3.4	35.7	-19±12	-2	0±1	16
Mex City, Volcano (26)	0.237±0.110	2.15	0.03	4.9	486.4	115±54	14	10±6	80
S Mexico/ Yucatan (27)	0.120±0.067	1.79	0.08	2.6	599.2	72±40	9	6±5	76

Table 8-19. TrMB regression details for particulate sulfur at Big Bend and HYSPLIT EDAS/FNL input 10-day trajectory endpoints.

Source Area	Coef.±SE	T	P	VIF	Mean Ends/ day	Pred S (ng/m^3) ± unc	% Pred S	Relative % ± unc	No. days hit
North Central States (4)	-0.092±0.083	-1.11	0.27	1.8	350.2	-32±29	-4	0±4	43
Northeast (5)	-1.264±1.486	-0.85	0.40	3.8	15.2	-19±23	-2	0±3	17
MO/IL/AR (10)	-0.144±0.125	-1.15	0.25	6.5	566.9	-82±71	-10	0±9	51
East Central States (11)	0.881±0.341	2.58	0.01	2.4	96.5	85±33	11	6±4	38
LA/MS (20)	0.175±0.085	2.04	0.04	5.8	745.1	130±63	17	10±8	62
FL/GA (21)	-0.176±0.095	-1.84	0.07	1.5	353.6	-62±34	-8	0±4	67
Pacific Northwest (1)	-0.026±0.175	-0.15	0.88	2.0	154.1	-4±27	-1	0±3	51
Northern Rockies (2)	-0.133±0.175	-0.76	0.45	3.4	294.1	-39±51	-5	0±7	55
Dakotas (3)	0.244±0.200	1.22	0.23	3.4	199.8	49±40	6	4±5	46
Southern California (6)	0.344±0.321	1.07	0.29	4.5	83.8	29±27	4	2±3	32
AZ/NM (7)	-0.152±0.247	-0.62	0.54	22.5	376.4	-57±93	-7	0±12	42
Central Plains (9)	-0.143±0.109	-1.32	0.19	4.4	543.7	-78±59	-10	0±8	59
Texas Panhandle (8)	0.525±0.545	0.96	0.34	9.9	121.6	64±66	8	5±8	44
West Texas (15)	-0.087±0.277	-0.32	0.75	14.1	285.7	-25±79	-3	0±10	36
North Central Texas (16)	0.031±0.154	0.20	0.84	4.5	342.5	11±53	1	1±7	50
Northeast Texas (17)	0.270±0.147	1.84	0.07	5.2	299.6	81±44	10	6±6	52
Southeast Texas (19)	0.184±0.071	2.59	0.01	4.4	1310.6	242±93	31	18±12	97
Baja California (12)	-0.417±0.438	-0.95	0.34	7.6	106.0	-44±46	-6	0±6	23
Northwest Mexico (13)	0.528±0.565	0.94	0.35	15.7	113.4	60±64	8	5±8	24
N Central Mexico (14)	0.051±0.242	0.21	0.83	3.6	120.2	6±29	1	0±4	28
Carbón I & II (18)	0.166±0.053	3.14	0.00	2.1	1762.8	292±93	37	22±12	100
W Central Mexico (22)	1.961±0.852	2.30	0.02	6.4	38.8	76±33	10	6±4	16
Central Mexico (23)	-1.593±0.624	-2.55	0.01	2.6	50.1	-80±31	-10	0±4	34
Monterrey Reg., MX (24)	0.092±0.066	1.39	0.17	2.2	930.2	86±61	11	7±8	89
SW Coast Mexico (25)	0.734±1.904	0.39	0.70	4.4	13.8	10±26	1	1±3	10
Mex City, Volcano (26)	0.339±0.180	1.88	0.06	2.2	215.7	73±39	9	6±5	53
S Mexico/ Yucatan (27)	0.047±0.108	0.44	0.67	1.8	358.7	17±39	2	1±5	64

8.2.3 Forward Mass Balance Regression (FMBR)

The Forward Mass Balance Regression (FMBR) is a hybrid receptor model in which receptor concentrations are assumed to be linearly related to airmass transport from a number of source regions to the receptor. The transport is estimated using a forward particle dispersion model simulating transport from the source regions to the receptor. The FMBR methodology is explained in section 2.3.2.2 and validated using the measured tracer concentrations and the REMSAD source apportionment results in sections 7.1.2 and 7.2.2, respectively. FMBR is identical in concept to TrMB, but FMBR is based on forward transport using plumes from the sources, while TrMB is based upon backward transport using back trajectories from the receptor.

The evaluation of FMBR was conducted using both the BRAVO MM5 and EDAS/FNL wind fields. It was shown that FMBR was able to properly apportion the measured perfluorocarbon tracer at Big Bend to the four tracer release sites in Texas, within the uncertainties of the technique. Therefore the technique was able to account for source contributions of inert species from sources 250–750 km from Big Bend. FMBR was also tested against synthetic sulfate concentrations and their apportionment to nine source regions including the Carbón facilities. The synthetic data was derived from the REMSAD model runs. Again, FMBR was able to properly apportion the synthetic sulfate to the nine source regions within the uncertainties of the technique. The results were sensitive to the length of time that the transport from the sources to the Big Bend region was tracked, and 10-day transport times produced the best results. Distant (western U.S. and eastern U.S.) source regions tended to be underestimated while the closer source regions in Texas and Mexico were overestimated. Based upon these results, FMBR was applied to the measured Big Bend sulfate data and the analysis was conducted for both wind fields.

In this application, the 24-hour observed fine particulate sulfur concentrations at the K-Bar Ranch in Big Bend were used. Multiple sulfur measurements were made at K-Bar so the median daily concentration for each day was used. These are the same data used in the TrMB analysis in the previous section. The airmass transport was estimated using the CAPITA Monte Carlo model driven by both the BRAVO MM5 and EDAS/FNL wind fields to estimate plume transport from about 670 virtual sources about 100 km apart evenly distributed throughout the United States and Mexico. Each plume was tracked for 10 days. These plumes were aggregated together to represent transport from 17 large source regions. The location of the virtual plumes and the source regions are presented in Figure 2-17. Section 7.2.2 describes how the Monte Carlo Model was run and how the source-to-receptor transport was derived from the resulting plumes.

There were two differences between the application of FMBR and TrMB to Big Bend's sulfate data. The EDAS/FNL wind fields were used in FMBR, but the CMC back trajectories generated by the EDAS/FNL wind fields did not pass all of the TMBR evaluation tests and were not used in that analysis. Also, the FMBR technique used a modified version of the source regions used in TrMB. It was found that the transport from some of the source regions were highly collinear with $r^2 > 0.5$. These source areas were merged and adjusted until the r^2 between any two source regions was below 0.5. This process reduced the 27 source regions to only 17 which are presented in Figure 2-18.

8.2.3.1 Results

The detailed regression results are presented in Tables 8-20 and 8-21 using the MM5 and EDAS/FNL wind fields, respectively. Figures 8-69 and 8-70 present the source attributions for

the four major regions, Mexico, Texas, the eastern U.S., and the western U.S., and the major subregions, Carbón and east Texas. Using either wind field, the performance of the regression was about the same with an r^2 of 0.36 an RMS error of 60%; however, the bias using the MM5 winds was only -6% but was -18% using the EDAS/FNL winds. When FMBR was applied to the REMSAD-simulated sulfate, the r^2 was 0.8. The reduction in the r^2 is due to either errors in the transport or nonlinearities in the atmospheric transformation and removal processes in the atmosphere for which the REMSAD model does not account.

Table 8-20. The FMBR regression results using the MM5 10-day plumes. The bolded rows have p values less than or equal to 0.1 derived from a two sized t test. The FMBR used the MM5-derived 10-day plumes.

Source Region	SO_2 Emission [1000 Tons SO2/yr]	Src/Sink ± Error	P Value	VIF	Attribution ± Error %
Southeast Texas	**537,000**	**36.4 ± 9.3**	**0.0002**		**24.4 ± 6.2**
Northeast Texas	476,000	0. ± 13.5	1		0. ± 4.3
West Texas	114,000	0. ± 5.	1		0. ± 2.7
Carbón I & II	**152,000 - 241,000**	**56. ± 12.6**	**0.00002**		**26.2 ± 5.9**
Monterrey Region, MX	**114,000**	**6.8 ± 3.4**	**0.05**		**18.3 ± 9.1**
Baja California	64,000	26.1 ± 44.1	0.55		1.4 ± 2.4
Northwest Mexico	140,000	0. ± 4.7	1		0. ± 3.
Central MX	44,000	0. ± 5.2	1		0. ± 4.2
SW Coast of MX	6,000	0. ± 31.3	1		0. ± 1.5
Mexico City & Volcano	2,160,000	17.8 ± 11.5	0.12		8.2 ± 5.3
S. Mexico/ Yucatan	0	3.5 ± 17.2	0.84		0.9 ± 4.3
North Central East	256,000	0. ± 34.7	1.00		0. ± 4.2
MO/IL/AR - LA/MS	2,100,000	8.3 ± 5.1	0.11		10.9 ± 6.8
East Central	**3,326,000**	**27.4 ± 15.3**	**0.08**		**9.6 ± 5.3**
FL/GA	1,377,000	0. ± 12.3	1		0. ± 4.
Western U.S.	740,000	0.05 ± 1.28	0.97		0.1 ± 2.6
Central Plains	445,000	0. ± 2.9	1		0. ± 3.7
Aggregated Regions					
Texas	**1,127,000**	**36.4 ± 17.2**	**0.04**		**24.4 ± 8.**
Mexico	**2,680,000**	**110.3 ± 59.7**	**0.067**		**55. ± 14.1**
Eastern U.S	7,060,000	35.7 ± 40.2	0.38		20.5 ± 10.4
Western U.S./Central Plains	1,200,000	0.1 ± 3.2	0.99		0.1 ± 4.5

Performance Statistics

Observed Sulfate Avg (µg/m3)	2.49
Predicted Sulfate Avg (µg/m3)	2.34
Bias (%):	-6.2
RMS error (%):	59
r^2	0.36
# Data Values	118

Table 8-21. The FMBR regression results using the EDAS/FNL 10-day plumes. The bolded rows have p values less than or equal to 0.1 derived from a two sized t test. The FMBR used the EDAS/FNL-derived 10-day plumes.

Source Region	SO_2 Emission	Src/Sink ± Error	P Value	VIF	Attribution ± Error
	[1000 Tons SO2/yr]				%
Southeast Texas	**537,000**	**11.4 ± 6.9**	**0.1**		**17.5 ± 10.6**
Northeast Texas	476,000	11.7 ± 7.9	0.14		6.6 ± 4.4
West Texas	114,000	0. ± 3.2	1		0. ± 3.8
Carbón I & II	**152,000 - 241,000**	**26.2 ± 8.5**	**0.003**		**20.4 ± 6.6**
Monterrey Region, MX	**114,000**	**7.1 ± 2.8**	**0.01**		**18.9 ± 7.5**
Baja California	64,000	0. ± 31.7	1.00		0. ± 3.7
Northwest Mexico	140,000	0.5 ± 4.8	2		0.5 ± 5.1
Central MX	44,000	0. ± 7.	1		0. ± 4.
SW Coast of MX	6,000	0. ± 28.6	1		0. ± 1.1
Mexico City & Volcano	**2,160,000**	**29.2 ± 16.3**	**0.08**		**7.1 ± 3.9**
S. Mexico/ Yucatan	0	29.9 ± 26.7	0.26		4.7 ± 4.2
North Central East	256,000	0. ± 42.7	1.00		0. ± 5.6
MO/IL/AR - LA/MS	2,100,000	6.2 ± 4.1	0.14		10.7 ± 7.2
East Central	**3,326,000**	**36.7 ± 15.**	**0.02**		**9.4 ± 3.8**
FL/GA	1,377,000	17.6 ± 14.6	0.23		4.2 ± 3.5
Western U.S.	740,000	0. ± 1.4	1.00		0. ± 4.8
Central Plains	445,000	0. ± 3.9	1		0. ± 7.
Aggregated Regions					
Texas	**1,127,000**	**23.1 ± 10.9**	**0.04**		**24.1 ± 12.1**
Mexico	**2,680,000**	**93. ± 54.5**	**0.09**		**51.6 ± 14.**
Eastern U.S.	7,060,000	60.5 ± 47.7	0.21		24.3 ± 10.4
Western U.S./Central Plains	1,200,000	0. ± 4.1	1.00		0. ± 8.5

Performance Statistics

Observed Sulfate Avg (µg/m3)	2.49
Predicted Sulfate Avg (µg/m3)	2.04
Bias (%):	-18.1
RMS error (%):	64
r^2	0.37
# Data Values	118

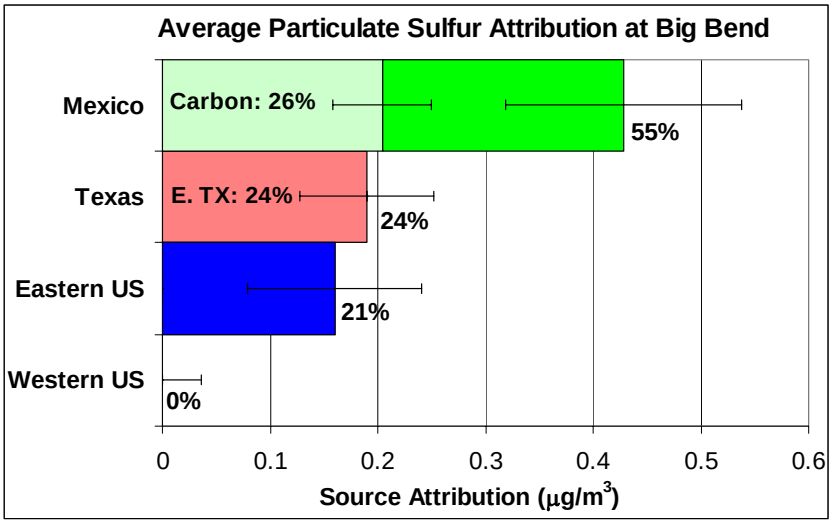

Figure 8-69. The average source attributions and standard errors to Big Bend's sulfate for the entire BRAVO time period (7/6–10/28/1999). The bolded labels are the relative contributions, i.e. the ratios of average absolute values. The FMBR used the MM5-derived 10-day plumes.

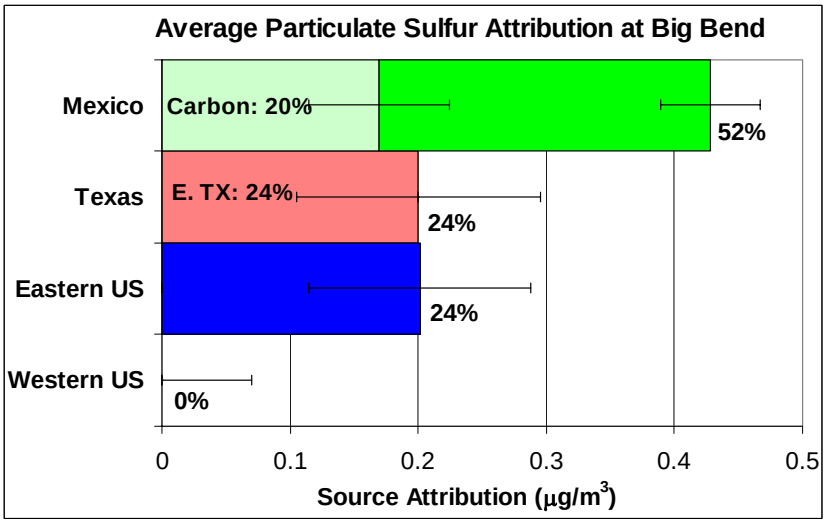

Figure 8-70. The average source attribution and standard errors to Big Bend's sulfate for the entire BRAVO time period (7/6–10/28/1999). The bolded labels are the relative contributions, i.e. the ratios of average absolute values. The FMBR used the EDAS/FNL-derived 10-day plumes.

As shown in Table 8-20, when using the MM5 wind fields, only four (southeast Texas, Carbón, Monterrey, Mexico, and the central eastern U.S.) of the 17 source regions were considered significant at p values of 0.1 or less. The two source regions encompassing MO/IL/AR - LA/MS and Mexico City and the Popocatepetl Volcano had p values less than 0.15. Note, each two letters in the MO/IL/AR - LA/MS source region represent a state in the eastern U.S. These 6 source areas accounted for nearly all of the sulfur contributions. As shown in Figure 8-69, Mexico was the largest average contributor to Big Bend's sulfur over the BRAVO period at about 55%. The Carbón and Monterrey Mexican subregions accounted for 26 and 18% of Big Bends sulfur, respectively. Texas accounted for about 24% of Big Bend's sulfur with all

of this coming from eastern Texas. The eastern U.S. accounted for the remaining 21%. The western U.S. had a predicted contribution of 0 with a standard error of 4.5%.

The source attribution using the EDAS/FNL wind fields produced similar results with Mexico accounting for 52% and Texas and the eastern U.S. each accounting for 24% of Big Bend's sulfur. The primary differences between the EDAS/FNL and MM5 results is that the EDAS winds had a smaller Carbón impact of 20.4 ± 6.6% compared to 26.2 ± 5.9% using the MM5 winds. In addition, the northeast Texas contribution was 6.6 ± 4.4% using the EDAS/FNL compared to 0. ± 4.3% when using the MM5 winds. These results are consistent with the fact that Big Bend back trajectories generated from the EDAS/FNL wind fields had greater transport from northeast Texas compared to those generated using the MM5 wind field (see chapter 4 and section 8.1.3).

8.2.3.2 Discussion

As discussed and demonstrated in chapter 7, the FMBR technique tends to overestimate the source contributions from nearby source regions and underestimate the contributions from more distant source regions. There are several explanations for this bias. First, common transport pathways between source regions result in collinearities in transport from neighboring source regions. For example, airmasses that traversed the eastern U.S. usually traversed Texas and northern Mexico en route to Big Bend (see section 8.1.3). Transport from more distant source regions usually occurs less frequently and the airmasses are more dispersed, decreasing their signal or impact on the receptor. If this signal is smaller than the error in the system, i.e. errors in the observations and transport, then the regression analysis cannot resolve the source's impact even though the source's actual contribution may be significant. This source attribution is then attributed to the collinear source region whose contribution is resolvable. A second potential cause is that the error in airmass transport tends to increase with transport time and distance. Therefore more distant source regions will have a larger transport error than nearby source regions. *White and Macias* [1987] showed that regression analyses are biased towards variables with less error.

In section 7.2.2, the FMBR technique was applied to a synthesis data set, generated by the REMSAD air quality model, where the sulfate concentrations and source contribution to Big Bend were known. This allowed the quantification of the FMBR biases on the synthesis data set. Presumably, similar biases exist in the application of the FMBR to the observed sulfate data, and the scaling of the FMBR results by these biases is a better estimate of the source attribution. These scaling factors were derived using the MM5 transport and are thus most appropriately applied to the FMBR-MM5 results.

The bias scaling factors and the scaled FMBR/MM5 source attribution of Big Bend's sulfate are presented in Table 8-22. As shown, both the Mexican and Texan source attributions decreased with Mexico decreasing from 55% to 43% and Texas from 24% to 17%. The contribution from the Carbón region also decreased to 22% for MM5. The eastern U.S. contribution increased, now accounting for 24% of Big Bend's predicted sulfate. The non-attributed contributions are the difference between the Mexican, eastern U.S., and Texan contributions from the total and can be thought of as the contributions from the western U.S. and the boundary conditions. This unaccounted contribution is 16% which is about equal to the contribution of the western U.S. and boundary conditions used to create the scaling coefficients. While the bias scaling factors were derived using the MM5 transport, similar biases should exist

in the FMBR using EDAS/FNL transport. Table 8-22 also presents the scaled FMBR-EDAS/FNL results which are similar to the scaled FMBR-MM5 results.

Table 8-22. The FMBR source attribution results for Big Bend scaled to account for biases that were estimated in section 7.2.2 (see Table 7-6).

		% Contribution ± Standard Error			
		Original Source Attribution		Scaled Source Attribution	
Source Regions	**Scaling Factors**	**MM5**	**EDAS/FNL**	**MM5**	**EDAS/FNL**
Carbón	0.84	26.2 ± 5.9	20.4 ± 6.6	22	17
Rest of Mexico	0.72	28.8 ± 13	31.2 ± 12	21	23
NE Texas	0.51	0. ± 4.3	6.6 ± 4.4	0	3.4
SE Texas	0.69	24.4 ± 6.2	17.5 ± 10.6	17	12
Rest of Texas	0.52	0. ± 2.7	0. ± 3.8	0	0
LA/MS & MO/IL/AR	0.8	10.9 ± 6.8	10.7 ± 7.2	8.7	8.5
E Central	1.54	9.6 ± 5.3	9.4 ± 3.8	15	15
Rest of E U.S.	1.5	0 ± 5.8	4.2 ± 6.6	0	6.3
[1]*Western U.S.*		0.1 ± 4.5	0. ± 8.5	0.1	**0**
[1]*GOCART BC*					
Mexico (all)		55. ± 14.1	51.6 ± 14.	43	40
Texas (all)		24.4 ± 8.	24.1 ± 12.1	17	15
Eastern U.S. (all)		20.5 ± 10.4	24.3 ± 10.4	24	29
[2]Non Attributed Contribution				17	16

1. The scaling factors were derived using a western U.S. contribution of 9% and boundary condition contribution of 7%.
2. The non attributed contribution is due to the scaling of the source contributions and is assumed to be due to a western U.S. contribution of 9% and boundary condition contribution of 7%.

Neither the MM5 nor the EDAS/FNL wind fields were shown to be superior at generating the forward transport for the FMBR technique in any objective analysis. Therefore it is not known which result, if either, is closer to the true source attribution. Since REMSAD was run with the MM5 wind fields, it could be expected that the FMBR-MM5 results would be more similar to REMSAD. This comparison is presented in chapter 9 which contrasts, compares, and reconciles all of the differences between the air quality and receptor modeling approaches. In this chapter it is shown that the FMBR-EDAS/FNL results are actually more similar to the REMSAD results. As shown in Table 8-22, the largest differences are that the FMBR-MM5 estimated larger source contributions from Carbón and southeast Texas, while the FMBR-EDAS/FNL estimated large contributions from northeast Texas and the rest of the eastern U.S. The transport from these source regions is collinear and the technique must properly divide the mass between these source regions. Collinearity inflates the standard errors and it is seen that the different source attributions using the two wind fields are within 1 to 1.5 standard errors. Thus, the techniques may have misappropriated mass between these source regions. The differences are not significant at even the 0.1 level. Also, the FMBR-MM5 source attributions

are larger for the closer source regions, e.g., Carbón and southeast Texas. As discussed, the FMBR most likely has positive biases for nearby sources. These biases appear larger for the FMBR-MM5 than the FMBR-EDAS/FNL results.